UAB
Universitat Autònoma de Barcelona

Development of novel therapeutic strategies against NF-κB Pathway in Diffuse Large B-cell Lymphoma

Marc Antoni Armengol i Cubillos

Doctoral Thesis

Development of novel therapeutic strategies against NF-κB Pathway in Diffuse Large B-cell Lymphoma

Marc Antoni Armengol i Cubillos

Departament de Bioquímica i Biologia Molecular

Facultat de Medicina

Universitat Autònoma de Barcelona

2023

This work has been carried out at the Institut d'Investigació contra la Leucèmia Josep Carreras (IJC), in Barcelona in the Lymphoma Translational Group, in order to obtain the Degree of Doctor in Biochemistry, Molecular Biology and Biomedicine

Dr. Gaël Roué

Director

Dr. Victor J. Yuste Mateos

Tutor

Doctoral Thesis

Development of novel therapeutic strategies against NF-κB Pathway in Diffuse Large B-cell Lymphoma

Marc Antoni Armengol i Cubillos

Departament de Bioquímica i Biologia Molecular

Facultat de Medicina

Universitat Autònoma de Barcelona

2023

This work has been carried out at the Institut d'Investigació contra la Leucèmia Josep Carreras (IJC), in Barcelona in the Lymphoma Translational Group, in order to obtain the Degree of Doctor in Biochemistry, Molecular Biology and Biomedicine

Als meus pares i germanes.

Rosa Maria, Antoni, Ingrid i Thaïs

“There's real poetry in the real world. Science is the poetry of reality”.

Richard Dawkins

PREFACE

The Experimental study presented in this doctoral thesis was performed at the Institut d'Investigació contra la Leucèmia Josep Carreras (IJC), in Barcelona in the Lymphoma Translational Group under the supervision of Dr. Gaël Roué (Group Leader at IJC). Part of this work has been co-financed by the European Regional Development Fund (ERDF) through the Interreg V-A Spain-France-Andorra (POCTEFA) program, project PROTEOblood (EFA360/19).

ABSTRACT

Although a high proportion of diffuse large B cell lymphomas (DLBCL) can be cured with combination of rituximab, cyclophosphamide, adriamycin, vincristine and prednisone, almost a third of the patients, corresponding mainly to the activated B-cell (ABC) subtype of the disease, does not achieve complete remission or relapse. It is believed that these tumors rely almost exclusively on constitutive nuclear transcription factor κB (NF-κB) signaling for their survival, a phenomenon that has been linked to a variety of genetic alterations that aberrantly activate the B cell receptor (BCR) and the Toll-like receptor (TLR) signaling pathways.

In this PhD dissertation we have evaluated the safety and efficacy of different approaches aimed at targeting the pathological overactivation of NF-κB in diffuse large B-cell lymphoma, with a special focus on the activated B-cell, hard-to-treat subtype of the disease. These approaches consist on one hand on the blockade of TLR signalling by direct inhibition of IRAK1/4 in association with BET bromodomain inhibition-mediated impairment of epigenetic reader's activity and on the other on the inhibition of ubiquitin-proteasome system signalling by means of a novel covalent inhibitor of HOIP, the LUBAC catalytic subunit.

For this purpose, we have developed innovative preclinical models of DLBCL such as Organotypic multicellular spheres and a chick embryo chorioallantoic membrane (CAM) model of ABC-DLBCL. With this cutting-edge technology, we have demonstrated that BET inhibitors offer synergistic antitumoral and pro-apoptotic activities with IRAK antagonist in vitro and in vivo. This effect is directly related to the downregulation of a set of NF-κB-regulated genes, with a predominant impact on CD44 and MCL-1 expression, with the consequent blockade of cell motility and triggering of tumor cell death. Additionally we have developed a pyrido[2,3-d]pyrimidine derivative, CpdA, that can efficiently and specifically bind to HOIP, resulting in the perturbation of LUBAC complex dynamic and in impaired downstream NF-κB signaling, exerting selective antitumor activity both in In vitro and In vivo models of DLBCL which is currently being evaluated for patentability.

These results highlight the importance of NF-kB pathways in DLBCL and the potential as therapeutic target that it presents, confirming that HOIP represents a promising therapeutic target for ABC-DLBCL, specially with activating MYD88 mutation, as new combinatorial treatment tackling both $MYD88^{p.L265P}$, as for example dual IRAK1 and IRAK4 inhibition, and

LUBAC could be developed in the search of synergistic effects which result in the control of the aberrant overactivation of the NF-kB pathway in these specific patients.

TABLE OF CONTENT

LIST OF FIGURES

LIST OF TABLES

LIST OF ABBREVIATIONS

ABC-DLBCL - Activated B-cell diffuse large B-cell lymphoma

A-DLBCL – Anaplastic diffuse large B-cell lymphoma

Ag – Antigen

ALL – Acute lymphoblastic leukaemia

BCR – B-cell receptor

BL – Burkitt Lymphoma

B-NHL – B-cell non-Hodgkin lymphoma

CAM - Chorioallantoic membrane

CB – Centroblast

CC – Centrocyte

CDK - Cyclin-dependent kinase

CDX - Cell line-derived xenograft

CLL - Chronic lymphocytic leukaemia

CLP – Common lymphoid progenitor

Cpd A – Compound A

DLBCL – Diffuse large B-cell lymphoma

DUBs - Deubiquitinating enzymes

EBV – Epstein-Barr virus

GC – Germinal center

GCB – Germinal center B-cell

GCB-DLBCL – Germinal center B-cell diffuse large B-cell lymphoma

GEP – Gene expression profiling

GSEA – Gene set enrichment analysis

HDACi - Histone deacetylase inhibitors

HGBL – High-grade B-cell lymphoma

HOIL-1 L - Heme-oxidized IRP2 ubiquitin ligase-1 L

HOIP - HOIL-1 L-interacting protein

HR – host response

HSC – Hematopoietic stem cell

Ig – Immunoglobulins

IHC – Immunohistochemistry

IKK - IκB kinase

IRAK1 - Interleukin-1 receptor-associated kinase 1

IRAK4 - Interleukin-1 receptor-associated kinase 4

IRAKi - Interleukin-1 receptor-associated kinase Inhibitor

ITAMs - Immunoreceptor tyrosine-based activation motifs

LUBAC - Linear ubiquitin chain assembly complex

MDM2 - Murine double minute 2

MYD88 - Myeloid differentiation primary response 88

MZ – Marginal zone

NF-Kb - Nuclear factor kappa-light-chain-enhancer of activated B cells

NHL – Non-Hodgkin Lymphoma

NOS – Not otherwise specified

NZF1 - NPl4-type zinc finger 1

OxPhos – Oxidative phosphorylation

PDO - Patient-derived organoids

PDX – Patient-derived xenografts

qPCR - Quantitative real-time PCR

SHARPIN - Shank-associated RH domain interactor

Srbc – Sheep red blood cells

Thf – T helper follicular

TLR - Toll-like receptor

TME – Tumor microenvironment

WHO – World Health Organization

INTRODUCTION

INTRODUCTION

1. B-CELL DEVELOPMENT

The immune system is responsible for protecting our organisms against pathogens. For this purpose, two immunological responses, with significant crosstalk between them, are known. The innate immune response, our first defensive line which depends on macrophages, dendritic cells, neutrophils, eosinophils, basophils, and natural killer cells to create an inflammatory environment. (1) On the other hand, the adaptive immune response, presents specificity against pathogens, triggered by B lymphocytes and T lymphocytes. These cells will produce effector and memory lymphocytes creating a faster and stronger response when exposed to the same pathogen for a second time. (2)

1.1. Lineage differentiation

A functional immune system requires a tight regulation of dynamic transcription-factor networks to activate and guide lineage-specific gene expression, limiting the differentiation options of hematopoietic stem cells (HSCs) (Figure 1).(3) This differentiation starts in the primary lymphoid organs (i.e. the foetal liver and bone marrow (BM)) and, during their lineage differentiation, B lymphocytes will migrate to the secondary lymphoid organs (spleen and lymph nodes (LN)) to complete their specialization. The BM, a soft, spongy tissue rich in blood vessels found in the centre of most bones, is differentiated into two types: yellow BM, made mostly of fat and contains stem cells that can become chondrocytes, adipocytes, or osteocytes and red BM, containing HSCs and where common lymphocyte progenitor development occurs leading to the expression of surface immunoglobulins (Ig) converting HSCs into pro- or pre-B cells.(4)

During this stage, DNA antigen receptor gene rearrangement in the variable regions of heavy chain (V(D)J recombination) takes place thanks to a combination of signalling pathways and activation of different transcription factors like IRF8, IRF4, IKZF3, IKZF1 among others. (5) Once this process is completed, these immature naïve B cells migrate across the circulatory system to the spleen to become transitional B cells (Figure 1).

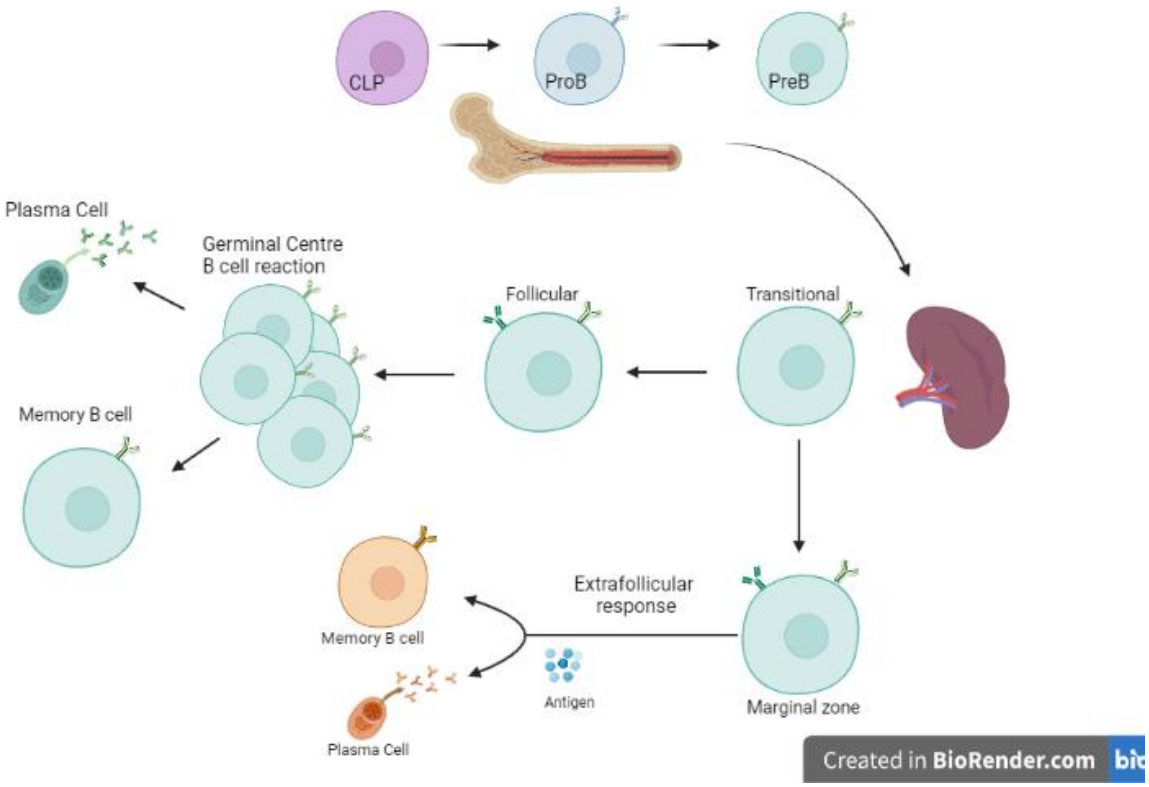

Figure 1. – B cell development and differentiation. Differentiation from common lymphoid progenitor (CLP) to memory B cell and plasma cell.

The spleen is the largest lymphatic organ in the body. It is surrounded by the marginal zone (MZ), a capsule formed of connective tissue, that extends inwards dividing the organ into lobules consisting of two additional types of tissue: the red pulp, where blood is filtered and macrophages reside, and the white pulp, where the T and B lymphocytes compartments are found. (6) B cells with affinity towards a specific antigen (Ag) are selected within a structure found in the white pulp known as germinal centre (GC) where these cells continue their development generating high affinity B cell receptors (BCRs). The BCR is composed of pairs of heavy (IgH) and light (IgL) chains that form surface antibodies which are coupled to a heterodimer formed by CD79A (Igα) and CD79B (Igβ).[62] Human lymphomas retain expression of BCR although the IgH locus is frequently altered by chromosomal translocations.[63] IgH and IgL are composed of constant regions that are fused to antigen

recognition variable regions, which are constructed from VH, DH and JH gene segments for IgH, and VL and JL gene segments for IgL. In the case of IgH, naïve B cells express IgM and IgD constant regions, but can change to either IgG, IgA or IgE constant regions following class switch recombination (CSR) in the GC. Finally, these cells complete their lineage differentiation forming plasma cells, a type of immune cell that produces large amounts of a specific antibody, or memory B cells, whose function is to memorize the characteristics of the antigen that activated their parent B cell during initial infection triggering an accelerated and robust secondary immune response when they encounter this antigen.(7,8)

1.2. Germinal Center Dynamics

As mentioned previously, GCs are developed in secondary lymphoid tissues, within B cell follicles. They are organized in two major zones (Figure 2): the dark zone, which contains large centroblasts, densely pack B cells, that are constantly proliferating and undergoing somatic mutation of their antibody variable region genes, and the light zone, where B cells, referred to as centrocytes, are selected in an Ag and T cell-dependent manner. This centrocytes will either re-entry the dark zone to undertake further rounds of somatic hypermutation or will give rise to high-affinity memory B cells and plasma cells, as GC B cells can migrate between both dark and light zone (Figure 2). (9,10)

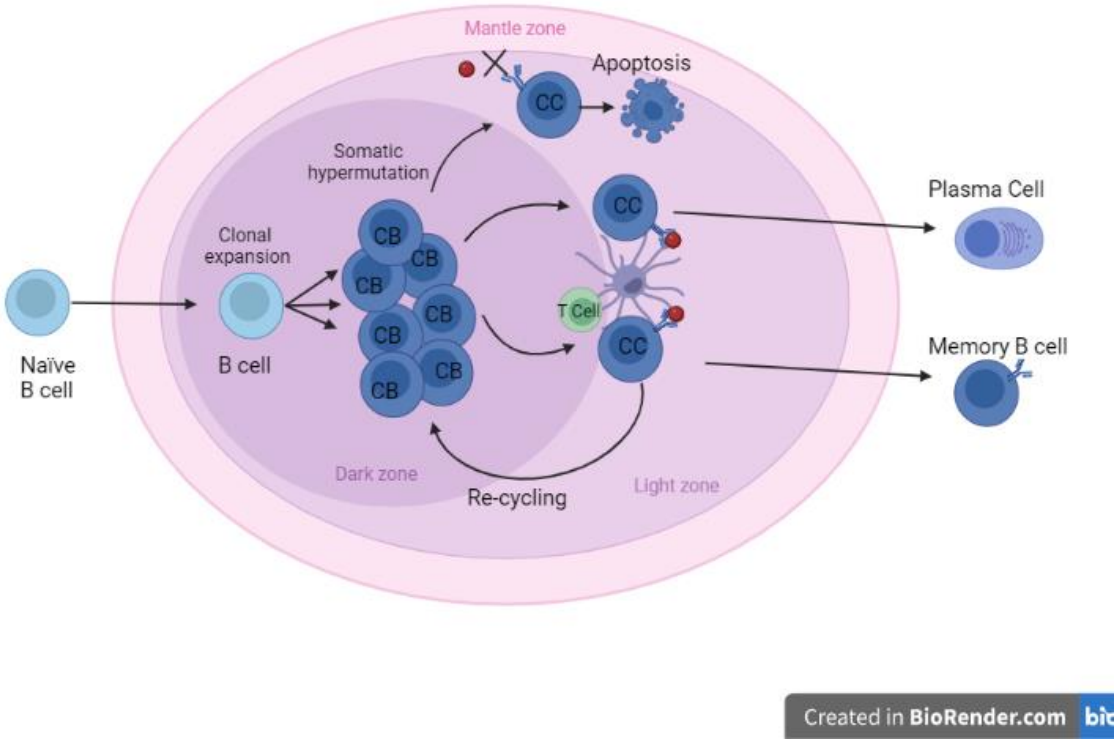

Figure 2. – GC dynamics between centroblasts and centrocytes. Centroblasts (CB) become centrocytes (CC). This centrocytes may differentiate into plasma cells or memory B cells or re-cycle toward a round of somatic hypermutation.

Plasma cells are terminally differentiated non-proliferative B cells that produce and secrete high affinity antibodies. These, will neutralize pathogens rapidly, and if there is an antigen-recall response, memory cells may re-enter the GC and undergo expansion and differentiate into plasma cells.(11)

In parallel, depending on microenvironment factors and BCR signalling, transitional B cells in the spleen complete their maturation into follicular B cells or marginal zone (MZ) B cells.(8) MZ B cells migrate into the MZ of the spleen and will be the first to be exposed to blood circulating Ag, triggering mainly a T-independent response. Once activated by an Ag, they will migrate into the red pulp and differentiate into plasma cells without need of T cells or GC formation.(12) However this MZ B cells are also known to interact with T cells and directly differentiating into plasma cells. (13)

As for follicular B cells, these will interact with T helper follicular (Thf) cells, resulting in full activation followed by clonal expansion of B cells, which will rapidly migrate into the centre of the follicle and proliferate forming an early GC. (14)

In the case of microenvironment forming cells, follicular dendritic cells (FDC), a specialized type of stroma, have a pivotal role in GC formation. These, will capture antigens after immunization and present it to B cells, triggering the entire response. (15)

2. Diffuse Large B cell lymphoma, activated B-cell subtype (ABC-DLBCL)

According to the Lugano staging system, DLBCL may be categorized in four stages with an additional four intermediate stages (Table 1), which correlate with an increasingly poorer prognosis. Apart from the stage, other parameters like age, extranodal involvement, biomarkers such as lactate dehydrogenase levels in blood or genetic alterations in *NFKBIA* and *NCOR1*, are used as prognosis predictors. (16)

The most frequent genetic alterations in DLCBL are translocations of *BCL6, BCL2, MYC*, and amplifications of proto-oncogene *c-Rel* (REL). These mutations are found in approximately 30 – 40% of all DLBCL cases. (17)

STAGE	
I	Involvement of one node or group of adjacent nodes • stage IE: single extra-lymphatic site in the absence of nodal involvement
II	Involvement of two or more nodal groups, same side of diaphragm • stage IIE: contiguous extra-lymphatic extension from a nodal site with or without involvement of other lymph node regions on the same side of the diaphragm.
III	Involvement of lymph nodes on both sides of the diaphragm; nodes above the diaphragm with spleen involvement • stage III(1): involvement of the spleen or splenic, hilar, celiac, or portal nodes • stage III(2): involvement of the para-aortic, iliac, inguinal, or mesenteric nodes
IV	Diffuse or disseminated involvement of one or more extralymphatic organs, or either: • Isolated extralymphatic organ involvement without adjacent regional lymph node involvement, but with disease in distant sites • involvement of the liver, bone marrow, pleura or cerebrospinal fluid

Table 1. – Lugano staging classification. Table adapted from (18)

2.1. Classification of high-grade B-cell lymphoma

High-grade B-cell lymphoma (HGBL) is used as a general term for B-cell lymphomas that are morphologically aggressive with multiple mitotic figures and a high proliferation rate. This morphology is linked with a very aggressive clinical behaviour. The concept was introduced in 2008 by the World Health Organization (WHO), grouping the different subtypes in 2 groups:

- HGBL with *MYC* and *BCL2* and/or *BCL6* translocations, characterized by translocations in the *MYC* and *BCL2* and/or *BCL6* genes. This category includes all NHL previously known as double/triple hit lymphoma. An estimate of 20-35% cases of DLBCL over-express *MYC* and *BCL2* proteins (called "double expressor lymphoma"), without oncogenic translocations of *MYC* and *BCL2* and/or *BCL6*. These double-expressor DLBCL are less aggressive, and in consequence treated differently and excluded from the HGBL family. (19)
- HGBL, not otherwise specified (NOS). This subtype includes aggressive B-cell lymphomas with mixed features of both DLBCL and Burkitt lymphoma (BL), blastoid-appearing large B-cell lymphomas, and cases lacking MYC and BCL2 or BCL6 translocations.(20)

The major types of HGBL are depicted on Table 2.

HIGH-GRADE B-CELL LYMPHOMA TYPES	
Diffuse large B cell lymphoma	Each year about 5,500 people are diagnosed with diffuse large B cell lymphoma (DLBCL). This makes up about 40 out of 100 cases (40%) of NHL in adults.
Burkitt Lymphoma	Burkitt lymphoma is the most common type of NHL in children. Adults can also be diagnosed, but it is more unusual. It can affect people with low immunity, such as people who have had an organ transplant or who have AIDS.
Lymphoblastic lymphoma	Very similar to acute lymphoblastic leukaemia (ALL). In lymphoblastic lymphoma, the abnormal lymphocytes are generally in the chest lymph nodes or thymus gland.
Treatment-related B cell lymphomas	They develop after an organ transplant or bone marrow transplant due to the immune-suppressors. It requires different treatment to other lymphomas.

Table 2. – Main subtypes of high-grade B-cell lymphomas

2.2. Physiopathology and molecular subtypes of DLBCL

Diffuse large B-cell lymphoma (DLBCL) is the most common type of non-Hodgkin lymphoma (NHL) among adults, with an annual incidence of 50 to 60 new cases per million people per year worldwide. This incidence, focused on Europe, results in 8,500 news cases and 4,000 deaths each year. The incidence of this type of tumour increases with age, ranging from <1/100,000 in children to 10–15/100,000 in people older than 65 years, having a median age of diagnosis of approximately 70 years.[17] It is characterized by the presence of large neoplastic B cells with a diffuse pattern of growth. This aggressive lymphoma can arise in virtually any part of the body, and the first sign of illness is the observation of a rapidly growing mass, associated in some cases with light symptoms such as fever, weight loss, and night sweats. Usually DLBCL arises *de novo*, but it can also represent a malignant transformation of other types of lymphoma, like follicular lymphoma (FL) or even leukaemia, like chronic lymphocytic leukaemia (CLL). Immunodeficiencies and infection with Epstein-Barr virus (EBV) are considered potential risk factors that may contribute to the development of subtypes of DLBCL. [18,19]

Although several DLBCL molecular classifications have been established, the two most commonly used are cell of origin (COO) and consensus cluster classification (CCC). COO classification (Figure 3) allows the division of DLBCL cases into different subtypes based on morphology and clinicopathology characteristics. Immunoblasts and centroblasts are large noncleaved cells with round or oval nuclei and a good prognosis, while plasmablastic lymphoma is a morphological form that varies immunophenotypically from other lymphomas. For instance, instead of the usual B-cell markers (CD20, CD79a) found in standard DLBCL, they express plasma cell markers (CD38, CD138). The anaplastic diffuse large B cell lymphoma (A-DLBCL) is an uncommon distinct morphologic variant of DLBCL characterized by large polygonal cells with bizarre pleomorphic nuclei.(21) The not otherwise specified (NOS) cases do not fit within any of the previous four subtypes. Gene expression profiling (GEP) and immunohistochemistry (IHC) is commonly used to classify DLBCL into germinal centre B cell (GCB) like, non-GCB, and double hit lymphoma.

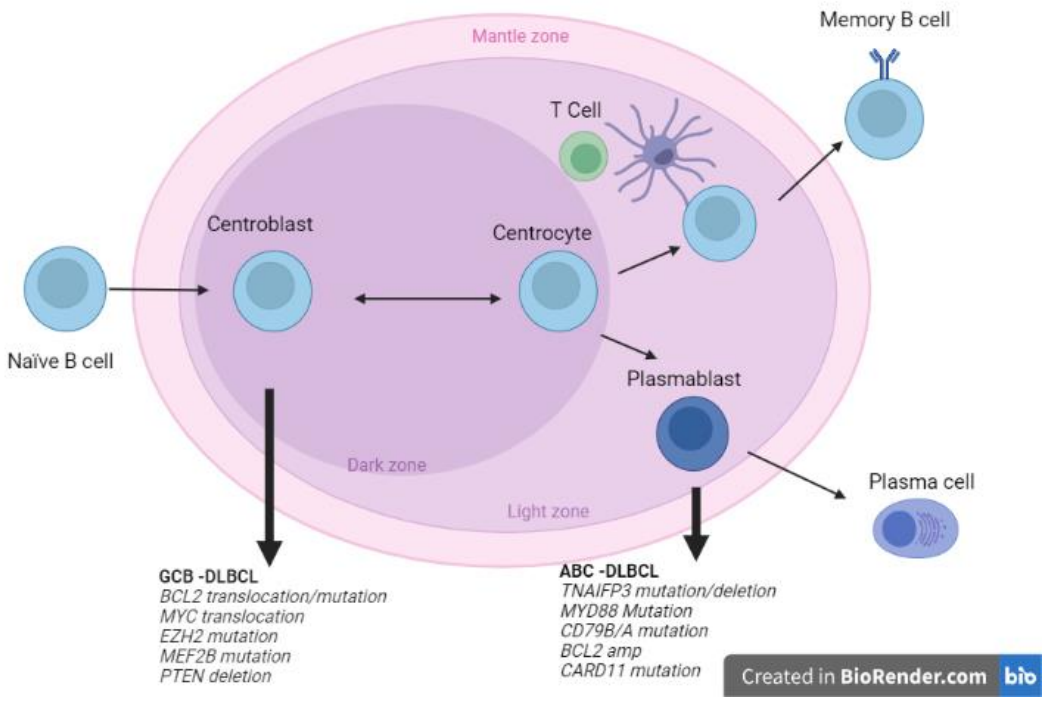

Figure 3. – Genomic alterations and cell of origin in DLBCL subtypes. Resume of the most common alterations (mutations, translocations, or deletions) associated with GCB or ABC-DLBCL subtypes.

Among GCB like and ABC-like subtypes (Table 3), the ABC group harbours a substantially worse prognosis than the GCB group. The molecular subclassification of these cases gives important information both prognostically and therapeutically. (22)

	GCB-DLBCL	ABC-DLBCL
Clinical Result (5-year overall survival)	59%	39%
Immunophenotype	$CD10^{+}$, $BCL2^{+}$, $BCL6^{+}$, $IRF4/MUM1^{-}$	CD10- BCL2±, BCL6±, $IRF4/MUM1^{+}$
Mechanism of carcinogenesis	REL amplification	Constitutive activation of NF-κB
Chromosomal translocation	Gain 12q12 t (14;18)	Trisomy 3 (FOXP1) gain 3Q Gain 18q21-q22 (BCL2) Deletion 6q21-q22 (BLIMP1)
Treatment	R-CHOP	R-CHOP shows poor results. Lenalidomide, bortezomib and ibrutinib should be added to treatment plan

Table 3 – Characteristics of germinal center B-cell and activated B-cell-diffuse large B-cell lymphoma.

ABC-DLBCL is associated with higher aggressiveness, lower survival rates and substantially worse outcomes when treated with standard chemoimmunotherapy consisting of cyclophosphamide, doxorubicin, vincristine, and prednisone (CHOP). These, have maintained stable even in the modern medicine era with the addition to CHOP of powerful chemotherapeutic agents such as the anti-CD20 monoclonal antibody rituximab (R-CHOP).(23) It represents approximately a third part of all lymphomas diagnosed and is characterized by chronic activation on BCR and Toll-like Receptor (TCR) signalling, which stimulates the nuclear factor kappa-light-chain-enhancer of activated B cells (NF-κB) activity via Bruton's tyrosine kinase (BTK) dependent signalling. A vast majority of this cases do not achieve complete remission or suffer relapse shortly after.(24)

On the other hand, the CCC classification, based on whole genome arrays and metabolic fingerprints, is used to classify molecular subtypes of DLBCL. One analysis, done by Chapuy et al, classifies DLBCL into in five clusters, termed C1–C5, each with a discrete genetic signature, as well as a cluster without any detectable alterations. (25)This classification is originated by the analysis of 304 DLBCL biopsies to identify candidate cancer driver genes. The study combines algorithms that classify mutations occurring more often than expected by chance (MutSigCV), mathematical models that identify clustering of missense mutations in 3-dimensional protein structures (CLUMPS), and a model to identify significant copy number variants and structural aberrations. (26) In contrast, another genomic DLBCL analysis classified 574 tumors into genetic subtypes using the GenClass algorithm that starts with an initial set of genetic aberrations and then examines all possibly re-assortments of cases into classes to classify for genetic heterogeneity. This approach distinguished four genetic subtypes, named MCD, BN2, N1, and EZB. This nomenclature relates with the initial alterations that generate each genetic subgroups: *MYD8*^{8L265P} and *CD79B* mutations in MCD, *BCL6* translocations and *NOTCH2* mutations in BN2, *NOTCH1* mutations in N1, and *EZH2* mutations and *BCL2* translocations in EZB.(27) Although resulting in different classification, both analyses revealed that the different molecular groups had significantly different clinical outcomes, highlighting that these novel molecular taxonomies are biologically and clinically meaningful.(26)

Lymphomagenesis covers from deregulation of transcriptional and epigenetic regulators in normal B cells to chromosomal alterations. These chromosomal alterations are due to the high degree of genomic instability present in these cells. Figure 3 depicts some of the major dysregulated pathways and oncogenic alterations.(28) Histone modification genes (*MLL2* and *CREBBP*) are recurrent mutations sites as *BCL6* deregulations, present in 35% of the cases.(29)

If we focus on COO classification, there are also specific mutations and deletions associated with specific groups of this DLBCL classification. For instance, the aberrant activation of BCR present in ABC-DLBCL is linked to *CD79B/A* and *CARD11* mutations, together with TLR pathway alterations like myeloid differentiation primary response 88 (MYD88) mutations.(28,29) In the case of GCB-DLBCL, *MYC* translocations, heterozygous somatic mutations of *EZH2* and somatic *BCL2* mutations are observed in 15%, 22% and 34% of patients respectively.

It is believed that this chronic activation of BCR and TCR confers extra survival to this type of tumours, vitally via NF-KB pathway, along which many mutations that overactivate both receptors signalling pathways have been described.(30) Point mutations in the BCR subunit CD79B, which are present in 21% of ABC-DLBCL, facilitate this chronic BCR signalling activation. (31) In cases that do not present these point mutations, an alternative pathway for constitutive NF-κB activation occurs through MYD88, a signal adaptor for the TLR (see section 2.3.2). A single oncogenic point mutation, known as $MYD88^{L265P}$, occurs in 30% of ABC-DLBCL, but is rarely observed in GCB-DLBCL.(32). This modification generates a chronic activation of both interleukin-1 receptor-associated kinase 1 (IRAK1) and interleukin-1 receptor-associated kinase 4 (IRAK4) which finally lead to an overactivation of NF-KB pathway and expression of related genes. (33)

2.3. ALTERED PATHWAYS IN ABC-DLBCL

Thanks to the implementation of powerful genomic technologies, remarkable progress has been made in the understanding of the pathogenesis of this disease. These studies have deepened our knowledge on genomic alterations that contribute to the initiation and maintenance of the tumour clone by disrupting biological functions known to be critical for the normal biology of its cells of origin. Some of these alterations are simplified in Figure 4. All the new data generated these past decades offers unique opportunities for the development of improved diagnostic and prognostic tools. Furthermore, some of these newly identified alterations are potential targets that are currently being explored for the development of novel therapeutic strategies.

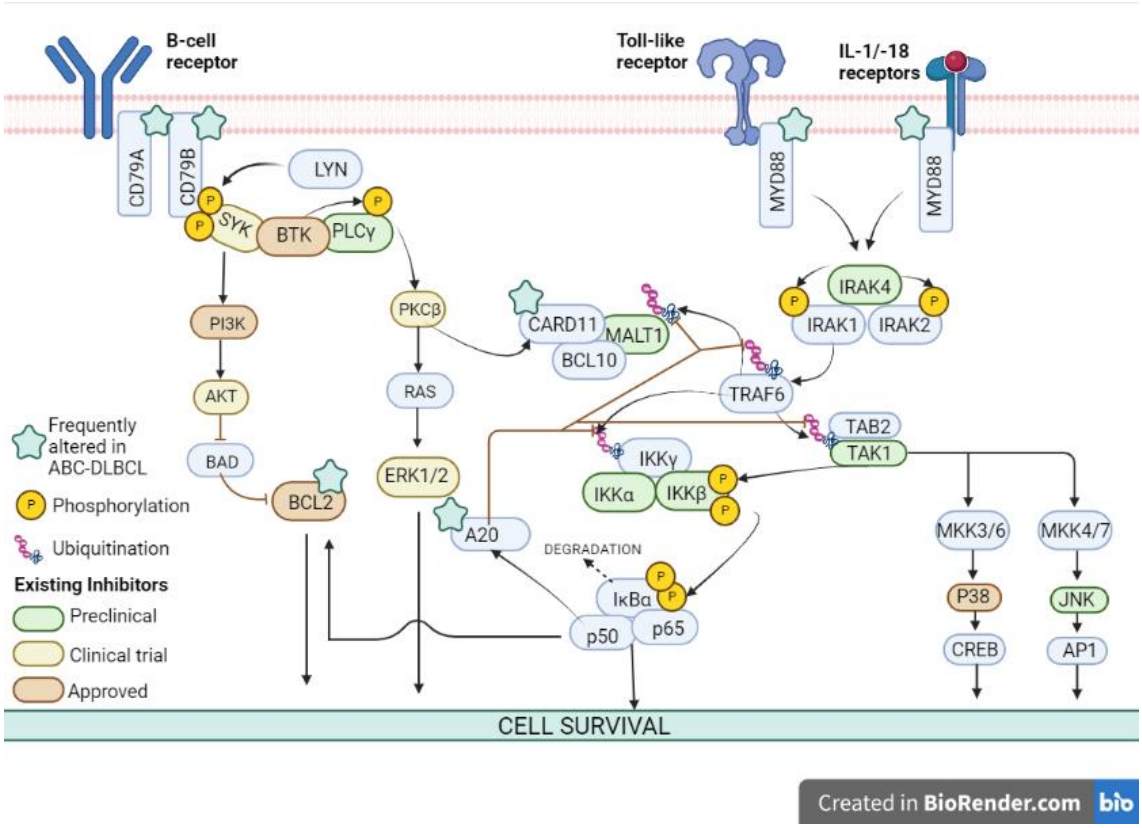

Figure 4. – Frequent altered pathways in ABC-DLBCL. Simplified altered pathways and targets with existing inhibitors in different stages of development.

2.3.1. NF-kB signaling canonical and non-canonical pathways; therapeutic targeting

AS highlighted previously, a hallmark of ABC-DLBCL is the constitutive activation of NF-kB pathway. Gene expression profiling in patient samples highlighted a preferential expression of NF-kB regulated genes in ABC-DLBCL when compared with the other major subtype GCB. This has also been shown in cell lines. The ABC subtype engages classical NF-kB pathway as they have a very fast turnover and phosphorylation of IkBα and an important degree of nuclear accumulation of the heterodimer p50/p65 in comparison with p50-c-rel heterodimer.(34) The suppression of this signaling pathway with IkB repressors or IKKβ inhibitors induces apoptosis in ABC-DLBCL but not in GCB-DLBCL cells.(34,35)

As a result of this constitutive activation of NF-kB, malignant cells are propelled to the plasma cell stage of differentiation mediated by the NF-kB target gene, interferon regulatory factor 4

(IRF4). In healthy lymphocytes IRF4 drives terminal differentiation transactivating *PRDM1*, which encodes Blimp-1. However, in ABC-DLBCL genetic lesions that inactivate Blimp-1 are frequently observed.(36) Altogether, this suggests a model by which NF-kB activation in ABC-DLBCL initiates plasmacytic differentiation via IRF4 transactivation but due to lesions inactivating Blimp-1 the cell fails to fully differentiate. This explains how tumor cells evade cell cycle arrest that typifies normal plasma cells.(37)

Production of cytokines in ABC-DLBCL is also a consequence of NF-kB constitutive activation. For instance, both interleukin 6 (IL-6) and interleukin 10 (IL-10) are secreted by ABC-DLBCL cells and signal for the activation of transcription factor signal transducer and activator of transcription 3 (STAT3), a dimerizing transcription factor and oncogene involved in cytokine growth signaling and cell survival pathways.(38) This STAT3 activation is demonstrated by high STAT3 protein level, phosphorylated STAT3 present in the nucleus and the existence of a signature of STAT3 target genes that typifies ABC-DLBCL.(39) As STAT3 physically interacts with NF-kB factors, ABC-DLBCLs with higher activation of STAT3 also present higher expression of NF-kB target genes, presenting an increased ability to transactivate their targets.(40) Due to this existing interaction, JAK kinase inhibitor, which results in a blockade of STAT3 phosphorylation, acts synergistically with IKKβ inhibitors in eliminating ABC-DLBCL tumoral cells. (39)

Certain mutations may also lead to a constitutive activation of the alternative NF-kB pathway. For instance, deletions/mutation of TRAF3, a negative regulator of the alternative NF-kB pathway is present in 15% of patients, and often coexist with *BCL6* translocations, all together preventing terminal B cell differentiation. (41)

2.3.2. TLR pathway: MYD88 and others

Aberrant Toll-like receptor (TLR) signaling is emerging as a potent driver of lymphomagenesis especially in the ABC-DLBCL subtype. To date, 10 distinct TLR's, members of the pattern-recognition receptors class, have been identified in humans.(42) All of them, except TLR3, require the MYD88 adaptor protein to relay downstream signaling. (42) Upon activation, MYD88 is recruited to the Toll/IL-1 receptor (TIR) domain of the activated TLR. (43) MYD88 then recruits members of the IRAK family to form the Myddosome complex. The assembly of this signaling supercomplex is hierarchical, which means that MYD88 first recruits IRAK4 and

this complex then recruits IRAK2 or the related IRAK1, both substrates of IRAK4 activity.(44) The formation of this complex is vital to bring the kinase domains close enough for phosphorylation-mediated activation to take place. (45) IRAK4 mediated phosphorylation of IRAK1/2 promotes TRAF6 recruitment causing the ubiquitination and activation of TAK1 finally leading to the activation of the NF-kB pathway. (46) The biological importance of this signaling pathway has been shown by RNA interference experiments which concluded that ABC-DLBCL cells require both IRAK1 and IRAK4 for their long-term survival.(32) However, additional genetic experiments with mutant kinases demonstrated that only IRAK4, but not IRAK1 kinase activity, was required for ABC-DLBCL survival, suggesting that IRAK1 is more of adaptor or scaffold for this complex rather than a real effector.(47)

Excessive TLR signaling driven by somatic gain of function MYD88 mutations has been described in numerous hematological malignancies including CLL(48), DLBCL (32), and Waldenström's macroglobulinemia (WM) (49). Specially interesting is the case of ABC-DLBCL where 29% of patients carry the p.L265P mutation at a highly conserved residue in the β-sheet of the hydrophobic core of the MYD88 TIR domain. In addition, these tumors have been shown to display MYD88$^{p.L265P}$-dependent NFκB activation and JAK-STAT3-, as well as type I interferon signaling leading to an oncogene addiction to MYD88$^{p.L265P}$ within this subtype of DLBCL.(32) Altogether, it is expectable that MYD88-dependent oncogenic NFκB signaling is an important contributor to lymphomagenesis, in a well differentiated subset of ABC-DLBCL. The observation that MYD88-mutant ABC-DLBCL is oncogene-addicted, supports that MYD88 signaling as a very promising drug target.

The potential of MYD88$^{p.L265P}$ mutation to trigger a malignant grow as been firmly confirmed through *In vivo* studies in mice. For these, a Cre-mediated recombination was performed to generate a conditional expression of Myd88$^{p.L252P}$ (in the orthologous position of the human MYD88$^{p.L265P}$ mutation) in B-cells. The model developed a lympho-proliferative disease and occasional transformation into clonal ABC-DLBCL with immunophenotypical and morphological features characteristic of human ABC-DLBCL.(50) In line with the frequent *BCL2* amplification that is observed in human ABC-DLBCL, lymphomagenesis could be accelerated in this animal model by adding to the Cre;Myd88$^{p.L252P}$ a conditional overexpression of BCL2, showing the existing interaction between BCL2 and oncogenic Myd88$^{p.L252P}$.(50)

2.3.3. BCR pathway: effect of BTK antagonists +/- epigenetic drugs

The BCR signalling starts with the phosphorylation of tandem tyrosines within immunoreceptor tyrosine-based activation motifs (ITAMs) found on the CD79A (Igα) and CD79B (Igβ) heterodimer. ITAMs then recruit and activate SYK kinase causing its autophosphorylation to generate the docking site for its effectors like BLNK and BTK. (51) SYK and SRC kinases can then activate BTK, which is recruited to the plasma membrane by the production of phosphatidylinositol (3,4,5)-trisphosphate (PIP3) by phosphoinositide 3-kinase (PI3-K).(52) PI3-K is activated through BCR-dependent phosphorylation of CD19 by Src-family kinases. Once BTK is recruited and activated in the BCR signalosome, it triggers a signalling cascade ending in the production of inositol trisphosphate (IP3) and diacylglycerol (DAG). IP3 binds to the IP3 receptor on the endoplasmic reticulum, initiating an extracellular calcium flux and activation of many calcium-dependent signalling and transcriptional programs. The combination of increased intracellular calcium and DAG production activates protein kinase C beta (PKCβ). The increase of intracellular calcium together with other factors results in the activation of the classical NF-κB pathway mediated by the formation of the CBM complex triggered by the phosphorylation of CARD11. BCR stimulation also initiates signaling through the ERK, MAPK and NF-AT pathways, which coordinate with NF-κB to promote B cell survival, proliferation, and differentiation.(53) ABC-DLBCL cases predominantly express an IgM-BCR, while GCB-DLBCL cases have typically switched to an IgG-BCR. This is due, in part, to mutations in the switch μ, region of the IgH gene in ABC DLBCL that interfere with its function to promote class switching from IgM to other isotypes. [62] This suggests the existence of a selective pressure for ABC-DLBCL to avoid CSR and maintain IgM-BCR expression which preferentially leads to mitogenic and survival signaling, among which we find NFκB, while IgG-BCR signaling favors plasma cell differentiation. [64]

Going deeper into our knowledge of the role of BCR signalling in ABC-DLBCL has led to the discovery of new targets and the development of precise therapeutic inhibitors against kinases involved in the pathway like BTK, SYK and PI3-K. as well as other downstream targets like mucosa-associated lymphoid tissue lymphoma translocation 1 (MALT1).(54) One of the most promising targets is BTK as it interconnects BCR signalling, TLR signalling, and chemokine receptor signalling. After the first failed BTK inhibitor LFM-A13 was discovered in 1999 (55), PCI-32765, now known as ibrutinib, designed by Celera Genomics/Pharmacyclics, was chosen

for preclinical development giving rise to the first-in-class inhibitor of BTK. The efficacy of ibrutinib in B-cell lymphoma was first reported in 2010 (56) but due to off-target side effects and emerging of resistance, the development of second generation of BTK inhibitors was initiated. The first was Acalabrutinib from Acerta Pharm/Astrazeneca (57) followed by Zanubrutinib by BeiGene (58).

There are similarities and differences among these three approved BTK inhibitors, as for instance all inhibitors are irreversibly covalently bound to cysteine 481 in the ATP binding pocket of BTK; ibrutinib is the most potent BTK inhibitor followed by zanubrutinib and acalabrutinib based on biochemical binding kinetics, but differences in biochemical potency were partly lost in cellular assays using human peripheral blood mononuclear cells or human white blood cells (all less than 10 nM); acalabrutinib had the lowest off-target rate and the highest selectivity followed by zanubrutinib and ibrutinib (59).

In the first phase II trial of ibrutinib monotherapy in relapsed/refractory DLBCL, objective responses were observed in 39% of patients with ABC DLBCL, translating into significantly longer overall survival (OS) in patients with ABC-DLBCL. Nonetheless, median progression-free survival (PFS) in ABC-DLBCL cases was very short (2 months), indicating that BTK monotherapy failed to eradicate the malignant cells in most patients.

Genetic analysis of biopsy samples from patients on the ibrutinib monotherapy trial revealed that patients with ABC-DLBCL whose tumours harboured both a CD79B mutation and a $MYD88^{L265P}$ mutation had an 80% response rate, whereas the response rate in the remaining ABC cases was only 30%.(60) This observation revealed a functional cooperation between the BCR and MYD88 pathways (60), leading to the discovery of a supramolecular complex termed the “My-T-BCR,” consisting of BCR, TLR9, and $MYD88^{L265P}$ along with many other proteins involved in NF-κB activation, including CARD11, BCL10, MALT1, and IκB. ABC DLBCLs that form an My-T-BCR complex are “addicted” to BCR signalling, explaining their exceptional response to ibrutinib monotherapy.

Seeing this short PFS, there has been a great interest in identifying other vulnerable mechanisms that can be therapeutically explored in combination with ibrutinib. In this sense, genetic silencing of mutant *MYD88* by treatment with histone deacetylase inhibitors (HDACi) enhanced ibrutinib efficacy in ABC DLBCL. Ibrutinib leads to decreased binding of mutant

MYD88 protein to BTK, resulting in reduced downstream NFκB signalling and increased apoptosis. The transcriptional downregulation of MYD88 by treatment with HDACi, together with ibrutinib therapy, reduces even more this aberrant constitutive binding showing a synergistic antitumoral effect by NFκB signalling blockade.(61) The blockade of MYD88-driven NF-κB activation indicating that dual inhibition of BTK and MYD88 is more effective as an antiproliferative strategy against ABC DLBCL and should be explored therapeutically.

2.4. Standard and current treatment regimens for ABC-DLBCL

Nowadays DLBCL is considered an aggressive but curable in most cases, with around 60% of patients presenting good response to treatment and prolonged survival. (62) However there is a remarkable heterogeneity in response rates within each subtype having great impact on prognosis.(29)

The standard frontline treatment for DLBCL remains chemo-immunotherapy with R-CHOP. (63) R-CHOP has achieved durable remission in around 60% of cases (62) however there is a specific group of patients that do not respond to R-CHOP or relapse shortly after remission, presenting very poor outcomes. This lack of response suggests that there is a differential response according to different DLBCL subtypes.

For instance, no efficient treatment is available against ABC-DLBCL as it can be seen in the high mortality and relapse index. However, an alternative option to finding new treatments is the search of complementary therapies to increase the tumour sensitivity towards existing treatments. Numerous randomized trials have attempted to improve R-CHOP by intensifying therapy or adding maintenance or novel agents to the existing backbone, especially for ABC-DLBCL, mainly focusing on adding different biologic agents targeting NFκB pathway and chronic BCR signalling to R-CHOP.(64) Some of the most important agents tested are proteasome inhibitors (bortezomib), BTK inhibitors (Ibrutinib), phosphatidylinositol-3 kinase (PI3K) inhibitors (idelalisib), Bromodomain inhibitors (JQ1 and CPI203), bispecific IRAK-1 and IRAK-4 inhibitors or CXCR4 inhibitors among others. Unfortunately, none of this has translated into improved patient outcome.(65–67)

These therapeutic strategies should not only focus on single agent approaches but should specifically be based on synergistic drug interactions. The major signalling nodes to be targeted are the NFκB pathway, as well as BCL2-driven apoptosis resistance. Based on the common ABC-DLBCL-associated genomic aberrations detailed above, several intervention strategies are conceivable (Table 4).

Target	Compound	Status
JNK	SP600125	Preclinical
MALT1	MI-2	Preclinical
P38	Losmapimod (GW856553X)	Phase 3 (ACS)
PI3Kδ	Idelalisib (CAL-101)	Approved (CLL, FL)
PIM1	AZD-1208 SGI-1776	Phase I (AML, terminated) Phase I (NHL, terminated)
PKCβ	Sotrastaurin (AEB071) Ensataurin (LY317615	Phase II (MCL, CLL, terminated) Phase III (NHL, failed
PLCϒ	U73122	Preclinical
STAT3	S3I-201	Preclinical
SYK	Entospletinib (GS-9973) Fostamatinib (R788)	Phase II (Multiple B-cell malignancies) Phase III (RA, ITP)
TAK1	5Z-7-Oxozeaenol	Preclinical
BCL2	Venetoclax (ABT-199)	Approved (CLL)
BTK	Ibrutinib (PCI-32765)	Approved (MCL, CLL)
ERK1/2	GDC-0994	Phase I (Solid tumours)
IKK	LY2409881, IMD-0354, TPCA-1	Preclinical
IRAK4	ND-2158, AS2444697, CA-4948	Preclinical
JAK1/2	Ruxolitinib (INCB018424)	Approved (myelofibrosis)

Table 4. – Targeted therapies currently under evaluation in ABC-DLBCL. Summary of recently identified targets and existing inhibitors in different stages of development.

2.5. Deregulation of Ub-regulating enzymes

Among the hallmarks of cancer, metabolic reprogramming includes enhanced biosynthesis of macromolecules, maintenance of redox homeostasis and altered energy metabolism. It is a highly regulated and complex process modulated by multiple signaling pathways, enzymes,

and transcription factor. It has been recently shown that ubiquitination and deubiquitination play a vital role in the regulation of metabolic reprogramming in cancer cells. Being one of the most important post-translational modifications, ubiquitination is a multistep enzymatic process with a role in various pathologies.(68) Ubiquitination is an ATP-dependent process that leads to the ligation of ubiquitin, a ubiquitously expressed protein consisting of 76 amino acids, to a substrate protein. The core enzymes in this Ubiquitin-activating enzymes (E1s), ubiquitin-conjugating enzymes (E2) and ubiquitin ligases (E3). Initially E1 binds to ubiquitin for activation, and then transfer activated ubiquitin to E2s and E3s finally transfer ubiquitin to substrates.(69) As E3 ultimately determine the target of ubiquitination and the specificity of substrate recognition, they are the mediators of proteasomal degradation or non-degradative signaling, being crucial in the normal functionality of UPS and control of intracellular components in healthy and malignant settings.

There are two known genes codifying for E1 activating enzymes, UBA1 and UBA6, around fifty E2 enzymes and over 600 E3 ligases within the human genome. This vast variety of ubiquitinating enzymes leads to different types of ubiquitination, resulting in disparate fates of substrate proteins. K48-linked polyubiquitination is the most widely studied type, which mainly labels proteins for 26S proteasome-mediated recognition and degradation.(70)

On the other hand, deubiquitination is catalyzed by deubiquitinating enzymes (DUBs) to remove ubiquitin from ubiquitinated proteins, thus reversing the ubiquitination process, in which the isopeptide bond between ubiquitin and its substrate can be cleaved by a specific DUB, resulting in monoubiquitins for its reuse in other ubiquitinating processes. More than 100 DUBs are known so far classified in five different families according to the presence of conserved catalytic domains: ubiquitin-specific proteases (UPS), ovarian tumor domain (OTU), Machado-Joseph domain (MJD) ubiquitin-C terminal hydrolases (UCH) and Jab1/MPN (JAMM) metalloproteases.(71) Dynamic conversion between ubiquitination and deubiquitination is closely related to various cellular functions and thus, its dysregulation results in multiple diseases, such as neurodegenerative diseases and cancer. Understanding of ubiquitination and deubiquitination may provide novel insights into the treatment of these diseases.(72)

Depending on the substrate specificity and on the affected signaling pathway, ubiquitin ligases and DUBs can act as either tumor promoters or tumor suppressors. Regulators of the cell cycle are among the main factors affected by aberrancies in the UPS pathway. As an

example, the cyclin-dependent kinase (CDK) inhibitor $p27^{KIP1}$ is highly expressed in quiescent cells; however, its expression dramatically decreases in tumor cells as it is sent for degradation in the proteasome.(73) Together with cyclin E/A/CDK2 complexes and the E3 S-phase kinase-associated protein 2 (SKP2), $p27^{KIP1}$ also constitutes a regulatory network engaged in a bidirectional crosstalk with the c-MYC proto-oncogene, whose stability, cell cycle regulation and senescence role are finely controlled by processes of phosphorylation and specially ubiquitylation.(74) The accumulation of c-MYC, together with the activation of the mechanistic target of rapamycin (mTOR)-dependent translation, is also regulated by F-box/WD repeat-containing protein 7 (FBW7), another E3 ubiquitin ligase which in healthy cells plays a crucial role as tumor suppressor and which loss of function, associated with mutations is frequently found in a variety of cancers. (75)

Besides cell cycle, expression of tumor suppressor p53 is also controlled by ubiquitination and deubiquitylation. The murine double minute 2 (MDM2 or HDM2 for humans), which binds to the transactivation domain of p53, impairing its transcriptional activity and mediating its transport from the nucleus to the cytoplasm for its degradation is found to be deregulated in cancers presenting p53 mutations.(76) USP10, the DUB that compensates MDM2 function, translocating to the nucleus and activating p53 is also frequently under-expressed in certain types of cancer. (77) UPS deregulation may also affect apoptosis signaling in particular due to aberrant accumulation of the anti-apoptotic MCL-1. The regulation of MCL-1 levels is dependent on the correct functioning of the E3s tripartite motif containing 17 (TRIM17), MULE and FBW7. (78,79)

Regarding NF-κB signaling, its essential modulator, NEMO, depends also on correct ubiquitination to carry out its normal function. Its mistaken ubiquitination is critical for genotoxic NF-κB activation and for the protection of tumor cells from DNA damage-induced cell death.(80) Dysregulation of the linear ubiquitin chain assembly complex (LUBAC)-mediated linear ubiquitination pathway is directly responsible of the erroneous ubiquitination of NEMO and posterior aberrant activation of NF-κB pathway. LUBAC is composed by Heme-oxidized IRP2 ubiquitin ligase-1 L (HOIL-1 L), HOIL-1 L-interacting protein (HOIP), and Shank-associated RH domain interactor (SHARPIN), being the function of HOIP controlled by the DUBs OTULIN and CYLD.(81)

2.5.1. TLR-LUBAC-NF-kB crosstalk in DLBCL

The ubiquitin-like (UBL) proteins of HOIL-1L and the ubiquitin-associated (UBA) of HOIP are indispensable for complex formation. However, the RING-in-between RING-RING (RBR) domain of HOIP, but not that of HOIL-1L, is responsible for linear ubiquitin formation, being HOIP the catalytic subunit. (82)

LUBAC is the only E3 that assembles linear polyubiquitin chains by peptide bonds between the C-terminal Gly76 of ubiquitin and the α-NH2 group of M1 of another ubiquitin moiety. LUBAC functions has a regulator of the canonical NF-κB pathway as it mediates the K63-linked ubiquitinations of NEMO. (83) Ubiquitinated NEMO, together with ubiquitinated RIP1 provides a scaffold for the recruitment of TGFβ-activated kinase 1 (TAK1)-TAB1-TAB2/3 complex. This complex is responsible for the activation of the canonical IκB kinase (IKK), composed of the kinase subunits IKKα, IKKβ and the regulatory subunit NEMO finally resulting in the proteasomal degradation of inhibitory IκBs, allowing the nuclear translocation of NF-κB. (84)

It has been shown that LUBAC overexpression results in NF-κB activity, and that knockdown of LUBAC components resulted in reduced basal and TNF-α-stimulated NF-κB activities.(85) In addition, it has been shown that activating single-nucleotide polymorphisms of HOIP are enriched in patients with ABC-DLBCL, and expression of HOIP, which parallels LUBAC activity, is elevated in ABC-DLBCL samples. Within the same study, it was revealed that HOIP overexpression protects B cells from DNA damage-induced cell death through NF-κB activation, indicating that HOIP facilitates lymphomagenesis by preventing cell death and augmenting NF-κB signaling. Furthermore, the pharmacological inhibition of LUBAC was shown to suppress the tumor growth in an *in vivo* mouse model. (86)

2.5.2. Pharmacological modulation of LUBAC signaling

HOIP is the main catalytic subunit of LUBAC, as it contains the E3 active site. So, targeting HOIP is synonym to targeting LUBAC signaling. HOIP is composed of three main domains: zing finger (ZF) domains, NPl4-type zinc finger 1 (NZF1), and NPl4-type zinc finger 2(NFZ2). NZF1

domain acts as a ubiquitin-binding site able to interact with NEMO and Lys63 ubiquitin chains, necessary for the recruitment of LUBAC in different pathways. (87)

At present, BAY11-7082, gliotoxin, peptidyl inhibitors of LUBAC, bendamustine, and α,β-unsaturated methyl ester-containing compounds reportedly inhibit the LUBAC activity.(87) However, BAY11-7082 has been shown to inhibit E2s, indicating that probably it is not a direct LUBAC inhibitor; (88) Gliotoxin indeed binds to HOIP suppressing LUBAC activity but presents cytotoxicity (89) and bendamustine suppresses LUBAC activity but presents several other E3s like MDM2 as off-targets.(90) It has been recently developed a novel family of thiol-reactive, α,β-unsaturated carbonyl-containing chemical compound, named HOIPIN (1 to 8) as potential LUBAC inhibitors. However, the detailed molecular mechanism and the pharmacological effects of HOIPINs have remained elusive.(87) Thus, makes so important to search for novel compounds targeting this altered pathway as a possible adjuvant therapy to combine with existing treatments to tackle tumors with LUBAC overexpression or NF-κB addicted tumors like ABC-DLBCL.

3. State of the art preclinical modelling of high-grade B-cell lymphoma

Models used in cancer research are constantly evolving toward more complex and physiologically relevant models for preclinical studies. Cancer models are either naturally existing or artificially prepared experimental systems that show similar features with human tumours, however the heterogeneous nature of human tumours is still a factor difficult to mimic in laboratories. Thorough investigation is constantly taking place on cancer models for deepening our knowledge in cancer invasion, progression, and early detection (Figure 5). These models give an insight into cancer etiology, molecular basis, host tumour interaction, the role of microenvironment, and tumour heterogeneity in tumour metastasis. These models are also useful to discover new biomarkers, targeted therapies, and are very helpful and cost-efficient in drug development.

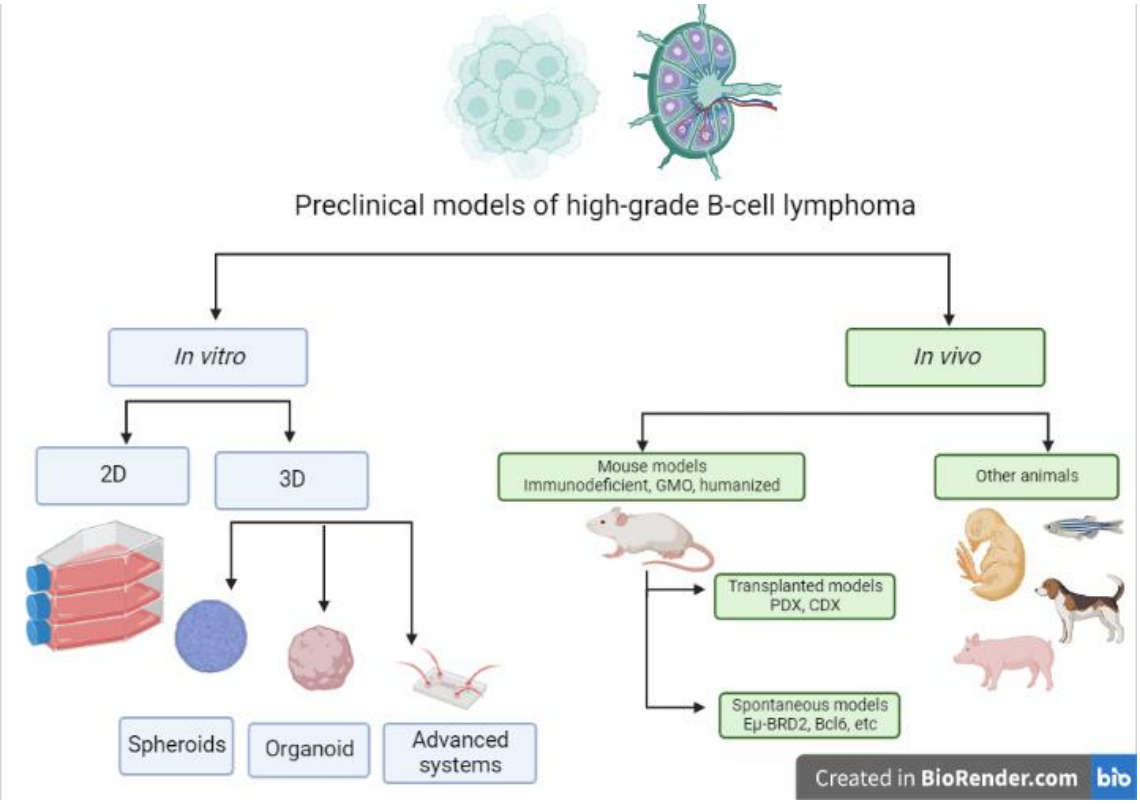

Figure 5. – Common existing In vitro and In vivo models used in lymphoma research.

From its outset, lymphoma research has relied on a wide variety of models, from cell monolayers to whole-organism studies, in particular mice. Over the years, advances in gene-editing, mouse models, and the rise of three-dimensional (3D) *in vitro* models have opened

the door to a vast variety of approaches to the study the biology and therapy responses in a more physiological environment. The generation of reliable models approximating human disease offers the potential to apply the obtained results in daily clinical practice.(91) Although non-preclinical model is ideal as all present limitations its development and application is key to fill the gap between preclinical research and translational medicine.

3.1. In vitro: 2D vs 3D models

2D models, based on the culture of cancer cell lines, is regarded as a ubiquitous feature of oncology as it presents similar gene expression patterns and features to those on primary human tumours. This model is widely used due its cost, high proliferation rates, limited cellular heterogeneity, immortality and easy to use characteristics.(92) In addition to the aforementioned advantages, 2D cultures are an extremely versatile model enabling the modification of the system even at the genetic level with novel gene-editing techniques like DNA base editors and RNA-programmable clustered regularly interspaced short palindromic repeats (CRISPR)-associated (Cas) nucleases.(93)

However, high-grade B-cell lymphomas, and all cancer types, complexity does not result only form genetic aberrations in the tumoral cells. Its survival and physiology deeply depend on the interaction of the malignant cells with the non-malignant cells forming the surrounding tumour microenvironment (TME). In the case of DLBCL TME involves the interactions of the malignant cells with healthy immune cells, like natural killer (NK) cells (±20% of total cell content), dendritic cells (DCs) (±15%), M2-type macrophages (±15%), CD4+ T cells (±10%), and CD8+ T cells (<5%). (94) These diverse interactions and the composition of the TME widely affect the disease's progression, response to treatment, acquisition of resistance and general pathophysiology.

In DLBCL, tumour cells represent between 60 and 80% of the total cellular content, therefore classical 2D models do not fully recapitulate the complexity of the disease.(91) The first approaches to fill this gap consisted on the elaboration of simple co-culture systems, by combining tumoral cell lines with other cell types as for instance stromal cells or some type of effector cell like M2-polarized macrophages. However, this models still lack the full

spectrum of interactions with the TME and the 3D structure of the region which also plays a vital role in disease behaviour and treatment response. (95) Organoids and organotypic spheroids fall in this last category.

The development of organoids as an *ex vivo* model system has revolutionized cancer research for the last decade. Organoids are the infinitesimal of human organs and tissues, and functional features and architectures of a selected organ are accurately mimic. The organoid cancer model is developed by tumour cells isolated from biopsies of cancer patient and cultured within an artificial extracellular matrix, specific culture systems which facilitate the formation of cancer organoid. (96) Patient-derived lymphoma organoids (PDOs) reproduce the actual interactions within a patient's own immune system to eradicate tumour cells, and recapitulate the transcriptional, mutational profile, and therapy response of the primary tumour.

This may be also performed with cell lines, by combination of the different cell types present in the tumour within an extracellular matrix. There is a variety of techniques and technologies to form cancer organoids or spheroids ranging from using commercially available extracellular matrix, synthesis of hydrogels to use as scaffold, (97,98), hanging drop method (99), magnetic levitation and bioprinting techniques (100) or chips and microfluidics systems (101) among others.

A major limitation of organoids involving different cell types is that the co-culture conditions require exhaustive optimization to achieve an equilibrium that suits all cell types involved. Additionally, patient-derived 3D models are often created from small biopsies, in part due to difficult access for researchers to big quantities of biological material, which may cause an underrepresentation of the complexity of the whole tumour, lack immune selection, and make it i*n vitro* manipulation challenging. Access to larger biopsies could facilitate optimizing these systems and broaden the scope of these models beyond drug screenings.(91)

Despite these limitations, cell-line-derived and patient-derived DLBCL spheroids have already been helpful in lymphoma research for example to deepen our knowledge in germinal centre dynamics and reactions (102), the TME and therapeutic potential and resistances (103). 3D models have been used to study epigenetic events within the GC, as for instance B cell proliferation mediated by enhancer of zeste 2 polycomb repressive complex 2 subunit (EZH2)

through the repression of Cyclin Dependent Kinase Inhibitor 1A (CDKN1A), which cannot be evaluated in mouse models due to biological limitations of the model. (104) These models have also been used for pharmacological evaluation of novel drug combinations to try and discover new anti-lymphoma regimens specially for ABC-DLBCL. (105)

Progress is leading to the development of even more complex systems such as organ-on-chip models and microfluidics-based platforms, which together recapitulate blood-flow conditions and accurately reproduce the cell interactions that occur in the DLBCL tumour microenvironment.(101) In comparison with 2D models, 3D models, and the coming combinations of this models with microfluidics devices, are prone to facilitate faster and more accurate drug development, because they recapitulate in more detail the TME of primary tumours.

3.2. In vivo: advantages of existing CDX and PDX models

Due to its genetic and physiological similarities, in the field of lymphoma research, mice have been the favourite animal model. In addition, the possibility of genetically modifying this specie has enabled the development of spontaneous lymphoma models to evaluate its arise and development like for example the Eμ-Myc,(106) Eμ-BRD2,(107) or Bcl6 (108) mouse models. These models have enabled us to understand important factors in this disease like the role of BCR signalling, identification of key factors in B cell development and transformation such as *BCL6, PAX5, PI3K, MEF2B* and *EZH2*,(91)(109) among others as well as the discovery of novel tumour suppressors and other potential therapeutic targets like Tet methylcytosine dioxygenase 2 (TET2).(110)

Xenograft mouse models, which are obtained by the implantation of human lymphoma cells into an immunodeficient mice are also very helpful and widely used. Within this model we find two subtypes: patient-derived xenografts (PDX), which result from the inoculation of cells obtained from patient samples, and cell line-derived xenograft (CDX), which is a gold-standard model used for the research and testing of anti-cancer therapies obtained from the inoculation of cell lines in mice. CDX models, are easy to generate and cellular material, as it comes from cultured cell lines, is abundant. However, these cell lines contain native mutations that may not be observed in the comparative human lymphoma.(111)(96) PDX, in

comparison, retain the genetic signature, refractoriness to treatment and TME as seen in patients enabling to do a thorough study of therapeutic regimens and personalized therapies for each individual patient. However, with this type of biological material, quantity is limited, and engraftment rates are usually low. In addition, immune-compromised animals are used to avoid rejection making it impossible to evaluate immunotherapies or directly the role of the immune system within the model.(112) By serial engraftments on different mice we can amplify the cells to increase the amount of biological material to work but this procedure, slowly leads to a loss of the primary tumour characteristics as well as increased costs and time required.

Humanized mice, immunodeficient mice populated with a human immune system, are also an option to study immune interaction and the effect of different immunotherapeutic agents in a living model. However, its establishment and application still face many challenges, including the major histocompatibility complex (MHC) incompatibility between immunocytes and tumours, the residual murine innate immunocytes, and the lack of specific-specific cytokines and the elevated price of humanized mice. (113) In addition, mouse xenograft models are costly, time-consuming and require large cohorts of animals, presenting several ethical issues that should also be considered when using mice in research. Due to growing pressure on reducing the number of animals used in experimentation and the need to comply with the 3R principles, the chicken embryo chorioallantoic membrane (CAM) assay appears as an attractive alternative to traditional animal models.

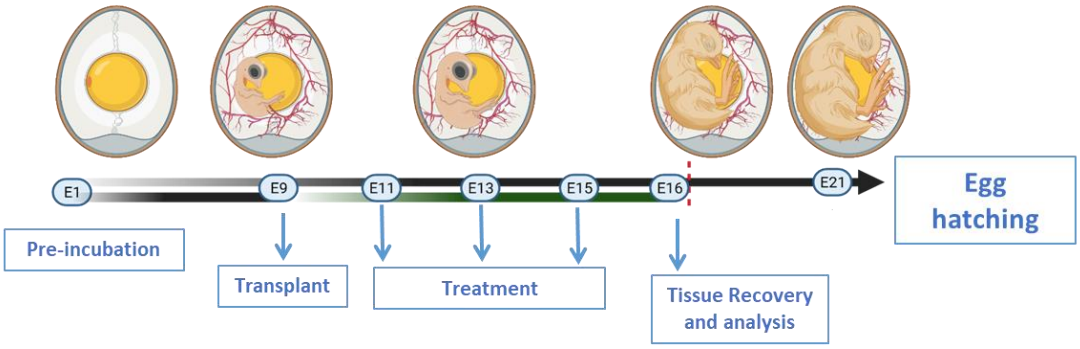

Figure 6. – Schematic representation of the CAM assay

The CAM is a highly vascularized extra-embryonic membrane tightly connected to the developing embryo through its vascular system circulatory system. This model, in comparison with other existing animal models, presents a series of advantages as for example its cost-effective, fast allowing the screening of a large number of pharmacological samples in a short time and presents fewer ethical issues;(114) as the chick embryo is unable to perceive pain from manipulations in the CAM tissue, which is not innervated and experiments are terminated before the development of centres in the brain associated with pain perception, making this a system not requiring animal experimentation permissions. Due to these characteristics' chick embryos are not considered as living animal until day 17 of development in most countries. (115)

Acellular matrix can be transplanted onto the CAM to provide a matrix for cells to grow. Xenotransplantation can also be performed easily and non-invasively as at the beginning of the chicken embryo development the immune system is immature, presenting an immunodeficient environment in the early stages of development when the cells are implanted. Within days, tumor formation occurs, and, in the case of aggressive tumours, metastasizing cells can colonize the embryo's organs via the circulatory system due to the angiogenesis irrigating the xenograft. (116) This spontaneous angiogenesis around the tumour provides the explants with nutrients and growth factors derived from the yolk sack and structures developing within chicken embryo. (117)

After the first 8 days of embryonic development, early lymphoid cells deriving from the yolk sac and spleen are usually recognizable in the thymus and 3 days later in the bursa of Fabricius, a specialized organ where hematopoiesis takes place, vital for B-cell development in birds, and cell-mediated immunity has been demonstrated by day 13–14.(118–120) On day 12 of embryonic development, the immune system is mature enough to respond to foreign tumour cells by infiltration of monocytes and inflammatory-like cells such as avian heterophils and opening the door to using the CAM model as an *In vivo* research model for immunotherapy. (121)

However, the CAM model presents certain limitations. For instance, embryo viability is largely variable (20–90%) and directly depends on biophysical parameters, like considerable changes in atmospheric temperatures, which leads to lower rates of fertilization and lower survival of embryos. Experiments are bounded to strict schedules as the eggs are only viable until day 17

of embryonic development and the development of immune system is also rigorously time framed. This be problematic when evaluating response to treatment depending on the mechanism targeted by the treatment or in the case of immunotherapy, it is totally dependent on the embryos immune system development. In addition, there is still a lack of reagents like for instance antibodies that are compatible with chicken tissue. Despite these limitations, the CAM model is technically simple, fast, and cost-efficient. Therefore, it can be easily set up as a model for bridging the *in vivo–in vitro* gap, and reduce the number of animals used in experimentation, especially in drug development, making it easier to comply with the 3R rule of animal experimentation at a global level.(122)

RATIONALE AND OBJECTIVES

RATIONALE AND OBJECTIVES

The overall objective of this dissertation is to evaluate the safety and efficacy of different approaches aimed at targeting the pathological overactivation of NF-κB in diffuse large B-cell lymphoma, with a special focus on the activated B-cell, hard-to-treat subtype of the disease.

The strategies challenged in this thesis are the following:

1. Blockade of TLR signalling by direct inhibition of IRAK1/4 in association with BET bromodomain inhibition-mediated impairment of epigenetic reader's activity.

2. Inhibition of ubiquitin-proteasome system signalling by means of a novel covalent inhibitor of HOIP, the LUBAC catalytic subunit.

MATERIAL AND METHODS

MATERIAL AND METHODS

Cell Lines

In both projects, four *MYD88*^{L265P} ABC-DLBCL cell lines (OCI-LY3, OCI-LY10, HBL-1, TMD8), one *MYD88*^{wt} ABC-DLBCL cell lines (U-2932) and four GCB-DLBCL with *MYD88*^{wt} (SUDHL-4, SUDHL-8, OCI-LY8 and KARPAS-422) were used. All cell lines were cultured in RPMI medium (Gibco) supplemented with 10% fetal bovine serum (FBS) (Biowest) except for OCI-LY10 which were cultured in Iscove's Modified Dulbecco's (IMDM) medium (Gibco) supplemented with 20% human serum, 1% L-glutamine (Corning) and 1% penicillin–streptomycin (Gibco). Hk follicular dendritic cells were cultured in Advanced-RPMI 1640 medium (Gibco) supplemented with 5% FBS, 1% antibiotics, 1% glutamine.

Primary samples

Healthy donors' peripheral blood mononuclear cells (PBMC) were isolated using Ficoll density gradient. Cryopreserved cells of lymph node biopsies from two ABC-DLBCL patients with either MYD88wt or MYDD88L265P were included in this study. Cell of origin and MYD88 mutational status were determined histologically using Hans's algorithm and allele-specific PCR, respectively. To prevent spontaneous apoptosis *ex vivo*, primary cultures were maintained in complete RPMI medium in the presence of the bone marrow-derived mesenchymal cell line StromaNKTert (Riken BioResource Center) at a 4:1 ratio. The ethical approvals for this project, including the informed consent of the patients, were granted following the guidelines of the Hospital Clínic Ethics Committee (IRB, reg. num. 2012/7498).

Proliferation assay

DLBCL cells and PBMCs ($4x10^4$) were seeded onto 96-well-plates and incubated with or without different drugs at the indicated doses. After the indicated time points, 5mg/ml of MTT (3-(4,5-dimethylthiazolyl-2)-2,5-diphenyltetrazolium bromide) reagent (Sigma-Aldrich) diluted in PBS was added and incubated for 4 hours (in the case of cell lines) or 6 hours (in the case of primary samples). The formazan precipitate was diluted in acidic isopropanol and the colorimetric assay was detected at 560nm using 750mm absorbance as reference wavelength with Synergy™ HTX Multi-Mode Microplate Reader (Biotek). Each measurement was made in triplicate. Values were represented using untreated control cells as reference.

Combination Index (CI) calculations

The combination index (CI) was calculated using CompuSyn software based on the Chou and Talalay's algorithm and the formula (CI) = (D)1 /(Dχ)1 + (D)2/(Dχ)2, where (Dx)1 represents the dose of the drug D1 alone that inhibits the growth of cells by 50% and (Dx)2 is the dose of the drug D2 alone that inhibits the growth of cells by 50%. For evaluation of interaction CI <0.8 indicate synergism, CI=1 indicates additivity and CI>1 indicates antagonism.

Western blot

Whole cell proteins were extracted from 10^7 DLBCL cells as previously described [11]. Proteins (30-50 µg/lane) were subjected to 10-12% SDS-PAGE, transferred onto PVDF membranes (Immobilon-P; Millipore) and probed with antibodies against MARCKS (Thermo Fisher), MCL-1 (Santa Cruz), IκBα (Cell Signaling Technology), CD44 (Bio-Rad), endogenous α-tubulin (Sigma-Aldrich), followed by incubation with anti-rabbit or anti-mouse secondary antibody (Cell Signaling Technology). Chemiluminescence detection was done using ECL Plus system (Thermo Fisher) and a Fusion FX imaging system (Vilber Lourmat). Band intensity was quantified using Image J software and normalized to housekeeping protein (GAPDH or

TUBULIN). If not otherwise specified, representative data from n = 3 experiments are shown. Antibodies used in this dissertation are listed in Table 6

RNA extraction, cDNA Synthesis and quantitative PCR (qPCR)

Total RNA was extracted using the RNeasy Mini Kit (Qiagen) according to manufacturer's instructions. Total RNA was retrotranscribed using the high-capacity cDNA Reverse Transcription Kit (Thermo Fisher) and quantitative real-time PCR (qPCR) was performed on a QuantStudio™ 7 Flex Real-Time PCR System (Life Technologies) using Sybr Green primers and Gotaq qPCR Sybr Green Master Mix (Promega). Primers used in this dissertation are listed in Table 5. The comparative cycle threshold method (ΔΔCt) was used to quantify the relative expression of each gene by means QuantStudio™ 7 software (Life Technologies) normalizing with a housekeeping gene (GAPDH, B-TUBULIN OR B-ACTIN).

Target gene	**Forward (5' to 3')**	**Reverse (5' to 3')**
CCL3	ATGCAGGTCTCCACTGCTG	GGGAGGTGTAGCTGAAGCA
IL6	GCAGAAAAAGGCAAAGAAT	CTACATTTGCCAAGAGC
IL10	GCCTTTAATAAGCTCCAAG	ATCTTCATTGTCATGTAGGC
MARCKS	CTCCTCGACTTCTTCGCCCAAG	TCTTGAAGGAGAAGCCGCTCAG
IRF4	TCAGCTCCTTCACGAGGATT	GAGCCAAGCATAAGGTCTGC
MCL1	TAGTTAAACAAAGAGGCTGG	ATAAACTGGTTTTGGTGGTG
CD44	CCAGAAGGAACAGTGGTTTGGC	ACTGTCCTCTGGGCTTGGTGTT
MYC	TGAGGAGGAACAAGAAGAT	ATCCAGACTCTGACCTTTTG
RNF31(HOIP)	GTTGGAAGACAAGGTTGAAG	GTGTCCATGGAACAGGTG
Human Alu Sequences	ACGCCTGTAATCCCAGGACTT	TCGCCCAGGCTGGTCGGGTGCA
HPRT Gallus gallus	CAGGCTCCACGTTTGTTACC	TTTCCCTCAGGCCTTCATCA
GAPDH	ACAGTTGCCATGTAGACC	TTGAGCACAGGGTACTTTA
β-ACTIN	GACGACATGGAGAAAATCTG	ATGATCTGGGTCATCTTCTC
HPRT	ATAAGCCAGACTTTGTTGG	ATAGGACTCCAGATGTTTCC

Table 5. – Primers used in this dissertation.

Gene expression and gene set enrichment analysis (GSEA)

Complementary RNA was hybridized on the HG-U219 GeneChip (Affymetrix) following standardized protocols. Scanning was processed in a Gene Titan instrument and analyzed with GeneChip Command Console Software (Affymetrix). Raw data were normalized using the Robust Multichip Analysis algorithm implemented in the Expression Console Software v1.1 (Affymetrix). An enrichment pathway analysis was done using the gene set enrichment analysis (GSEA) desktop application version 2.0 (http://www.broadinstitute.org/gsea/) in order to find significant gene signatures using experimentally derived custom gene sets (lymphochip.nih.gov). Data has been deposited at the Gene Expression Omnibus (GEO) of the National Center for Biotechnology Information (GSE159915).

Flow cytometry analysis

Apoptosis was determined by cytofluorimetric detection of phosphatidylserine exposure after dual staining with annexinV-propidium iodide on an Attune acoustic focusing cytometer (Thermo Fisher). For intracellular detection of *IL6* transcripts, DLBCL cultures were labeled with an IL-6 Hu-Cyanine 5 SmartFlare RNA detection probe (Merck), and percentage of cells with detectable contents of *IL6* mRNA was determined by flow cytometry. For F-actin measurement, HBL-1 y OCI-LY3 cells were pre-incubated for 24 hours with 0.5 µM CPI203 and/or 50 µM IRAKi, followed by a 24-hour stimulation with 0.5 µM hyaluronic acid (Sigma-Aldrich). Cells were then PFA-fixed, labeled with 50 µg/ml phalloidin-TRITC (Sigma-Aldrich). Recounting of red fluorescent cells was performed on a H5505 microscope by means of a 20X/1.30 NA oil objective (Nikon) with the use of Isis Imaging System v5.3 software (MetaSystems GmbH). Antibodies used in this dissertation are listed in Table 6.

Xenograft mouse model

NOD/SCID IL2R γnull (NSG) mice were inoculated subcutaneously with 10^7 OCI-LY3 cells and after 13 days, when tumor volume reached 100 to 200 mm3, animals were randomized into three groups of 5 mice each, and were dosed with intraperitoneal (i.p.) injection of 2.5 mg/kg CPI203 twice a day (BID) and/or i.p. administration of 7.5 mg/kg IRAKi (BID), or an equal volume of vehicle, in a five/two (on/off) schedule. Tumor volumes were measured every 2-3 days with external calipers and calculated as: $V = 1/2 \times a \times b2$, where a and b represent the length and width, respectively. After 11 days, animals were euthanized according to institutional guidelines and tumor samples were excised.

Immunohistochemistry

Tissue samples were formalin-fixed overnight and paraffin-embedded (FFPE) and sections of 4µm were cut. Formalin-fixed and paraffin-embedded slides were deparaffinized with xylenes and rehydrated using standard protocols before being incubated with 10amM Sodium Citrate (Ph 6) for antigen retrieval.

For DAB (3,3 – Diaminobenzidine) immunostaining, all slides were incubated with 0,3% H_2O_2 to block endogenous signaling and a blocking solution to minimize unspecific IgG binding (5% goat/donkey serum depending on the origin of the secondary antibody; 4%BSA and 0.5% Tween-20 in PBS) followed by overnight incubation with the primary antibody and an incubation with HRP-conjugated antibody of 1 hour. The staining was developed using DAB peroxidase substrate kit (Vector), counterstained with hematoxylin (de) and mounted in Dibutylphthalate Polystyrene Xylen Solution (DPX). Hematoxylin and eosin (H&E) staining were performed after rehydration step with serial hematoxylin and eosin incubations.

All slides were analyzed in a Leica DM2000 microscope (Leica Microsystems). Antibodies used in this dissertation are listed in Table 6.

Primary Antibodies	Source	Reference
IMMUNOBLOTTING		
IRAK1-pThr209	Thermo-Fisher	PA5-38633
IRAK1	Cell Signaling	4504
IRAK4-pThr345	Abnova	MAB2538
MCL-1	Santa Cruz	sc-819
β-actin	Santa Cruz	sc-47778
IKBα	Cell Signaling	9242
CD44	Bio-Rad	MCA2726T
MARCKS	Thermo-Fisher	PA5-12210
MYC	Cell Signaling	5605
Tubulin	ProteinTech	66240-1-Ig
RNF31 (HOIP)	Cell Signaling	99633

FLOW CITOMETRY		
Annexin V-FITC	Invitrogen	550474
IMMUNOHISTOCHEMISTRY		
p-Histone3	Abcam	ab32107
P50	Abcam	ab209795
Activated caspase-3	BD	550557

Table 6. – Antibodies used in this dissertation.

Generation of HOIP^{KO} cell lines

0.5 x 106 HBL-1 cells were electroporated using a on a Nucleofector™ 2b (program A030, Lonza) with 36 pmol SpCas9 Nuclease V3, 44 pmol CRISPR-Cas9 tracRNA ATTO 550, 44 pmol Alt-R CRISPR-Cas9 crRNA Hs.Cas9.RNF31.1.AS (RNF31-HOIP KO 5´- CAGGAGCAATCTCTCTCAAT AGG-3`) (IDT-Integrated DNA Technologies).

Design and Synthesis of HOIP inhibitor

For the design of out HOIP inhibitor, combinatorial substitution of α-β unsaturated moieties (described as covalent warheads to cysteines) in the different substitution positions of a pyrido[2,3-*d*]pyrimidine scaffold, leading to the generation of a new chemical library. After HOIP subunit modelling, the chemical library was screened through different molecular modelling techniques such as, covalent docking and molecular dynamics simulations to assess

the best HOIP binding candidates. Then, the synthetic route to obtain some of the candidates was described and finally synthesized at IQS using microwave assisted methodologies.

Drug Affinity Responsive Target Stability (DARTS)

Whole cell proteins were extracted from 10^7 DLBCL cells as previously described. Protein extracts were splitted into aliquots of 4µg/µL and incubated for 2 hours at 37ºC with concentrations of HOIP inhibitor ranging from 100nM to10µM. Digestion of the protein extracts was performed by incubating the extracts at 37ºC with increasing concentrations of pronase. Digestion was stopped after 30 minutes by addition of SDS loading buffer and heating the samples to 95ºC for 5 minutes and subjected to 10-12% SDS-PAGE electrophoresis, followed by Western blot detection and quantification of HOIP and β-Tubulin. Figure 6 depicts schematic workflow.

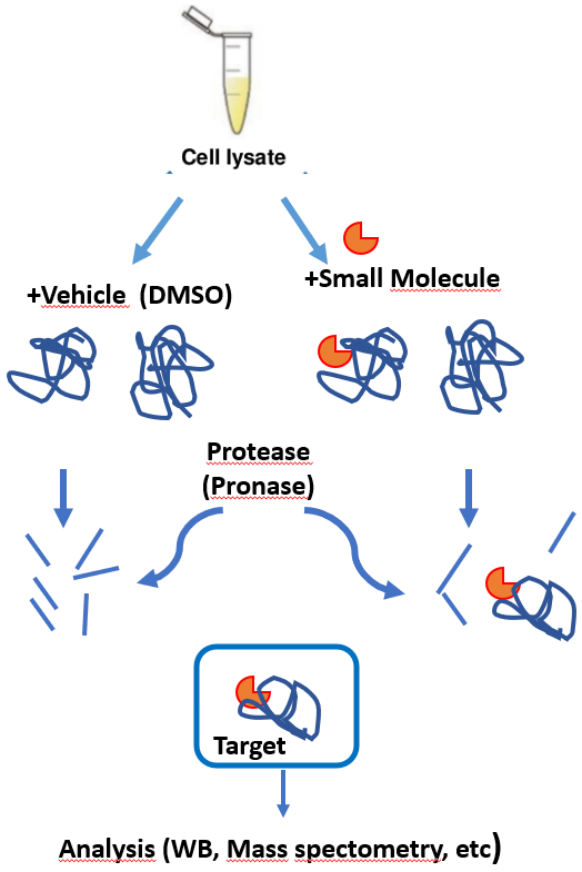

Figure 7. – DARTS workflow scheme.

Chick embryo chorioallantoic membrane (CAM) model

Fertilized white Leghorn chicken eggs were purchased from Granja Santa Isabel, S. L. (Córdoba, Spain) and incubated for 9 days at 37ºC with 55% humidity and constant movement. At day 9 of their embryonic development, eggs were cleaned with alcohol 70º and a window of an approximate 2 cm-diameter was drilled on top of the air chamber of the eggshell. Then, HBL-1 cells were resuspended in 25 µL Advanced RPMI medium containing 5% FBS and 100 U/mL penicillin and streptomycin and 25 µL Matrigel (Cultek). The mix was incubated for 15 min at 37 ºC and subsequently implanted into the CAM of each egg. The window was then covered with sterile tape and the eggs were placed back in the incubator. At days 12 and 14 of their embryonic development, 100 µmol/L of HOIP inhibitor or vehicle (DMSO) diluted in RPMI medium were administered topically on tumor-bearing eggs. On the 16th day of development, chick embryos were sacrificed by decapitation. Tumors were excised and weighed to determine tumor growth. Liver, spleen, bone marrow and brain were recovered and processed for metastasis analysis by ALU sequence RT-qPCR. ALU sequences are repetitive DNA sequences that are widely dispersed within the human genome. The name Alu derives from restriction enzyme site, Alu I, within the repetitive sequence. In humans, Alu sequences represent about 6-13% of genomic DNA. Detailed experimental timeline is described on Figure 8.

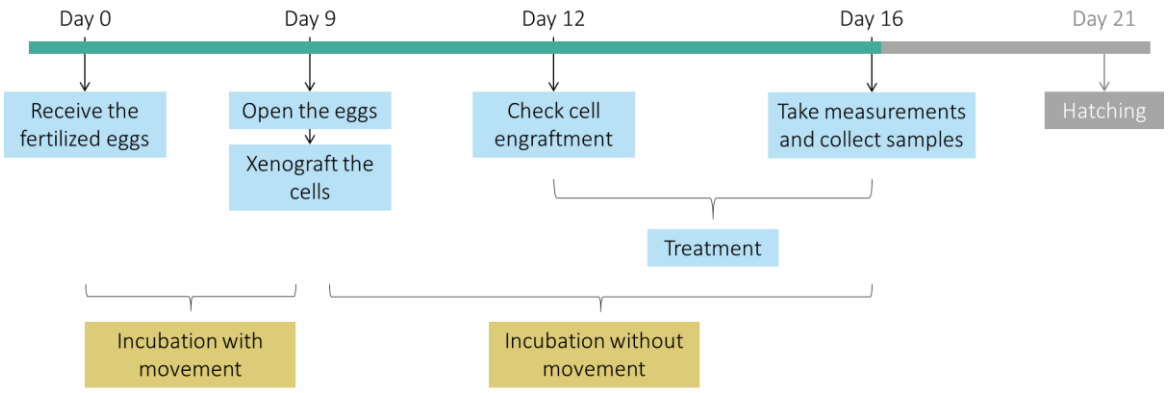

Figure 8. - CAM assay experimental timeline.

Obtention of monocytes and differentiation to M2 macrophages

The isolation of monocytes was performed using Ficoll density gradient from healthy donor's blood samples. To enrich the sample of monocytes, RosetteSep™ Human Monocyte Enrichment Cocktail (Stemcell™ Technologies) was added to negatively select unwanted cells by targeting them with tetrameric antibody complexes binding to non-monocyte cells and making them precipitate within the Ficoll density gradient. This monocyte enriched cell population was then cultured in Advanced-RPMI 1640 medium supplemented with 5% FBS, 1% antibiotics, 1% glutamine, and 100 ng/mL M-CSF (Peprotech) to differentiate into macrophages. To further polarize them to M2, IL-4 (Prepotech) was added at a concentration of 10ng/ml.

Generation of lymphoma spheroids by magnetic bioprinting

Multicellular spheres were performed by seeding cells in a 1:4 ratio (TME cells : malignant cells) in conditioned medium (Table 7). Subsequently, they were incubated with NanoShuttle™ (Greiner Bio-One) considering the ratio 1 µl/100.000 cells, and subjected to a magnetic field. Visual monitoring was performed by inverted microscopy (Figure 30.) and cell viability was determined with trypan blue (Thermo Scientific). Organotypic multicellular spheres were then assessed by fluorescence analysis and H&E staining.

Statistical analysis

Unless otherwise specified, the data are depicted as the mean ± SD of three independent experiments. Prism 4.0 (GraphPad Software) was used to perform all statistical analyses, using Student's t-test or nonparametric Mann-Whitney test/ANOVA for comparisons between two groups of samples. Results were considered statistically significant when $p<0.05$.

Conditioned medium for 3D bioprinting
RPMI
FBS 1%
Peniciline/streptomycin 1%
L-Glutamine 1%
Collagen 50 µg/mL
FGF 20ng/ml
EGF 20ng/ml
IL-2 500U/ml
B27 1x
M-CSF 20ng/ml
IL-4 500U/ml

Table 7. – Conditioned medium for organotypic multicellular spheres culture.

RESULTS

RESULTS

1. SIMULTANEOUS BLOCKADE OF TLR SIGNALING AND EPIGENETIC READERS EXERTS SYNERGISTIC ACTIVITY IN MYD88^{MUT} ABC-DLBCL

1.1. IRAK1/4 inhibition displays limited antitumoral activity in ABC-DLBCL with MYD88^{L265P} mutation

A set of three well characterized ABC-DLBCL cell lines harbouring MYD88L265P mutation, HBL-1, OCI-LY3 and OCY-LY10, were cultured for 24 or 72 hours in the presence of a selective and orally bioavailable IRAK1/4 inhibitor (IRAKi, Merck-Sigma) [15], and drug response was analysed by MTT assay. As a control, three GCB-DLBCL cell lines (SUDHL-4, SUDHL-8 and OCI-LY8) with MYD88^{wt} were analysed in the same settings. As shown on Figure 9, we observed only a partial and transitory response to the compound in ABC-DLBCL cells when using this later at the physiological dose of 50 µM.

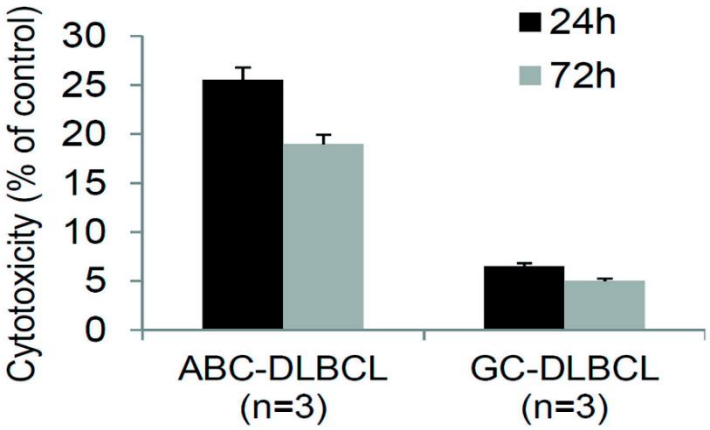

Figure 9. – IRAK inhibition presents a modest, but specific against ABC-DLBCL, antitumoral activity. MTT assay shows that IRAKi (50µM) elicited a partial and transitory response in ABC-DLBCL cell lines, while GCB-DLBCL cell lines were almost completely resistant to the compound.

The mean cytotoxicity of IRAKi decreased from 25.5% at 24 hours to 19% at 72 hours, respectively, despite an efficient blockade of IRAK1 and IRAK4 phosphorylation at Thr209 and Thr345 residues, respectively, in the three MYD88-mutated cell lines (Figure 9). Interestingly, the destabilization of the anti-apoptotic member of the BCL-2 family, MCL-1, previously

reported as a key mediator of IRAKi activity in preclinical models of T-ALL [15], was not sufficient to confer a significant cytotoxicity to the compound (Figure 10).

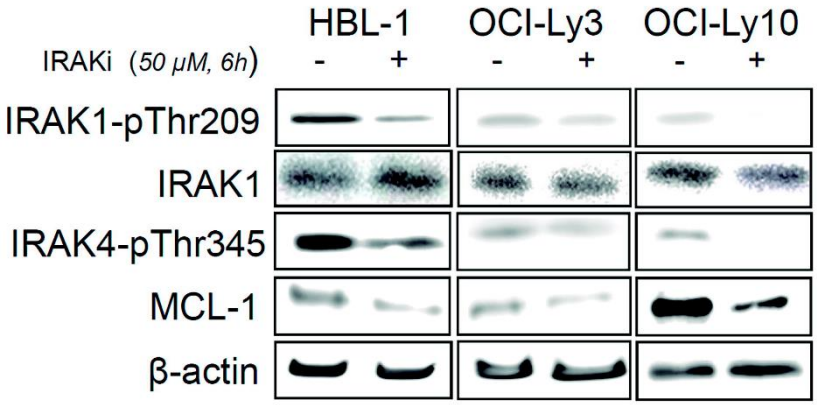

Figure 10. - IRAKi efficiently blocks the phosphorylation of IRAK1 at Thr29 and IRAK4 at Thr345 in the three ABC-DLBCL cell lines with MYD88^{L265P}. β-actin was used as a loading control.

A gene expression profiling (GEP) analysis of these three cell lines exposed for six hours to the inhibitor showed that IRAKi slightly affected the expression of NF-κB-related genes, with a mean normalized enrichment score (NES) < 1, when considering the three main gene sets modulated by the drug according to GSEA analysis (Figure 11). Importantly, the expression of several NF-κB-regulated genes known to promote ABC-DLBCL pathogenesis, including *IL6*, *IL10*, *IRF4* and *CCL3*, were either unaffected or even increased after treatment with IRAKi (Figure 11 and Table 8).

CUSTOM GENE SETS[1]	SIZE	IRAKi *vs* control		Combo *vs* IRAKi	
		NES	FDR q-val	NES	FDR q-val
BLIMP B-CELL REPRESSED	64	2.44	<0.0001	2.16	<0.0001
NFKB_ALL_OCILY3_LY10	58	1.76	0.007	1.99	<0.0001
NFKB_BOTHOCILY3ANDLY10	34	1.84	0.003	1.46	0.056
NFKB_K1106	17	1.62	0.013	0.93	0.705
PAX5 REPRESSED	62	1.37	0.086	-0.87	0.804
XBP1_TARGET_ALL	70	0.89	0.957	-0.93	0.737
PLASMA CELL VS B-CELL	37	-1.30	0.217	0.91	0.689
NFKB_ OCILY10_ONLY	16	-1.20	0.244	1.89	0.002

[1] Raw microarray data were normalized using Expression Console Software v1.1 (Affymetrix) and gene signatures were determined with GSEA version 2.0 (Broad Institute, Cambridge, MA USA) using custom gene sets (http://lymphochip.nih.gov/signaturedb/index.html).

Table 8. - Modulation of gene expression by IRAKi and IRAKi/CPI203 combination in DLBCL cell lines. Raw microarray data were normalized using Expression Console Software v1.1 (Affymetrix) and gene signatures were determined by GSEA version 2.0 (Broad Institute, Cambridge, MS, USA) using a custom gene set.

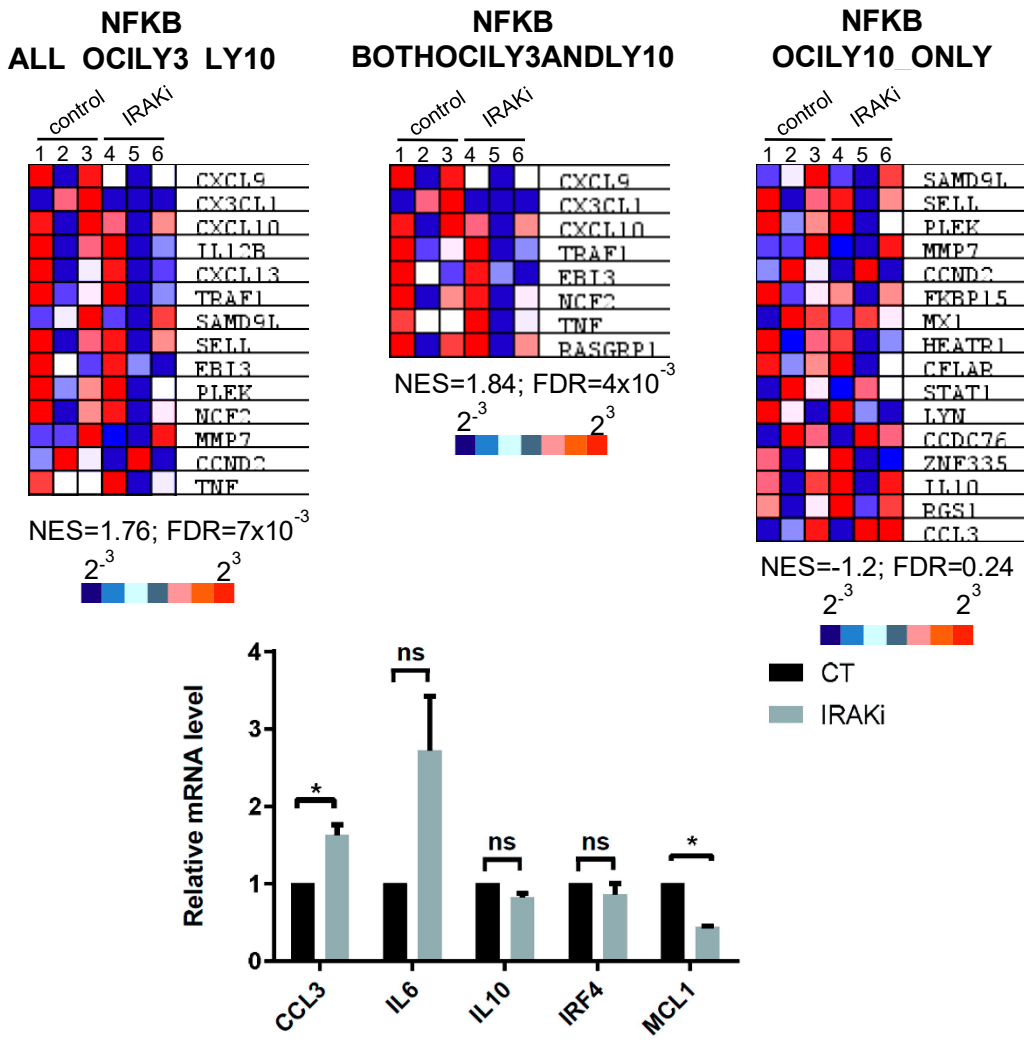

Figure 11. – IRAK inhibition does not significantly affect NF-κB gene signature expression. A) Gene expression signatures of NF-κB in the three cell lines exposed to IRAKi as above, highlighting that IRAKi treatment slightly affects this pathway. The leading edge of each gene set is displayed in a heat map. Gene sets with a false discovery rate (FDR) below 0.05 were considered to be significant. B) RQ-PCR analysis of the predominant NF-κB regulated genes shows limited activity of IRAKi single agent treatment in ABC-DLBCL cell lines with MYD88^{L265P} in relation with incomplete inhibition of the pathway.

Consistently, in an OCI-LY3 mouse xenograft model the compound used at either 1 mg/kg or 5 mg/kg doses failed to elicit a significant tumour growth inhibition (Figure 12). Altogether, these results suggest that concomitant blockade of IRAK1 and IRAK4 signalling does not achieve significant antitumor activity in MYD88^{L265P} ABC-DLBCL possibly due to an insufficient silencing of NF-κB gene signature.

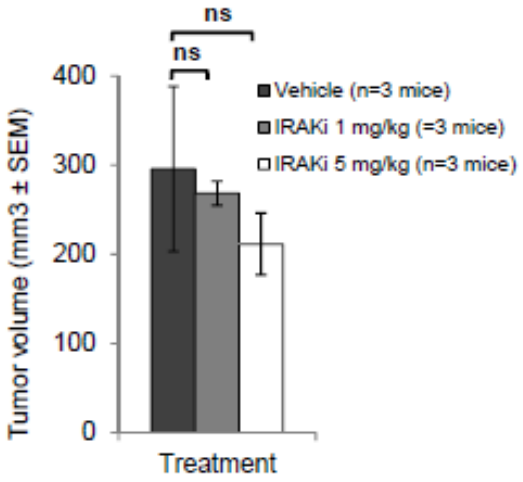

Figure 12. –IRAK inhibition has modest antitumoral activity in In vivo models of ABC-DLBCL. Nine NOD scid gamma (NSG) mice were inoculated subcutaneously with 10^7 OCI-LY3 cells. Two weeks later, they started to be dosed daily dose with 1 or 5 mg/kg IRAKi (intraperitoneal., twice a day) or an equal volume of vehicle (n=3 animals per group) in a five/two (on/off) schedule. After 3 weeks, animals were euthanized, and tumor volumes were recorded ex vivo.

1.2. BET bromodomain inhibition cooperates with IRAKi in *in vitro* and *in vivo* models of ABC-DLBCL

We then considered the possibility to enhance the efficacy of the compound in $MYD88^{L265P}$ ABC-DLBCL by combining IRAK blockade with the BET bromodomain inhibitor CPI203 (kindly provided by Constellation Pharmaceuticals), as this BRD4 antagonist has been shown to effectively suppress a NF-κB gene signature that includes *IL6*, *IL10* and *IRF4*, in the ABC subtype of DLBCL [8]. After exposing the same ABC-DLBCL cell lines as above to a 0.5 µM dose of CPI203, followed by a 24-hour treatment with 50 µM IRAKi, a new GEP analysis was performed. As shown in Figure 12, IRAKi-CPI203 combination induced a significant downregulation of NF-κB-related genes with a mean NES>1.9, when compared to IRAKi single agent. Among the genes included in the NFKB_ALL_OCILY3_LY10 gene set, a selected list of 19 genes underwent a ≥ 2- fold increase in their rank metric score between this analysis and the previous one (Table 9), suggesting that their increased modulation may be associated with the combinational effect of IRAKi and CPI203. From this list, we identified only 4 genes (*LTA*, *MARCKs*, *CD44* and *HEATR1*) that were not included in the core component of the NF-κB target genes affected by either IRAKi or CPI203 single agents, but which were significantly downregulated upon treatment with the drug combination.

GENE SYMBOL	RANK METRIC SCORE			NFKB_ALL_OCILY3_LY10 CORE ENRICHMENT		
	CT *vs* IRAKi	IRAKi *vs* combo	ratio	CT *vs* IRAKi	CT *vs* CPI203	IRAKI *vs* combo
NFKBIA	-0.0496	-0.7811	15.7	-	-	-
BATF	0.1380	1.9920	14.4	-	Yes	Yes
LTA	0.0390	0.5093	13.0	-	-	Yes
MARCKS	0.0369	0.4726	12.8	-	-	Yes
IL6	0.1045	1.0530	10.1	-	Yes	Yes
CD44	0.0498	0.3837	7.7	-	-	Yes
CFLAR	0.1573	1.1140	7.1	-	Yes	Yes
MX1	0.1948	1.3040	6.7	-	Yes	Yes
MX1	0.2341	1.3320	5.7	-	Yes	Yes
RASGRP1	0.0655	0.2800	4.3	-	Yes	Yes
IRF4	0.1176	0.3699	3.1	-	-	-
STAT1	0.0998	0.3125	3.1	-	Yes	Yes
NFKB2	0.1674	0.4954	3.0	-	-	-
HEATR1	-0.1842	-0.5230	2.8	-	-	Yes
CD83	0.5992	1.5090	2.5	-	-	-
SAMD9L	-0.2272	-0.5635	2.5	Yes	Yes	Yes
CCR7	0.6529	1.5950	2.4	-	-	-
TRAF1	0.7852	1.7170	2.2	Yes	Yes	Yes
IL12B	0.3663	0.7928	2.2	Yes	Yes	Yes

Table 9. - Differential modulation by IRAKi/CPI203 drug combination of a selected set of NF-kB-regulated genes in ABC-DLBCL cell lines with MYD88^{L265P}. A selected set of NF-kB-regulated genes are differentially modulated by IRAKi/CPI203 drug combination in ABC-DLBCL cell lines with MYD88^{L265P}.

Among these genes likely associated with the differential activity of IRAKi-CPI203 combination vs either single agent, we were unable to detect significant levels of LTA and HEATR1 transcripts in the 3 ABC-DLBCL cell lines (data not shown). In contrast, upon exposure to IRAK we could detect a 1.2 to 2-fold transcriptional increase of MARCKS and CD44, together with IL6 and IL10 used here as hallmarks of NF-kB activation, in the three cell lines. These genes

were all reduced to 0.5-fold in cells treated with the drug combination (Figure 13 and Table 9).

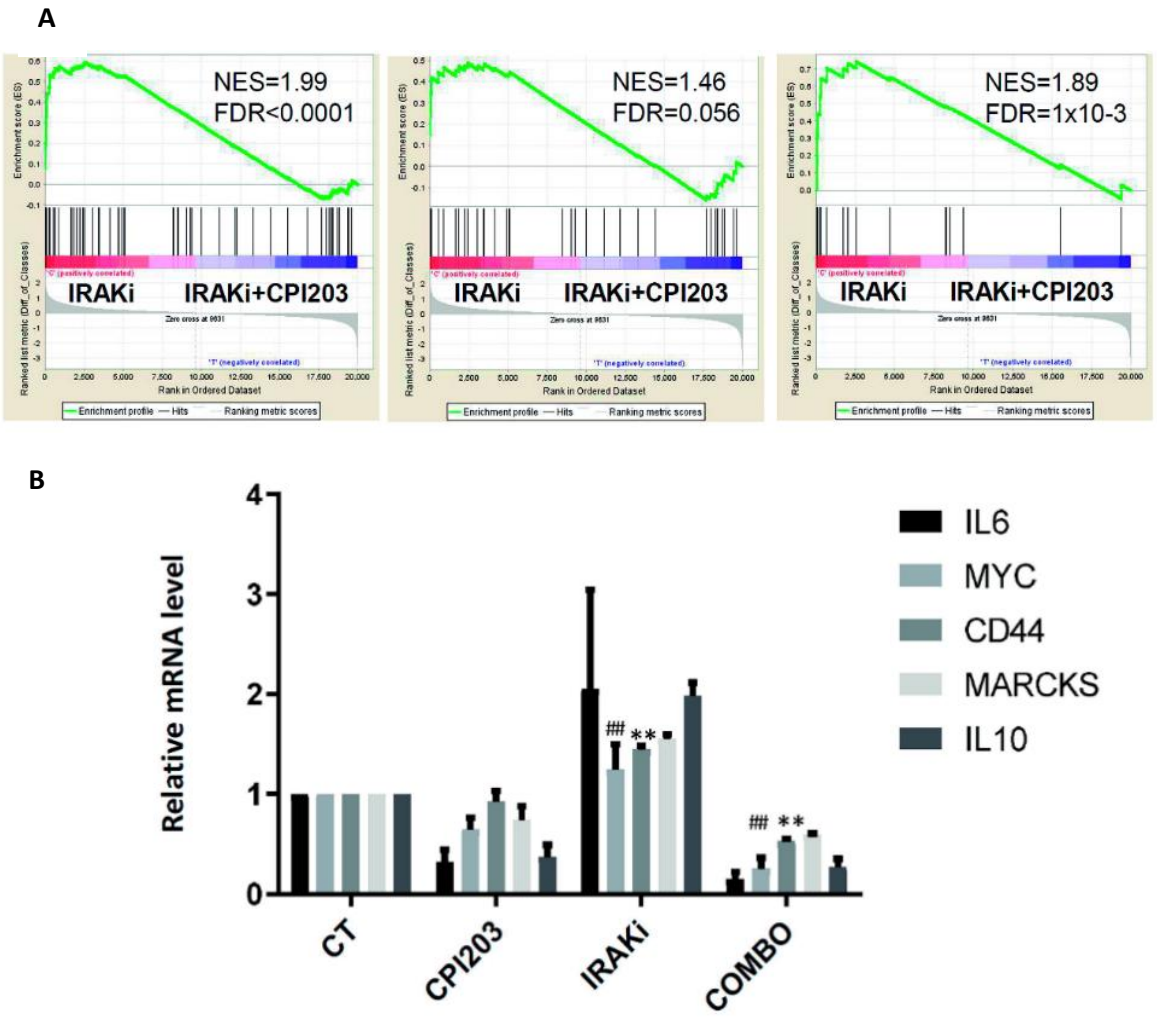

Figure 13. – IRAKi-CPI203 combination induces a significant downregulation of NF-κB-related genes. **(A)** Enrichment plots from GSEA analysis comparing IRAKi single agent versus IRAKi-CPI203 combo in the three cell lines treated for 6 hours (Affymetrix HG-U219; GSEA), showing a significant improvement of NF-kB signature decrease by the addition of CPI203 to IRAKi. **(B)** RQ-PCR analysis of NF-kB downstream genes in the three cell lines exposed to IRAKi, CPI203 or CPI203-IRAKi combo as before. (*p=0.01; **p<0.0001).

Accordingly, IRAKi-CPI203 treatment led to the accumulation of the intracellular inhibitor of NF-κB, IκB, and consequent reduction in CD44 and MARCKS protein levels, while IRAKi and CPI203 single agents slightly affected the expression of these factors (Figure 14). As expected, in two out of the three cell lines, CPI203-based treatments led to the decrease in MYC protein and mRNA, used here as hallmarks of BRD4 inhibition (Figures 13B and 14).

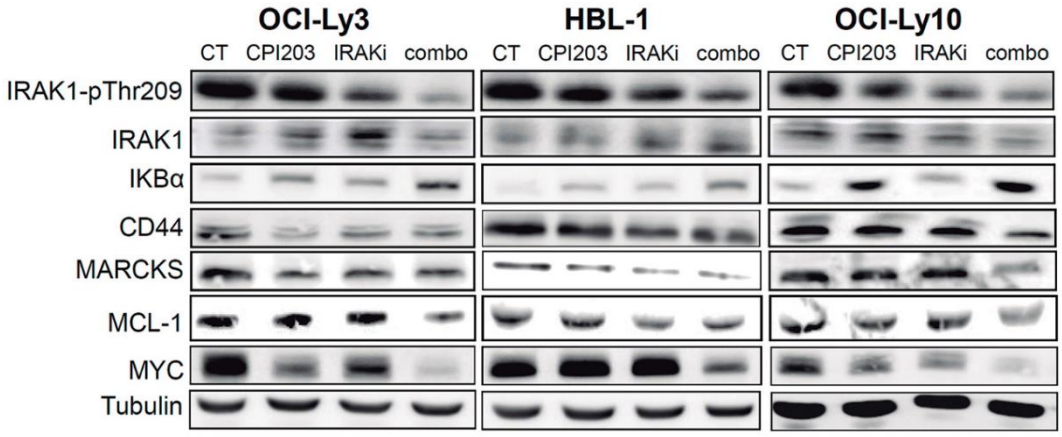

Figure 14. – BETi CPI203 synergizes with IRAKi in ABC-DLBCL mediated by the inhibition of NF-kB downstream pathways. The combination led to intracellular accumulation of IkBα and subsequent downregulation MYC, CD44, MARCKS and MCL-1 proteins in ABC-DLBCL cells with MYD88L265P.

In link with the increased blockade of NF-kB signalling, the addition of CPI203 synergistically improved IRAKi cytostatic effect in the three cell lines, as attested by an 86% blockade in cell proliferation, significantly higher than the 19% activity achieved by IRAKi single agent (CI = 0.52, Figure 14 left panel). Importantly, the cooperation between the IRAKi and CPI203 involved a remarkable downregulation of MCL-1 (Figure 13), which was accompanied by a 36% increase in the relative apoptosis rate when compared with IRAKi and CPI203 used separately (Figure 15 right panel).

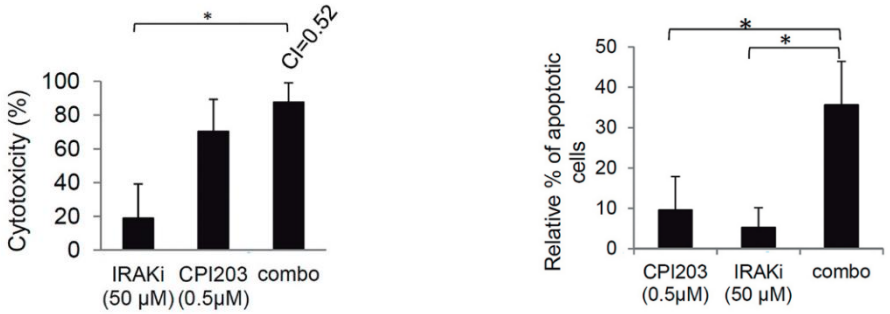

Figure 15. - Cytotoxicity and apoptosis increase with dual treatment. **Left Panel:** OCI-Ly3, OCI-Ly10, HBL-1 cells were exposed for 24 hours to 0.1-0.5 µM CPI203 and/or 50-500 µM IRAKi. Cytotoxicity was evaluated by MTT assay and combination index (CI) was determined using the Calcusyn software. Shown are the cytotoxicity and the mean CI value calculated for cell treatment with 0.5 µM CPI203 and 50 µM IRAKi. **Right Panel:** The drug combination led to a synergistic antitumoral effect *in vitro* in these 3 cell lines, inducing a median 36% increase in apoptosis rate when compared to single agent treatments (*p<0.04)

To further validate the activity of the drug combination in primary ABC-DLBCL samples, cells from lymph node biopsies from two DLBCL patients with either MYD88^{wt} or MYDD88^{L265P} were co-cultured in the presence of a feeding stromal monolayer and exposed for 24 hours to the different drugs as above. While it was almost inactive in MYD88^{wt} cells, the drug combination induced a 16% augmentation in relative apoptotic cell death in the MYD88^{L265P} primary co-culture (Figure 16, left panel). This phenomenon was accompanied by a 12% decrease in the fraction of cells with high contents in *IL6* mRNA, a percentage superior to what was observed upon treatment with each drug alone (Figure 16, right panel).

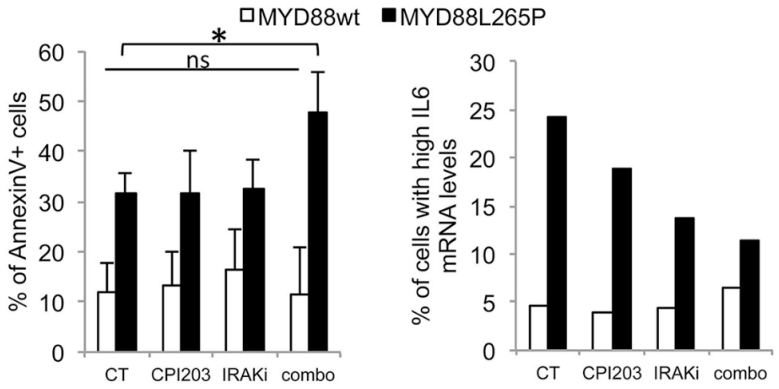

Figure 16. – Antitumoral activity and IL6 quantification in patient samples. ***Left panel:*** antitumoral activity of CPI203 (0.5 µM) and/or IRAKi (50 µM) was evaluated after a 24-hour culture of primary lymph node biopsies from ABC-DLBCL patients with either MYD88^{wt} or MYD88^{L265P} by cytofluorimetric quantification of AnnexinV+ cells. *Right panel*: DLBCL cultures treated as above were labeled with an IL-6 Hu-Cyanine 5 SmartFlare RNA detection probe (Merck Millipore), and percentage of viable cells with high contents in IL6 mRNA was determined by flow cytometry.

Collectively, this last set of results suggest that BET bromodomain inhibition cooperates synergistically with IRAK1/4 inhibition by avoiding the reactivation of NF-kB-regulated genes, thus promoting apoptotic cell death specifically in ABC-DLBCL cell lines and primary samples with MYDD88^{L265P}.

To assess the efficacy of the drug combination *in vivo*, NSG mice were subcutaneously injected with OCI-LY3 cells, and tumor-bearing animals received daily doses of either IRAKi (5 mg/kg, i.p., BID), CPI203 (2.5 mg/kg, i.p., BID), the combination of both agents, or the equivalent volume of vehicle, for 11 days. Figure 17 shows that CPI203 and IRAKi single agents induced a 31.5% and 46.3% reduction in tumor growth, respectively, while the combination of both drugs significantly improved this effect with a 65.6% decrease in tumor volume, when compared to vehicle-receiving animals (* p=0.011; ** p=0.007).

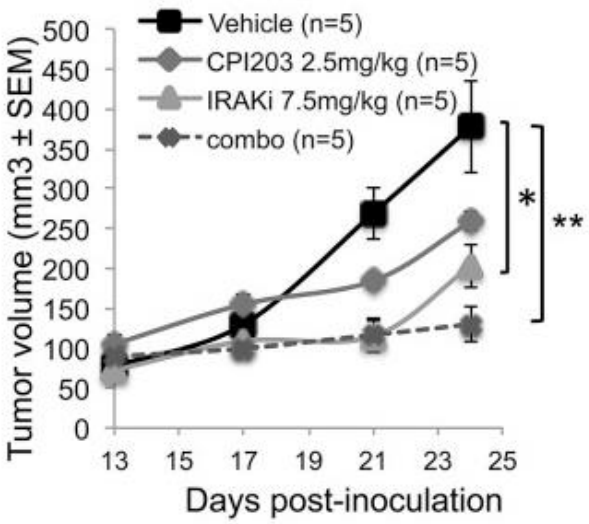

Figure 17. – Tumor growth kinetics in in vivo model. NOD/SCID IL2Rγ-null (NSG) mice were inoculated subcutaneously with 10^7 OCI-LY3 cells and after 13 days, tumor-bearing animals (n=5 mice per group) received intraperitoneal (i.p.) injection of 2.5 mg/kg CPI203 (BID) and/or i.p. administration of 7.5 mg/kg IRAKi (BID), or an equal volume of vehicle, for 11 days, in a five/two (on/off) schedule. Tumor volumes were measured each 2-3 days with external calipers.

Histological analysis of the corresponding tumors revealed an improved reduction of mitotic index together with an accumulation of apoptotic cells by the combination therapy, as assessed by phospho-histone H3 and activated-caspase-3 staining, respectively (Figure 18). In agreement with *in vitro* results, an enhanced reduction in the levels of CD44 and MCL-1, and an improved downregulation of nuclear p50 used as readout of NF-κB activity, were observed in the combination group when compared with the other arms (Figure 18). Collectively, these results confirmed our *in vitro* observation that the combination of IRAK1/4 inhibitor with the BET inhibitor CPI203 synergistically enhances the antitumoral properties of each single agent in ABC-DLBCL, mainly through the blockade of NF-κB signaling, followed by the downregulation of MCL-1 and the induction of apoptosis.

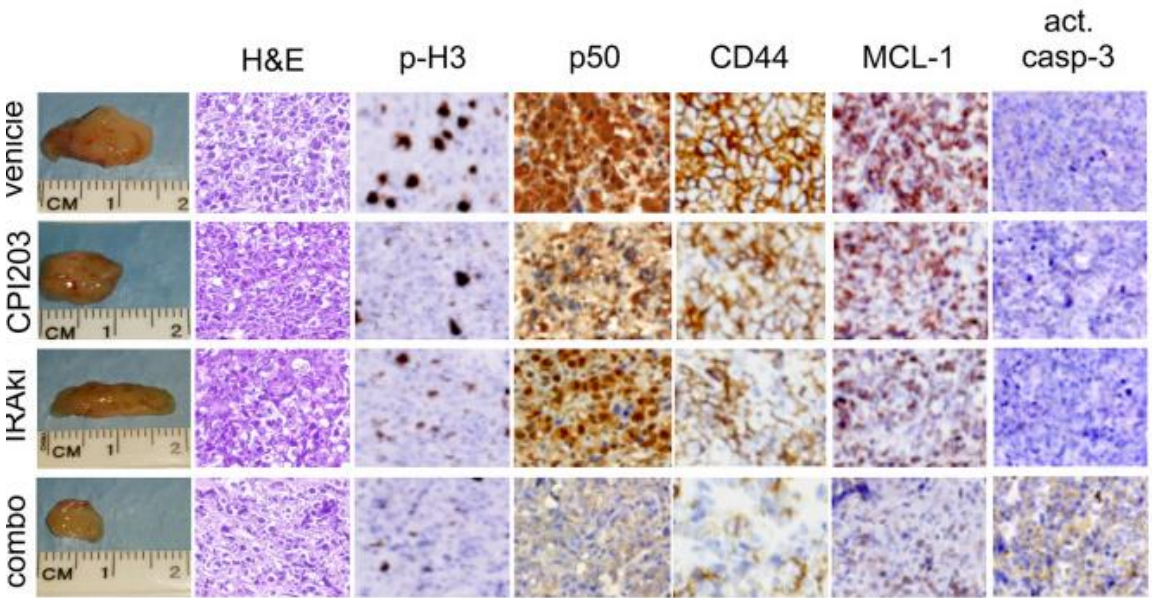

Figure 18. - Immunohistological analysis of consecutive tumor sections from representative animals. A notable decrease in mitotic index and in the NF-κB-regulated CD44, as well as a strong downregulation of MCL-1 and induction of apoptosis is seen in IRAKi-CPI203 combo group.

1.3. Dual blockade of IRAK and bromodomain activities favors the disruption of NF-kB-CD44 axis

Among the different above-mentioned genes, we and others have identified CD44 expression and IL-6 serum levels as potent prognostic markers in DLBCL [16,17]. To investigate the role of these two factors in the response of ABC-DLBCL cell lines to IRAKi-based treatment, HBL-1 and OCI-LY3 cells were stimulated with 0.5 µM of the CD44 ligand, hyaluronic acid (HA), or exposed to a 5 µg/ml dose of the IL-6 blocking antibody tocilizumab, prior to a 72-hour treatment with the drugs. In the case of HA, cells were exposed to IRAKi (50 µM) +/- CPI203 (500 nM0.5 µM), while effect of tocilizumab pre-treatment was evaluated in IRAKi-treated cells. Cell response was determined by fluorescence microscopy recounting of cells with high contents in F-actin and by MTT assay, respectively. As shown on figure 19 left panel, both IRAKi and CPI203 were able to block actin polymerization by 50.4% and 54.5%, respectively, while the drug combination achieved a total 77.9% decrease in cells with high contents in F-actin following stimulation of CD44 by HA.

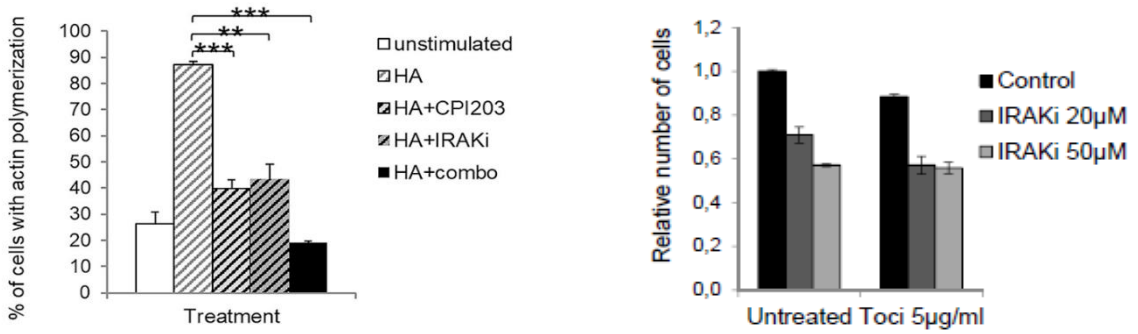

Figure 19. – Combinatorial inhibition of IRAK and Bromodomain disrupts NF-kB-CD44 axis. **Left panel)** HBL-1 y OCI-LY3 cell lines were preincubated for 24 hours with 0.5 mM CPI203 and/or 50 mM IRAKi, followed by a 24-hour stimulation with 0.5 mM HA, labelling with 50 mM Phalloidin-TRITC (Sigma-Aldrich) and recounting of red fluorescent cells on a Nikon H5505 microscope by means of a 20X/1.30 NA oil objective (Nikon) with the use of Isis Imaging System v5.3 software (MetaSystems GmbH) (***P<0.001). **Right panel)** Cells were exposed 24h to 20 or 50 µM dose of IRAKi together with 5 µg/ml Tocilizumab (Toci) showing no differences in cell death when exposed to both concentration of anti-IL-6 antibody.

In contrast, the anti-IL-6 antibody failed to sensitize ABC-DLBCL cells to IRAKi-based treatment (19 right panel), suggesting that the modulation of this cytokine alone was not essential for the activity of the compounds. Thus, these results suggest a significant activity of the drug combination towards CD44 downstream signalling, while IL-6 expression may not be directly involved in the effect of these agents.

2. HOIP AS A NOVEL THERAPEUTIC TARGET IN ABC-DLBCL

2.1. Design of a novel covalent inhibitor of HOIP

Our partners from the group of Pharmaceutical Chemistry at Institut Químic de Sarria (IQS) undertook a computational study that consisted of a combinatorial substitution of several α-β unsaturated moieties to be used as covalent binding warheads to the catalytic cysteine residue of HOIP. The resulting chemical library was used on subsequent molecular docking to assess the best HOIP binding candidates. Four candidates were synthesized and after a preliminary trial in a panel of ABC-DLBCL cell lines, we isolated compound A (Cpd A), a covalent irreversible inhibitor of HOIP with a pyrido[2,3] pyrimidine core, which is used along this part of this dissertation (Figure 20).

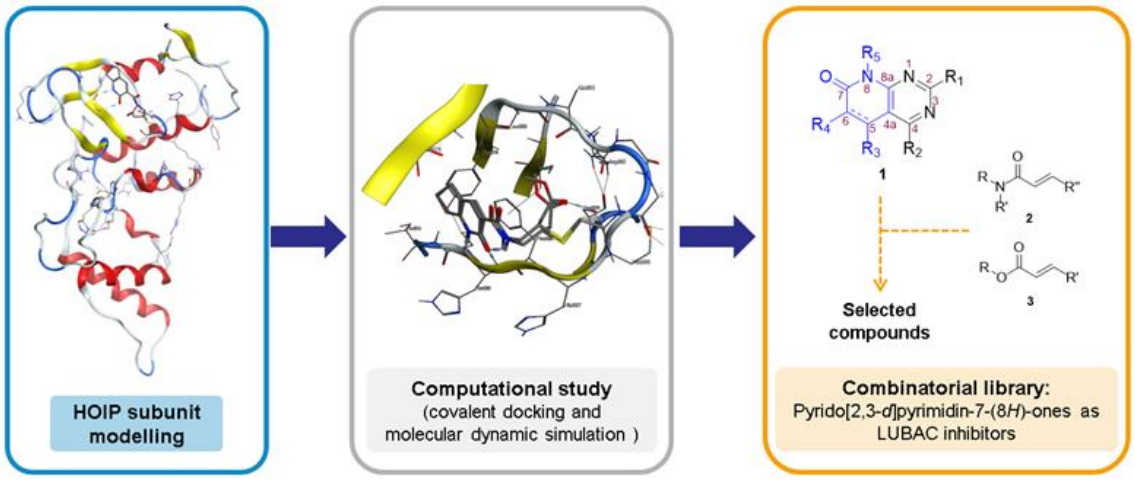

Figure 20. – Computational routes used for the selection and synthesis of Cpd A.

To validate the specificity of Compound A to its target HOIP we carried out a Drug Affinity Responsive Target Stability (DARTS) assay, which constitutes a relatively quick and straightforward approach to identify potential protein targets for small molecules. This assay relies on the protection against proteolysis conferred on the target protein by interaction with a small molecule. As shown on Figure 21, Compound A binds to HOIP giving certain degree of protection against proteolysis, which is not seen in the case of β-Tubulin which shows a similar degree of degradation independently of the concentration of Compound A. As expected,

higher concentrations of Compound A, protect HOIP from pronase digestion as seen by a preserved detection of HOIP by western blot. As the concentration of Cpd A is decreased, levels of HOIP protein detected are reduced even at low concentrations of pronase, becoming nearly anecdotal in absence of Compound A (Control (DMSO) panel). Thus, these results suggest a specific activity of our experimental compound towards HOIP.

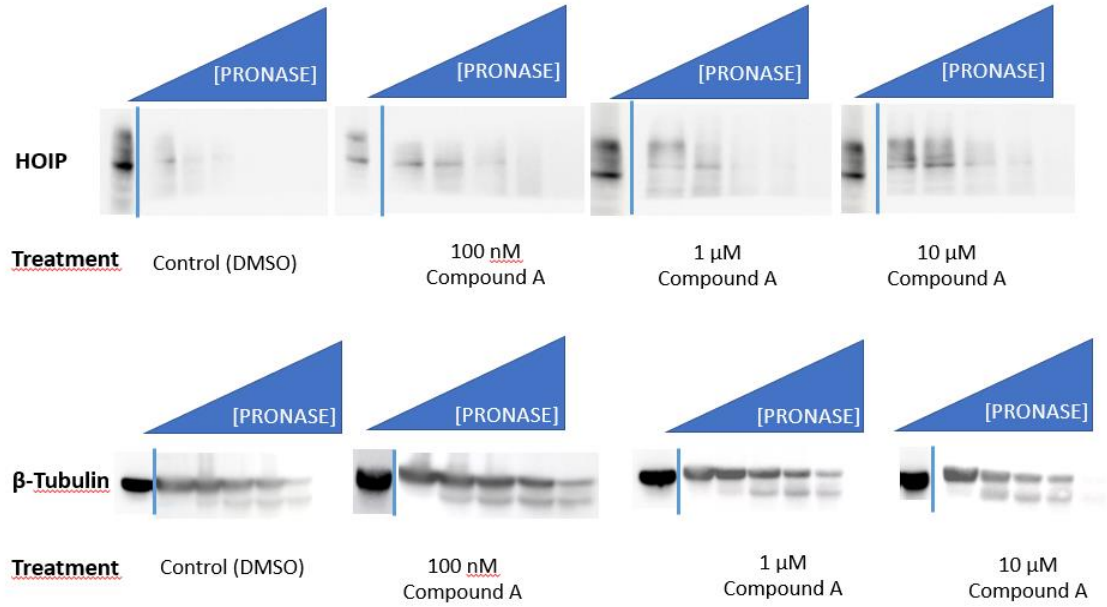

Figure 212. - DARTS assay shows specificity of Cpd A towards HOIP.

2.2. Single agent activity of HOIP antagonist in preclinical models of ABC-DLBCL

2.2.1. In vitro 2D models (HOIP^{wt} vs HOIP^{KO})

A set of five well characterized DLBCL cell lines of both GCB (KARPAS422 and U2932) and ABC subtype (HBL-1, OCI-LY3 and TMD8), were cultured for 24 or 48 hours in the presence of Cpd A, and drug cytotoxic activity was analysed by MTT assay. As shown on Figure 22, we observed only a partial response to the compound in the form of an increase in cytotoxicity in the different cell B cell lymphoma cell lines of up to a 50% after 48h of treatment. IC_{50} on the different cell lines are displayed on Table 10.

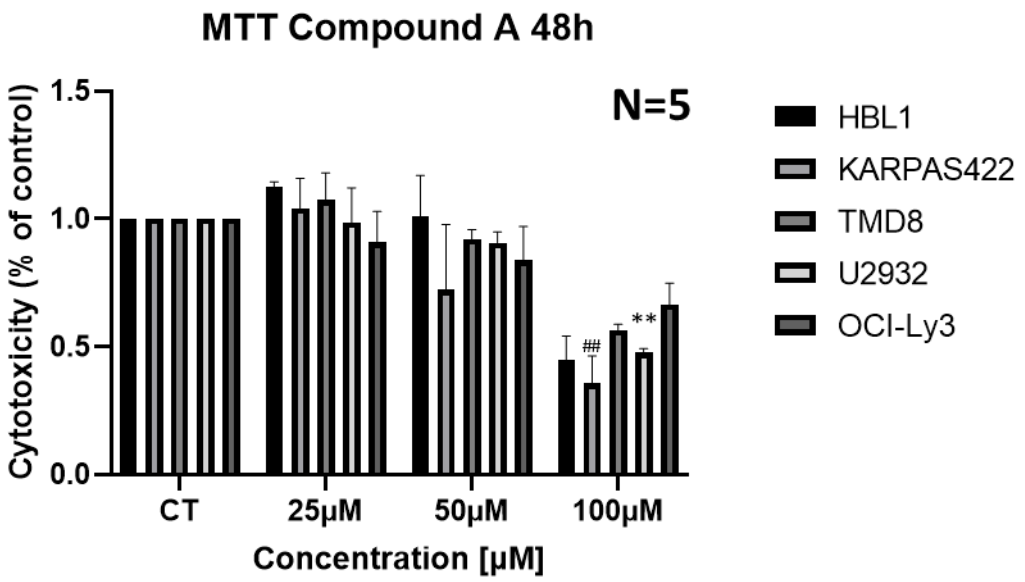

Figure 223. – Cytotoxic effect of Cpd A in a panel of DLBCL cell lines. MTT assay shows that the novel HOIP inhibitor elicits a partial blockade of DLBCL cell proliferation upon a 48h exposure to increasing concentrations of the molecule.

Cell line	IC50 (48h)
HBL1	72.2263µM
KARPAS 422	58.43µM
TMD8	>100µM
U2932	69.87µM
OCI-Ly3	>100µM

Table 10. – Compound A IC_{50} in the five different DLBCL cell lines after a 48-hour treatment.

We then evaluated if this cytotoxic effect could be related to the blockade of the NF-kB pathway, resulting in the downregulation of the NF-κB-regulated genes known to promote ABC-DLBCL pathogenesis, as before. For that aim, we analysed the expression of five bona fide NF-kB-regulated factors at both mRNA and protein levels, respectively by RT-qPCR and western blot (Figure 23.) Treatment with Compound A led to a 2-fold accumulation of the intracellular inhibitor of NF-κB, IκBα, and accordingly, several NF-kB regulated factors underwent a reduction in protein levels, reaching 72% in certain cell lines and determined factor (like MCL-1), supported by a consistent reduction in mRNA levels (up to 60%). Other factors associated with NF-κB activation like CD44 also experience a downregulation upon exposure to Cpd-A of between a 40 and an 86% in protein levels depending on the cell line.

The effective suppression of a NF-κB gene signature is further validated as *IL6* and *IRF4* levels underwent a dramatic reduction compared to basal levels (-81% and -86% reduction respectively). Interestingly, *MYC* was also decreased by 40% at both transcriptional and protein levels upon HOIP inhibition, warranting the exploration of combination therapies.

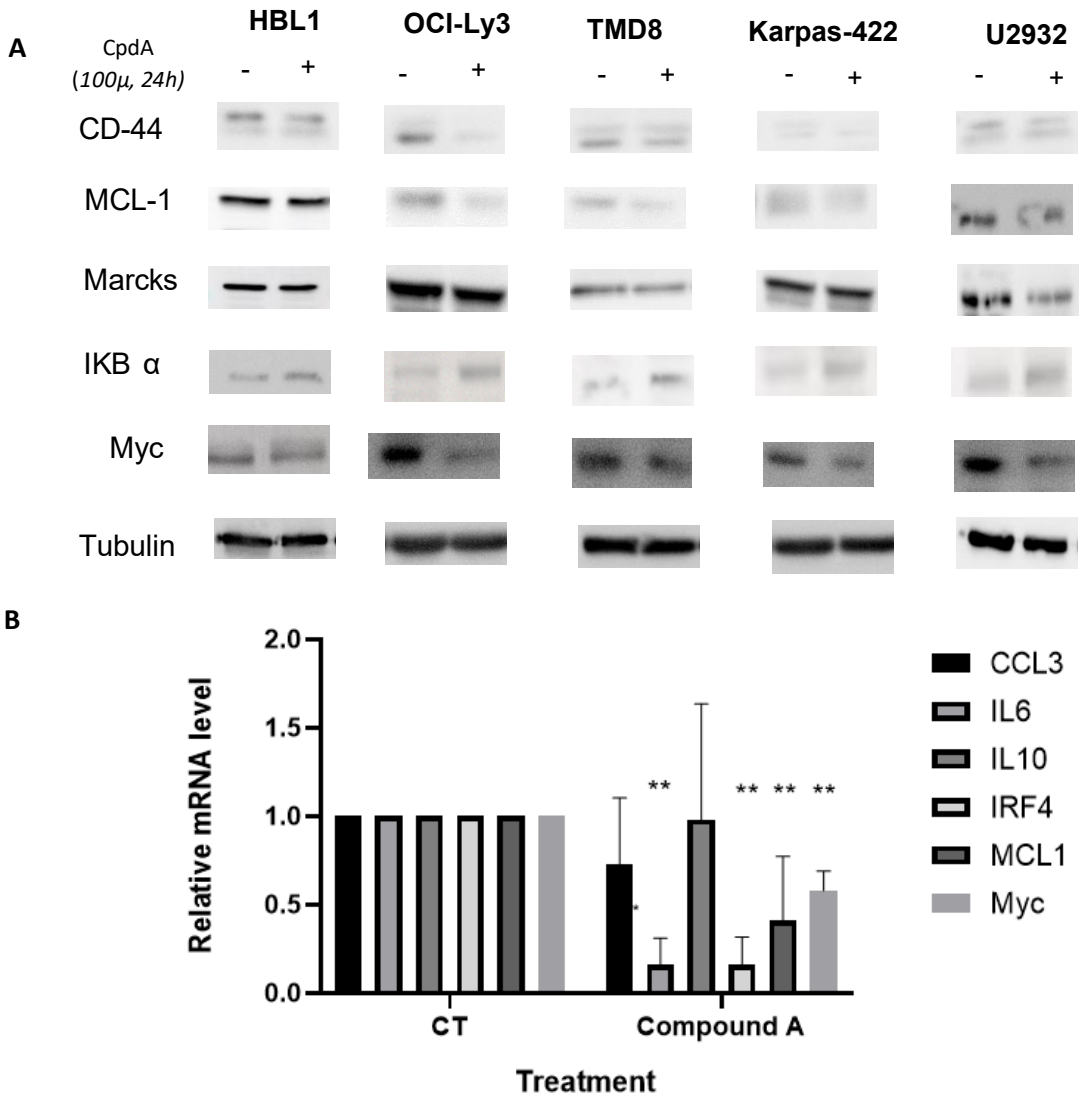

Figure 234. – Cpd A-mediated HOIP blockade results in the inhibition of NF-κB signaling pathways. A) This blockade led to intracellular accumulation of IκB, and subsequent downregulation of MYC, CD44, MARCKS and MCL-1 proteins in ABC-DLBCL cells with MYD88^{L265P}, ABC-DLBCL with MYD88^{wt} and a GCB-DLBCL cell line. B) RT-qPCR analysis of NF-κB downstream genes exposed to CpdA as before further demonstrates the inhibition of this downstream pathway.

Importantly, no significant cytotoxic effect was noticed in peripheral blood mononuclear cell (PBMC) cultures obtained from 4 different healthy donors (Figure 24.), suggesting a specific activity of Cpd A towards malignant B cell.

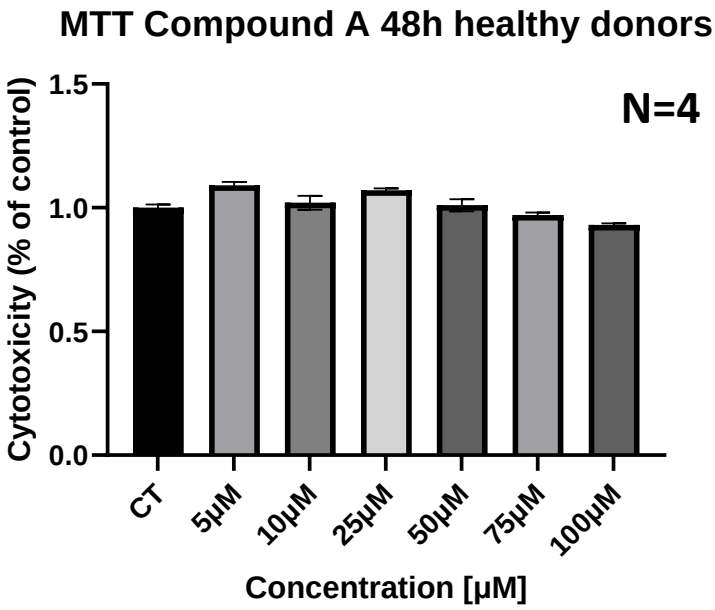

Figure 245. – Cpd A is safe in healthy PBMC cultures. MTT assay shows that the novel HOIP candidate inhibitor has no effect on peripheral blood mononuclear cells (PBMC) of healthy donors after 48h of treatment.

To confirm the specificity of Cpd A at targeting exclusively HOIP, we CRISPR-engineered a HBL1-HOIP knock-out (KO) cell line. For this purpose, protein extracts from the CRISPR pool were obtained to confirm a decrease in HOIP protein expression (Figures 25B and 25C) and then exposed for 48h to our molecule. We found after densitometry analyses of western blot membranes a decrease of close to 60% on HOIP protein levels in the pool (Figure 25C), in accordance with an almost complete abrogation of Cpd A cytotoxic effect at 48 hours (Figure 25A).

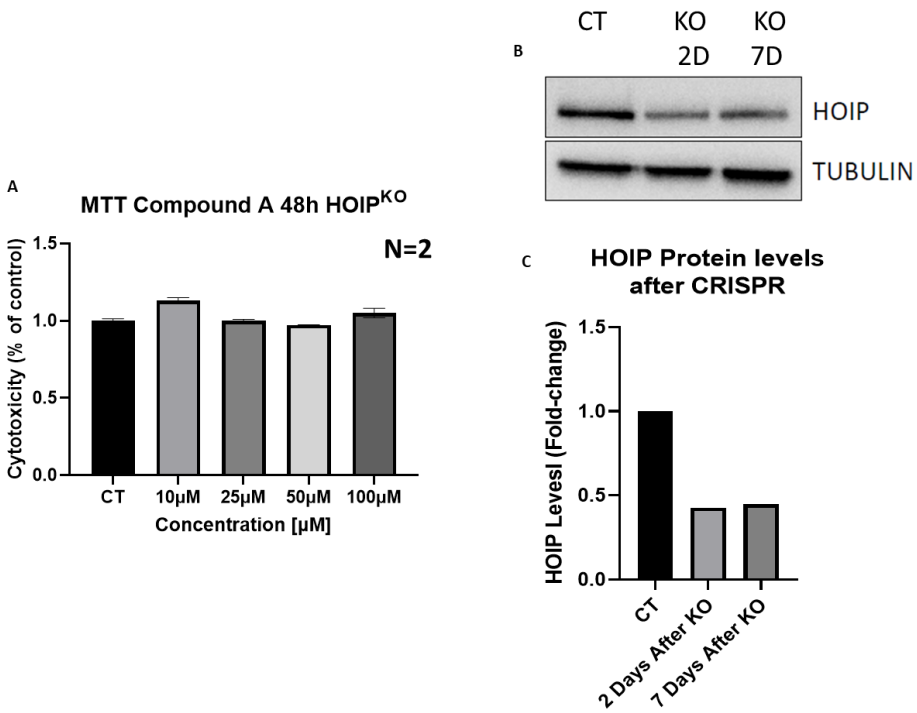

Figure 256. – Cpd A loses activity in a CRISPR-engineered HBL1–HOIP^{KO} cell line. A) MTT assay shows that the novel HOIP inhibitor loses its cytotoxic effect in a genetically engineered cell line with reduced HOIP expression. B) Western Blot analysis of the pooled HOIP knock-out cell line after 2 and 7 days after electroporation. C)Densitometry analysis of western blot membrane quantifying the reduction of HOIP protein levels to a 40% after CRISPR mediated knock-out.

2.2.2. Efficacy and safety of Cpd A in an in vivo (CAM-derived) xenograft model of ABC-DLBCL with MYD88^{L265P}

To further address whether Compound A maintains its antitumor activity and its safety profile *in vivo*, we developed and established a chick embryo chorioallantoic membrane (CAM) model of ABC-DLBCL using the HBL1 cell line. This non-animal model has long been used in cancer research to study angiogenesis, tumour growth and metastasis, and treatment responses as mentioned in the introduction of this dissertation. For this assay, cells were deposited in matrigel medium on top of chick embryo membrane at day 9 after fertilization in a total of 20 eggs, 10 for control group and 10 for treatment with Compound A group. Each egg received two doses (day 12 and 14 after fertilization) of Compound A at 100 µM or DMSO (in the case of the control group) on the site of cell engraftment.

After day 16, eggs were opened and, to assess the toxicity of the treatment, embryos were weighted showing no difference in weight or visual features (size, feather, and beak formation) between the control and the treatment group (Figure 26, right panel). Most importantly, the weighting of the harvested tumours pointed out a significant impairment of tumour growth in eggs treated with compound A, suggesting that the antitumoral activity seen in *in vitro* models was maintained in *in ovo* models (Figure 26, left panel).

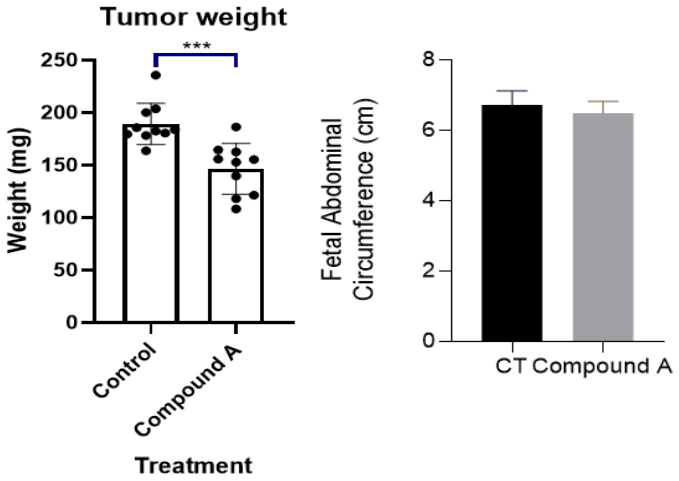

Figure 267. - Tumor weight and fetal abdominal circumference at ED 16. Cpd A significantly impairs tumor growth without exerting toxic effects during the embryo development.

Embryos were sacrificed and brain, liver, spleen, and bone marrow were recovered for quantification of infiltrated tumour B cells. For this purpose, organs were mechanistically disaggregated, and total DNA was extracted for qPCR-mediated detection of human specific ALU-sequences. As shown on Figure 27, treatment with compound A reduced the capacity of the tumour cells to migrate to other organs, being this metastatic capacity significantly impaired in brain (-42.5%, P-value=0.001), in bone marrow (-79%, P-value<0.0001), and in liver (-33.7%, P-value=0.0223). Regarding the spleens, a reduction of 62.4% in cell infiltration was detected, although not statistically due to the large variation in the control group (P-value=0.082).

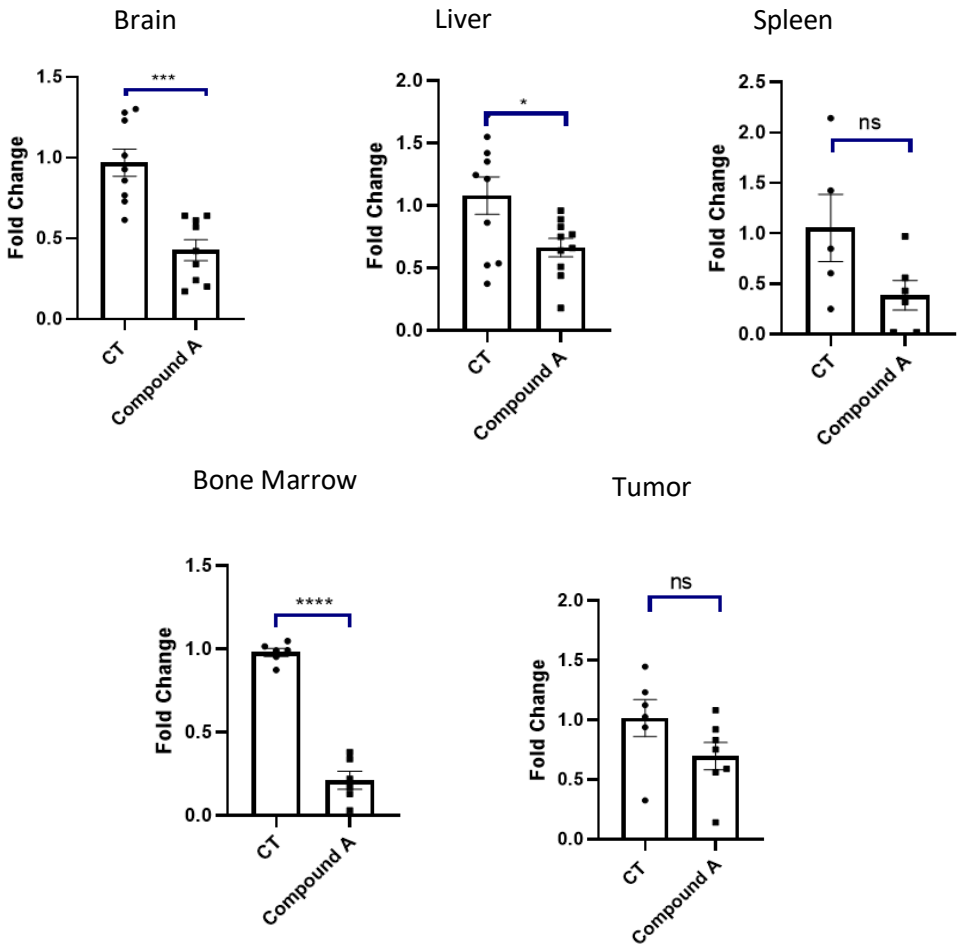

Figure 278. – Cpd A blocks tumoral B-cell migration and infiltration. Detection of human ALU sequences by QRT-PCR. The exposure to two fixed doses of Cpd A significantly impairs ABC-DLBCL migration and invasion of different tissues within the chicken embryo. (P-values: * = 0.0223; ***=0.001; ****<0.0001).

2.3. Development of in vitro multicellular 3D models of B-cell lymphoma.

A variety of different 3D cell culture platforms exist, from protein gels to nano-patterned plates, with wells <1 µm patterned within the well where cells aggregate. While these systems approximate tissue environments to varying degrees, they have technical and cost limitations, such as long fabrication times, specialized equipment, and either attachment to stiff substrates that influence cell behaviour or detachment that makes 3D cultures difficult to handle.

We set up a three-dimensional (3D) *in vitro* model of B-NHL using the Nanoshuttle technology. For this purpose, lymphoma cells were pre-incubated overnight with a magnetic nanoparticle assembly, containing gold, iron oxide and poly-L-lysine (Nano-shuttle), to allow cell attachment to the magnetic nanoparticles. At day 0, cells were resuspended in medium in an ultra-low adherence 96-well plate and a magnetic drive was placed below the well plate. Because of the magnetic field, cells were attracted to the same spot within the well, where they aggregated and started interacting between them to form larger 3D structures (Figure 27). Once the structures were fully formed, the therapeutic agents (compounds, antibodies, etc…) could be added to each well at specific concentrations. Drug activity could be assessed on 3D cultures using the same readouts as in classical 2D cultures, including MTT, western blotting, immunofluorescence, ADCP, ADCC, etc... The magnetic nanoparticles have been shown to not affect cell proliferation and metabolism or induce an inflammatory response [1] and similarly, exposure to the magnetic field generated by our magnets, which ranges between 30–500 G has no major effect on cell proliferation, metabolism or inflammatory response [1,2] although magnetic fields of higher strength (800–4,000 G) have been shown to influence cell behaviour.[3]

Multicellular DLBCL spheroids were generated using a panel of DLBCL cell lines like Karpas-422-GFP, HBL-1, TMD8, etc, in association with ectopic components of the lymphoid tumour microenvironment (TME), including dendritic follicular cells (HK cell line)(123) and M2-polarized macrophages, previously described to support the growth of DLBCL tumours.(124)

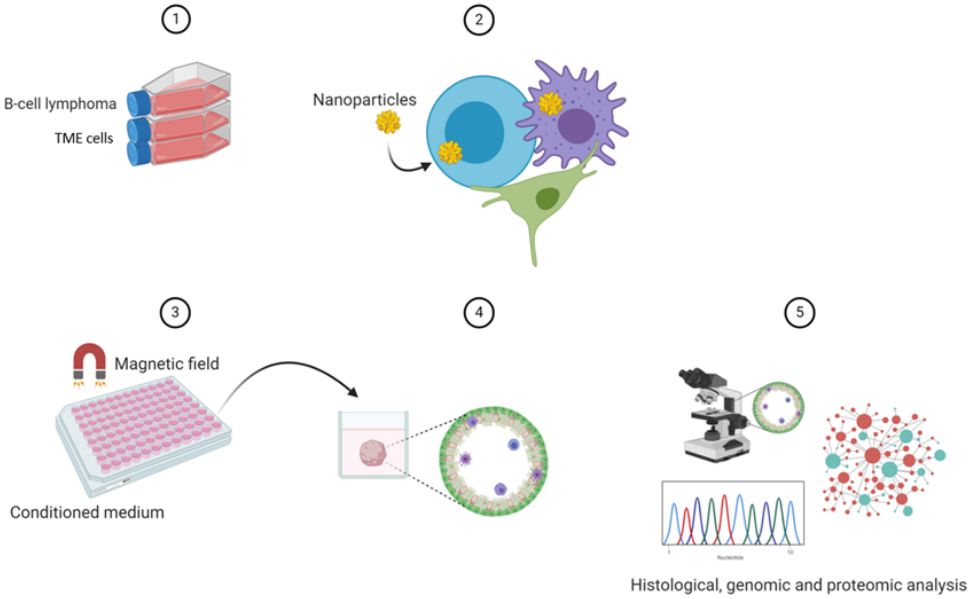

Figure 98. – 3D culture system by magnetic bioprinting.

Since there was no background in the literature on the 3D bioprinting cell culture system for the study of DLBCL and its microenvironment, we first carried out multiple standardization procedures, starting with a single cell population to determine the appropriate volume of nanoparticles, the optimal incubation time, the medium composition, and the cell density. The data shows the formation of multicellular spheres with a uniform structural conformation with an organized and continuous edge and with intercellular spaces (Figure 29).

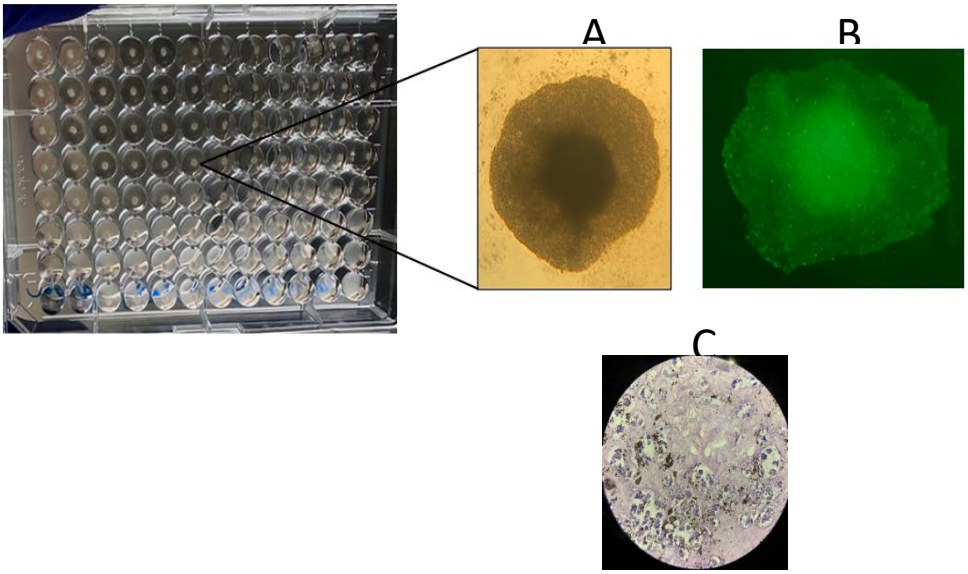

Figure 109. - Evaluation of organotypic multicellular spheres. Morphologic characteristics (A), fluorescence (B) and histological (C) of DLBCL multicellular spheroids.

In addition, DLBCL organotypic multicellular spheres may be mechanically disrupted and B cells purified using the CD20+ magnetic separation kit (EasyStep, Stemcell Technologies) to store cellular pellets at for subsequent molecular analysis when required.

One of the first troubleshooting we found, is that polarized M2 macrophage populations in the spheres had tendency to disappear within the first 7 to 10 days of 3D culture, making it difficult to evaluate the stability of the spheroids before proceeding to evaluate drug effect on them. This was due to macrophage death or lose of polarization. To try and increase both macrophage lifespan and M2 polarization we tested supplementing macrophage culture media with M-CSF alone or together with IL-4. After 14 days of cell culture both stimulating medias showed significant increase in both macrophage viability and M2 polarization by flow cytometry analysis of Annexin V staining and CD206 expression respectively (Figure 30. top panels). If the culture of the spheroids was to be extended for a week the combination of M-CSF and IL-4 showed significant increase of both variables in comparison with unstimulated or stimulated only with M-CSF macrophage cultures (Figure 30, lower panels, and Figure 31).

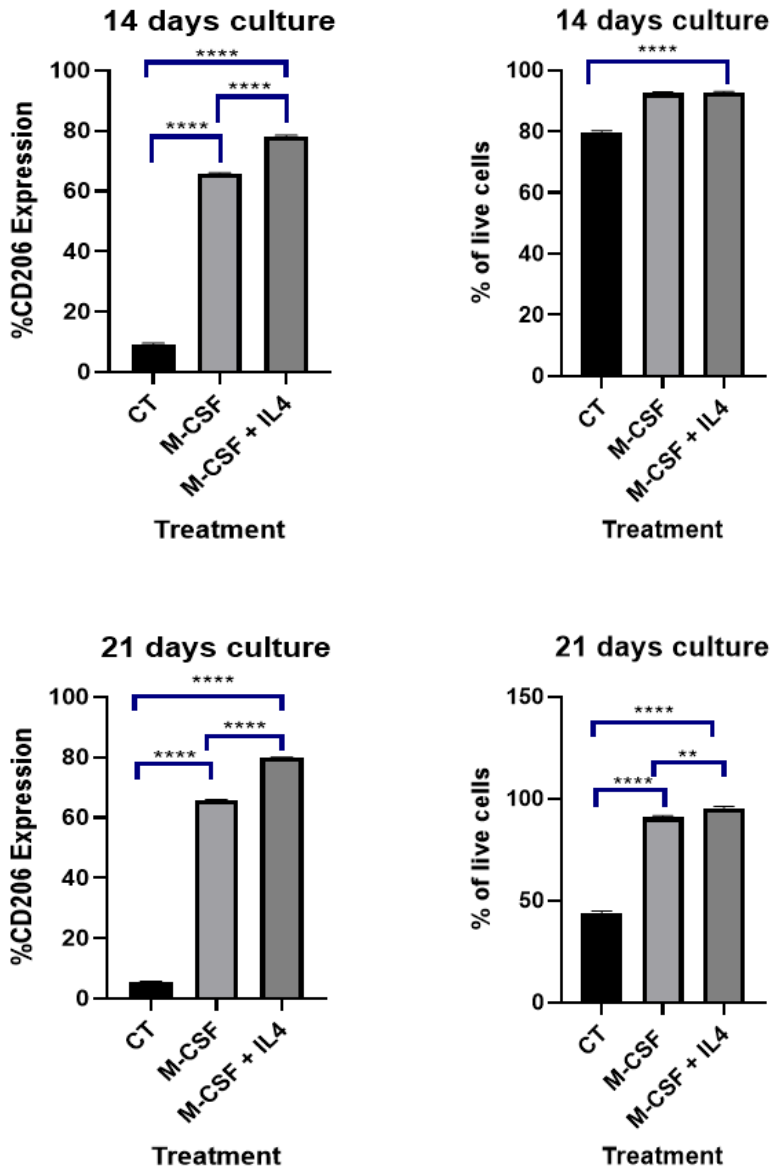

Figure 30. - Macrophage viability and CD206 expression. Top panels after 14 days in culture. Lower panels after 21 days in culture. (P-values: **=0.0016; ****=<0.0001)

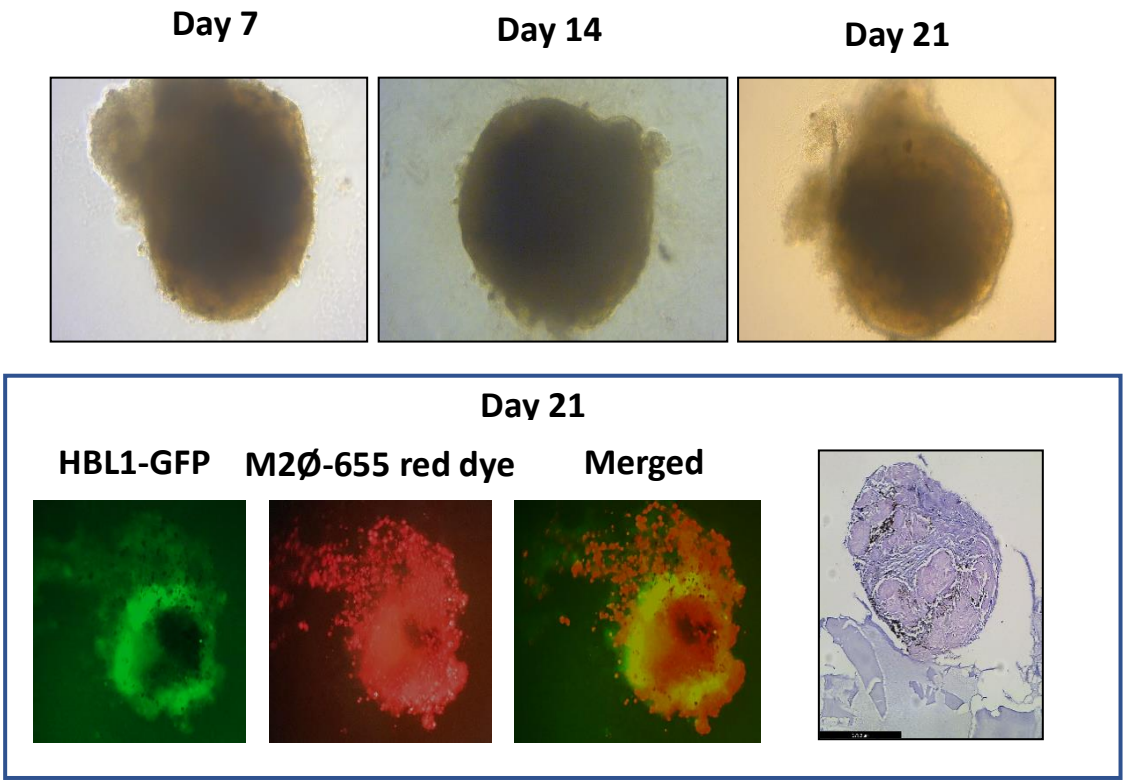

Figure 31. – Organotypic multicellular spheres. Spheroids maintain their structure and cell viability for 3 weeks. At day 21, histological analysis shows architecture resembling a lymphoma biopsy.

In line with this dissertation, DLBCL cell line (Karpas-422 – GFP^+) 3D spheroids were generated adding into the model primary M2-polarized macrophages and in presence or absence FDCs and maintained in culture for 2 weeks. After this time the malignant B-cells were sorted by GFP expression and labelling of CD20. Protein extracts were obtained and send to the laboratory of Dr Pierre Lutz, from the Institut national de la santé et de la recherche médicale (INSERM – Toulouse) and collaborator within the POCTEFA-Proteoblood project in which this dissertation is based. Our collaborators purified the ubiquitome of these cells using a novel system and workflow base on Tandem Ubiquitin Binding Entities (TUBEs), which are engineered protein domains that bind specifically to polyubiquitin chains, followed by a mass spectrometry analysis (Figure 32).

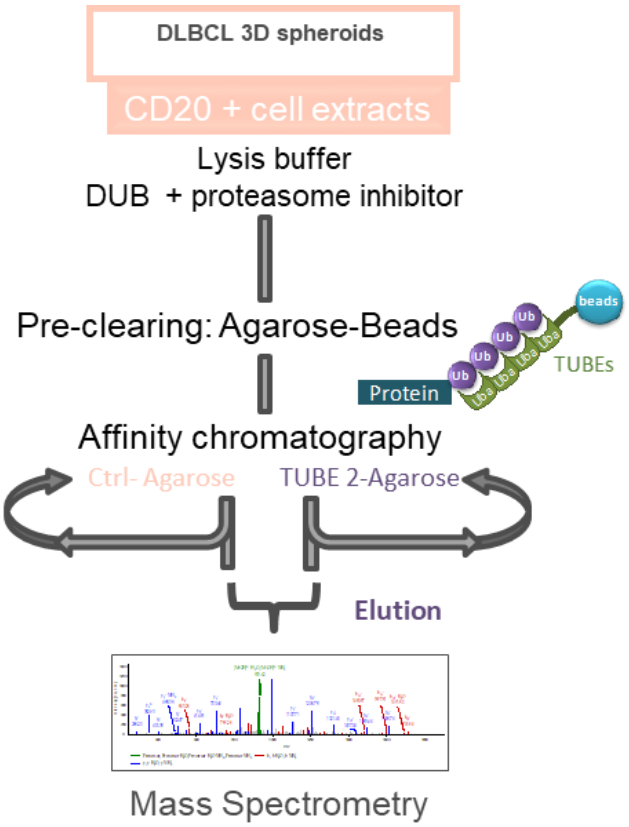

Figure 3211. – Workflow of DLBCL ubiquitome analysis coupling 3D tumor modeling to TUBES-Mass spectrometry analysis.

Interestingly, the complexity of the ubiquitome was related with the complexity of the microenvironment as more ubiquitinated proteins were detected by western blot in ubiquitome purified samples originated in more complex 3D organoids (Figure 33A). This result, was further validated by the analysis of mass spectrometry data, as shown on the heatmap below (Figure 33B) as a high proportion of ubiquitinated proteins are enriched in spheroids formed by coculture of DLBCL cells, M2 macrophages and FDCs when compared with simplified models formed by DLBCL cells and M2 macrophages alone. As we expected, within these enriched ubiquitinated proteins we found HOIP (Figure 33C), which gives an extra level of interest for this target as we demonstrate that its ubiquitination gets enriched

in *in vitro* models that better represent the complex microenvironment of DLBCL and the biological and physiological reality in patients.

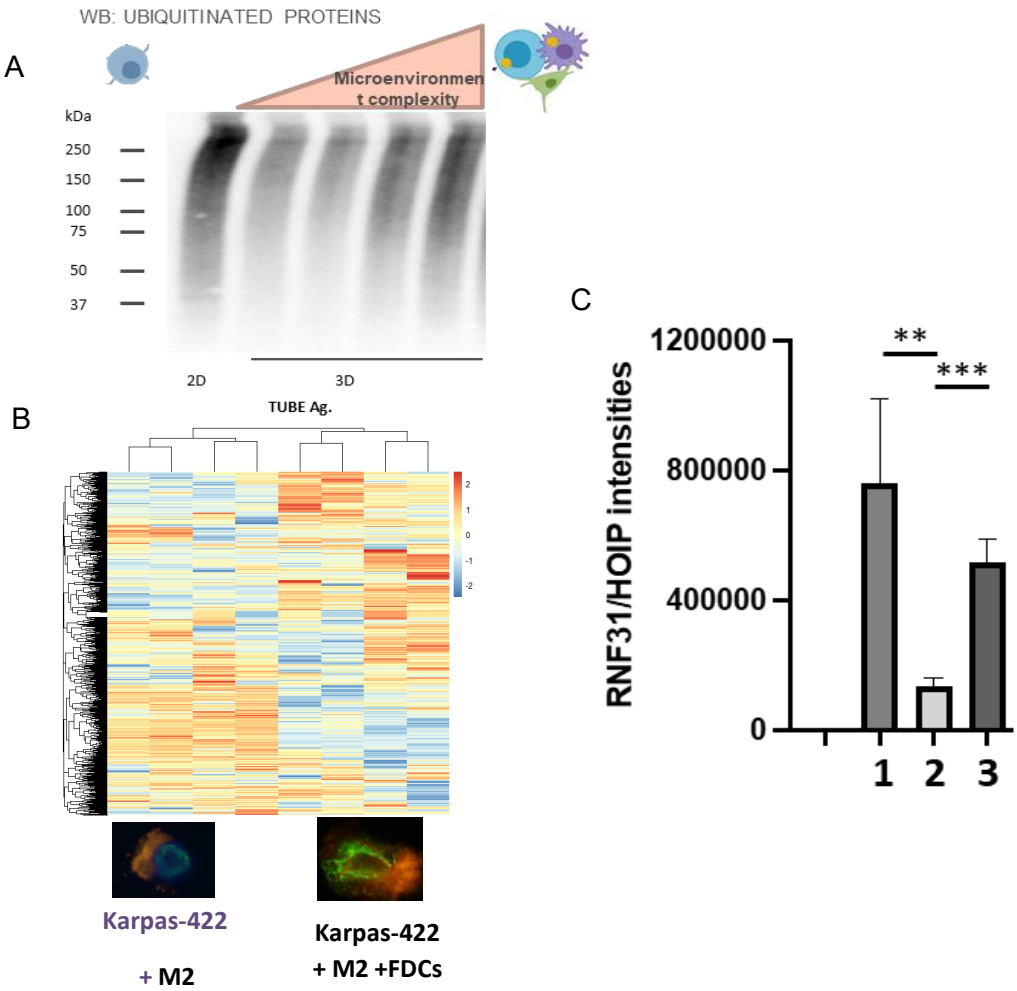

Figure 33. – Ubiquitome gets enriched as microenvironment complexity increases. A) Western blot of ubiquitinated proteins after purification with TUBEs in 3D spheroids with increasing levels of complexity. B) Heatmap of ubiquitinated proteins comparing spheroids consisting of DLBCL cell line and M2 macrophages vs. DLBCL cell line, M2 macrophages and FDCs. C) TUBES-MS quantification of HOIP contents within the ubiquitome of DLBCL conventional monoculture (1), DLBCL 3D spheroids (2) and DLBCL + M2 macrophages 3D spheroids (3).

Apart from these results and this dissertation, our novel 3D model for lymphoma based on magnetic bioprinting, has already been used in the testing of several compounds and is part of various works already published by our research group, which can be found in the annexes of this dissertation. However, CpdA has still not been trialled at the time of the drafting of this dissertation.

DISCUSSION

DISCUSSION

NF-kB transcription factors are major drivers of tumour initiation and progression. NF-kB signalling is constitutively activated by genetic alterations or environmental signals in many human cancers, where it contributes to almost all hallmarks of malignancy, including sustained proliferation, cell death resistance, tumour-promoting inflammation, metabolic reprogramming, tissue invasion, angiogenesis, and metastasis.(125) These characteristics make the NF-kB pathway a very attractive therapeutic target in a broad range of human cancers, as for instance DLBCL, as its constitutive activation is a hallmark of this pathology, specially the ABC subtype.

Currently, however, there is no clinically useful NF-kB inhibitor to treat oncological patients, owing to the preclusive, on-target toxicities of systemic NF-kB blockade. Thus, there is a need to develop new alternatives to tackle these pathways in a diversity of human pathologies.(126)

SIMULTANEOUS BLOCKADE OF TLR SIGNALING AND EPIGENETIC READERS EXERTS SYNERGISTIC ACTIVITY IN MYD88MUT ABC-DLBCL

Pathological activation of the Toll-like receptor signalling adaptor protein MYD88 underlies many autoimmune and inflammatory disease states. In the ABC subtype of DLBCL, the oncogenic MYD88^{L265P} mutation (detected in around 30% of cases) promotes cell survival by spontaneously assembling the myddosome, (a protein complex containing IRAK1 and IRAK4), which leads to IRAK4 kinase activity, IRAK1 phosphorylation, and NF-κB signalling, thus being making this mutation one of the most prevalent activating mutation in this malignancy.(32) Within MYD88 downstream signalling cascade, IRAK4 accounts for almost all of the biological functions of the adaptor protein, and pharmacological inhibition of IRAK4 is highly effective in MYD88^{L265P} ABC-DLBCL cultures and tumour xenograft models. (127)

However, it was recently reported that pharmacological inhibition of IRAK4 kinase activity mainly affected TLR-dependent cytokine production, with no alteration in the formation of the myddosome and with only a minimal effect on NF-κB signalling.(128) Selective inhibition of IRAK1 also displayed cytotoxicity in MYD88-mutated cell lines, either alone or in combination with ibrutinib.(129) Dual IRAK1/4 inhibition has shown promising activity in primary samples and mouse models of Waldenström's macroglobulinemia (WM), a lymphoid malignancy where mutations of MYD88 at p.L265P are found in 95-97% of the cases.[20] Based on these data and considering that IRAK1 and IRAK4 are both required for oncogenic MYD88 signalling in DLBCL, there is a great interest in exploring the impact of concomitant blockade of both kinases in MYD88-mutated tumours.(32)

Here we demonstrate that dual inhibition of IRAK1 and IRAK4 kinases leads to modest cytostatic activity in $MYD88^{L265P}$ ABC-DLBCL cells, in relation with the incomplete inactivation of NF-κB transcriptional activity. The mechanisms underlying this partial blockade of NF-κB signalling are still to be determined. A possible explanation may reside in the described stabilization of $MYD88^{p.L265P}$ by the heat shock protein HSP110 which facilitates chronic NF-κB activation in lymph node biopsies of patients with ABC-DLBCL.(130) HSP110 chaperoning activity might be engaged in ABC-DLBCL in response to endoplasmic reticulum stress and the adaptive mechanisms that are triggered upon dual IRAK1 and IRAK4 blockade in these cells.(131)

Considering the entire TLR signalling pathway and the effect of MYD88 p.L265P mutation, it seemed logic that the inhibition of IRAK1 and IRAK4 should reduce tumour survival in ABC-DLBCL. Although the use of a bispecific inhibitor for IRAK had a cytotoxic effect, especially in ABC-DLBCL cell lines, this effect was partial (25.5%) and transitory decreasing from 25.5% to 19% in only 48h. When checking by western blot its capacity to inhibit activation of IRAK proteins it demonstrates its effectiveness especially towards IRAK1. However, the residual activated protein molecules, should not be sufficient to maintain the whole pathway functioning and over activate NF-kB. Moreover, after treatment with IRAKi, some NF-kB related genes which are involved the pathogenesis of ABC-DLBCL, such as IL6 or CCL3, are unaffected or even increased in at least one of the studied cell lines. Why only some cell lines respond in such way is still being studied, although previous research showed strong apoptotic effect in ABC-DLBCL.(132)

Thus, suggests the existence of parallel pathways resulting in the pathological activation of NF-kB related genes. As it was shown that the use of BET bromodomain inhibitors such as CPI203 effectively suppresses NF-kB gene signature, the combination of both drugs was suggested.(133) Consistently with what was expected, the combination of both agents did indeed show a synergistic effect when evaluating cytotoxicity, increasing the antitumoral effect from 19% when using IRAKi as single agent to an astonishing 86% when treated with the combination. However, so statistically significant difference is seen between CPI203 alone and the combination treatment. On the other hand, it is true that the combination has an increased effect that should be considered in further research.

Similar effect is seen when evaluating NF-kB related gene expression where IRAKi as single agent tends to increase gene expression, which is reduced dramatically when using combinatory treatment. However, as mentioned above, effect is not significantly different between CPI203 and combination although both agents together synergize reducing such expression. These results strongly agree with 17 previous reports focused on T-cell acute lymphoblastic leukaemia using the same inhibitory agents.

Interestingly, cytotoxicity effect is also seen in primary lymph node biopsies from DLBCL patients. However, it has been difficult to obtain fresh viable biopsies to proceed with the project, resulting in a difficult to extrapolate data obtain from only one biopsy. To assure the strength and significance of these results more biopsies should be included in the study which hopefully will happen within the following months.

When evaluating the efficiency and possible side effects of the treatments *in vivo*, the combination of both agents significantly improved the antitumoral effect of the treatment causing a tumour volume reduction of up to 65.6%, more than the double obtained by single agent therapy. Importantly, no serious side effects were observed on the tumour bearing animals. However only one cell line was used in animals. Seen the *in vitro* results, it is probable that this response could vary between the 3 studied cell lines, although no significant differences should be expected.

Although IRAK inhibition shows modest effects both in cytotoxicity and gene regulation in both *in vivo* and *in vitro* models, it is shown that BET inhibition is an efficient strategy to counteract NF-κB activity. In addition, it has been shown that it offers synergistic antitumoral and pro-apoptotic activities with IRAK inhibition, opening the door to its combination with

other existing drugs to reduce tumoral survival. For instance, seen the mortality and relapse rates of ABC-DLBCL patients, all positive results, for minimum that they may seem, should be taken into consideration as they may shed light to the discovery of efficient therapies that finally affect survival rates and patient's life quality.

LUBAC INHIBITION AS A NOVEL THERAPEUTIC TARGET IN ABC-DLBCL

Ubiquitination is a post-translational modification that plays many vital roles in protein degradation, ensuring a precise functioning, both spatial and temporal, of intracellular proteins. Its deregulation has been shown to contribute directly to the appearance and progression of various types of cancer, including DLBCL, the focus of this dissertation.(71) Thus, this highly regulated system has been for years an active research area for drug discovery which has resulted in a series of approved drugs and a vast list of possible new targetable candidates. (68) HOIP, the catalytic subunit of LUBAC, specifically conjugates linear (Met1) ubiquitin chains to various target proteins in the canonical NF-κB pathway playing a pivotal role in its normal and dysregulated signalling.(134) As it has been widely discussed in this dissertation, the inappropriate and sustained activation of NF-κB pathway is a signature feature of DLBCL, especially the more aggressive ABC-DLBCL.

It has been reported that two germline polymorphisms affecting HOIP are enriched in ABC-DLBCL patients (7.8%) although being rare in healthy individuals. These polymorphisms increase HOIP activity and therefore LUBAC enzymatic activity, and NF-κB engagement.(135) The majority of ABC-DLBCLs in patients with these HOIP SNPs also harbour the $MYD88^{L265P}$ mutation, previously evaluated in this dissertation. Given that LUBAC plays a pivotal role in NF-κB activation we speculated that LUBAC may be an interesting target to tackle aberrant NF-κB activation and consequently ABC-DLBCL. With our new 3D lymphoma models, that better represent the complex microenvironment of DLBCL and the biological and physiological reality in patients, we have demonstrated that a high proportion of ubiquitinated proteins are enriched in spheroids presenting TME with a higher degree of complexity when compared to simplified 2D models. Within these enriched ubiquitinated proteins we found HOIP, further supporting our interest for this target. In addition, a mouse model with augmented expression of HOIP in B cells has been recently developed. This

overexpression of HOIP, interestingly, facilitates DLBCL-like B-cell lymphomagenesis driven by MYD88-activating mutation.(86)

As a result of all this preliminary data, we then undertook a computational study based on a systematic substitution of several α-β unsaturated moieties to be used as covalent binding warheads to the catalytic cysteine residue of HOIP. This study resulted in a vast library of compounds which underwent *In silico* molecular dockings to assess the best HOIP binding candidates. After this computational evaluations four candidates were selected for synthesis of which finally we isolated compound A (Cpd A), a covalent irreversible inhibitor of HOIP with a pyrido[2,3-d]pyrimidine core, with high specificity towards HOIP, as we have confirmed both by DARTS and also by developing a CRISPR-engineered HOIP-knockout ABC-DLBCL model that presents a 60% decrease in HOIP protein levels and does not respond to the treatment .

As for the activity of our experimental compound, we have shown in this dissertation that Cpd A presents selective antitumor activity in a panel of DLBCL cell lines, including several ABC-DLBCL lines, with mean IC50 at 48hours of 90.7± 13.09 μM while presenting no toxicity on normal B cells isolated from healthy patients. We demonstrated that this antitumoral activity is due to a blockade of NF-κB signalling, leading to a reduction both at gene and protein level in the expression of several downstream effectors like IRF4 with an 86% of decrease, IL6 with around 80% of decrease in expression levels as well as the antiapoptotic factor MCL-1 which expression falls to below 50. Interestingly, MYC is also downregulated upon exposure to Cpd A. This effect should be further studied as downregulation of such an important factor in several In addition we have developed a functional ABC-DLBCL model *In ovo* based in the CAM assay showing that Cpd A is safe, as no alterations were observed in the embryo development further validating our results in healthy donor's PBMC, while presents antitumoral activity by achieving a tumor growth inhibition of 25%, in comparison with vehicle treated arm, and significantly abrogates lymphoma infiltration specially in brain by a 60.5% and a remarkable 89% in bone marrow.

Altogether, our results confirm that HOIP represents a promising therapeutic target for ABC-DLBCL, specially with activating MYD88 mutation, as new combinatorial treatment tackling both $MYD88^{p.L265P}$, as for example dual IRAK1 and IRAK4 inhibition, and LUBAC could be developed in the search of synergistic effects which result in the control of the aberrant overactivation of the NF-kB pathway in these specific patients. This possible synergism has

already been suggested, as mentioned previously in this dissertation as it has been shown that overexpression of HOIP increases NF-kB activation and enhances proliferation of B cells upon MYD88 dependent signal activation. (86)

Finally, we present her a potential pharmacological hit against HOIP, in the form of a pyrido[2,3-d]pyrimidine derivative which successfully and specifically block HOIP, resulting in NF-κB disruption and selective antitumor activity in this aggressive subtype of B-cell lymphoma. This opens the possibility of patenting Cpd A, option that is currently being evaluated and work in an optimized and perfected structure with higher antitumoral activity to move on in the development of a novel anti-HOIP therapy for DLBCL, especially ABC-DLBCL, and other NF-kB dependent pathologies.

CONCLUSIONS

CONCLUSIONS

From the results obtained in this dissertation we can conclude that, on one hand:

1. IRAK1/4 inhibition is modestly effective in in vitro and in vivo models of ABC-DLBCL in which this strategy achieves a partial inhibition of NF-κB signalling. However, this effect is observed in a reproducible manner in cell lines, patient samples and ABC-DLBCL xenograft models.
2. We confirm that BET inhibition by itself is an efficient strategy to counteract NF-κB activity in preclinical models of MYD88mut ABC-DLBCL as it shows cytotoxic effect and a reduction of NF-kB gene signature.
3. In addition, BET inhibitors offer synergistic antitumoral and pro-apoptotic activities with IRAK antagonist in vitro and in vivo. This effect is directly related to the downregulation of a set of NF-κB-regulated genes, with a predominant impact on CD44 and MCL-1 expression, with the consequent blockade of cell motility and triggering of tumour cell death.

And on the other hand:

1. HOIP represents a promising therapeutic target in aggressive B cell lymphoma.
2. A pyrido[2,3-*d*]pyrimidine derivative can efficiently and specifically bind to HOIP, resulting in the perturbation of LUBAC complex dynamic and in impaired downstream NF-κB signalling.
3. CpdA is safe and exerts selective antitumor activity both in *In vitro* and *In vivo* models of DLBCL.
4. A patentability study is ongoing during the writing of this dissertation.

BIBLIOGRAPHY

BIBLIOGRAPHY

1. Immunity I. CHAPTER 14 Innate Immunity. Immunology. 2006;125(2 Suppl 2):1–4.
2. Haven N. Innate immunity : impact on the adaptive immune response Ruslan Medzhitov and Charles A Janeway Jr. Health San Francisco. 1997;9(1):4–9.
3. Laiosa C V., Stadtfeld M, Graf T. Determinants of lymphoid-myeloid lineage diversification. Annu Rev Immunol. 2006;24:705–38.
4. Boothby MR, Hodges E, Thomas JW. Molecular regulation of peripheral B cells and their progeny in immunity. Genes Dev. 2019;33(1–2):26–48.
5. Nutt SL, Kee BL. The Transcriptional Regulation of B Cell Lineage Commitment. Immunity. 2007;26(6):715–25.
6. Mebius RE, Kraal G. Structure and function of the spleen. Nat Rev Immunol. 2005;5(8):606–16.
7. Kurosaki T, Kometani K, Ise W. Memory B cells. Nat Rev Immunol. 2015;15(3):149–59.
8. Yam-Puc JC, Toellner KM, Zhang L, Zhang Y. Role of B-cell receptors for B-cell development and antigen-induced differentiation. F1000Res. 2018;7(0).
9. Nakagawa R, Calado DP. Positive Selection in the Light Zone of Germinal Centers. Front Immunol. 2021;12(March):1–8.
10. Allen CD, Okada T, Cyster JG. Germinal Center Organization and Cellular Dynamics Role of the GC in Antibody Responses. Immunity. 2008;27(2):190–202.
11. De Silva NS, Klein U. Dynamics of B cells in germinal centres. Nat Rev Immunol. 2015;15(3):137–48.
12. Maclennan ICM. GERMINAL CENTERS Further ANNUAL REVIEWS. Annu Rev Immunol. 1994;12:17–39.
13. Attanavanich K, Kearney JF. Marginal Zone, but Not Follicular B Cells, Are Potent Activators of Naive CD4 T Cells. The Journal of Immunology. 2004;172(2):803–11.
14. Mintz MA, Cyster JG. T follicular helper cells in germinal center B cell selection and lymphomagenesis. Immunol Rev. 2020;296(1):48–61.
15. Kranich J, Krautler NJ. How follicular dendritic cells shape the B-cell antigenome. Front Immunol. 2016;7(JUN).
16. Pileri SA, Tripodo C, Melle F, Motta G, Tabanelli V, Fiori S, et al. Predictive and prognostic molecular factors in diffuse large b-cell lymphomas. Cells. 2021;10(3):1–15.
17. Xu PP, Zhong HJ, Huang YH, Gao XD, Zhao X, Shen Y, et al. B-cell Function Gene Mutations in Diffuse Large B-cell Lymphoma: A Retrospective Cohort Study. EBioMedicine. 2017;16:106–14.
18. Cheson BD, Fisher RI, Barrington SF, Cavalli F, Schwartz LH, Zucca E, et al. Recommendations for initial evaluation, staging, and response assessment of hodgkin and non-hodgkin lymphoma: The lugano classification. Journal of Clinical Oncology. 2014;32(27):3059–67.

19. Tsai CC, Su YC, Bamodu OA, Chen BJ, Tsai WC, Cheng WH, et al. High-grade b-cell lymphoma (Hgbl) with myc and bcl2 and/or bcl6 rearrangements is predominantly bcl6-rearranged and bcl6-expressing in Taiwan. Cancers (Basel). 2021;13(7).

20. Zayac A, Landsburg DJ, Hughes M, Ayers EC, Girton M, Hu M, et al. High-Grade B-Cell Lymphoma, Not Otherwise Specified (HGBL, NOS): Characteristics, Treatment, and Outcomes from 17 Academic US Centers. Blood. 2021 Nov 5;138(Supplement 1):455.

21. Alaggio R, Amador C, Anagnostopoulos I, Attygalle AD, Araujo IB de O, Berti E, et al. The 5th edition of the World Health Organization Classification of Haematolymphoid Tumours: Lymphoid Neoplasms. Leukemia. 2022;36(7):1720–48.

22. Solimando AG, Annese T, Tamma R, Ingravallo G, Maiorano E, Vacca A, et al. New insights into diffuse large b-cell lymphoma pathobiology. Cancers (Basel). 2020;12(7):1–22.

23. Howlader N, Mariotto AB, Besson C, Suneja G, Robien K, Younes N, et al. Cancer-specific mortality, cure fraction, and noncancer causes of death among diffuse large B-cell lymphoma patients in the immunochemotherapy era. Cancer. 2017;123(17):3326–34.

24. Roschewski M, Phelan JD, Wilson WH. Molecular classification and treatment of diffuse large B-Cell lymphoma and primary mediastinal B-cell lymphoma. Cancer Journal (United States). 2020;26(3):195–205.

25. Chapuy B, Stewart C, Dunford AJ, Kim J, Kamburov A, Redd RA, et al. Molecular subtypes of diffuse large B cell lymphoma are associated with distinct pathogenic mechanisms and outcomes. Nat Med. 2018 May 1;24(5):679–90.

26. Weber T, Schmitz R. Molecular Subgroups of Diffuse Large B Cell Lymphoma: Biology and Implications for Clinical Practice. Vol. 24, Current Oncology Reports. Springer; 2022. p. 13–21.

27. Schmitz R, Wright GW, Huang DW, Johnson CA, Phelan JD, Wang JQ, et al. Genetics and Pathogenesis of Diffuse Large B-Cell Lymphoma. New England Journal of Medicine. 2018 Apr 12;378(15):1396–407.

28. Pasqualucci L. The genetic basis of diffuse large B-cell lymphoma. Curr Opin Hematol. 2013;20(4):336–44.

29. Pasqualucci L, Dalla-Favera R. The Genetic Landscape of Diffuse Large B-Cell Lymphoma. Semin Hematol. 2015;52(2):67–76.

30. Hoesel B, Schmid JA. The complexity of NF-κB signaling in inflammation and cancer. Mol Cancer. 2013;12(1):1.

31. Young RM, Shaffer AL, Phelan JD, Staudt LM. B-Cell Receptor Signaling in Diffuse Large B-Cell lymphoma. Semin Hematol. 2015;52(2):77–85.

32. Ngo VN, Young RM, Schmitz R, Jhavar S, Xiao W, Lim KH, et al. Oncogenically active MYD88 mutations in human lymphoma. Nature. 2011;470(7332):115–21.

33. Knittel G, Liedgens P, Korovkina D, Seeger JM, Al-Baldawi Y, Al-Maarri M, et al. B-cell-specific conditional expression of Myd88p.L252P leads to the development of diffuse large B-cell lymphoma in mice. Blood. 2016;127(22):2732–41.

34. Eric Davis R, Brown KD, Siebenlist U, Staudt LM. Constitutive nuclear factor κB activity is required for survival of activated B cell-like diffuse large B cell lymphoma cells. Journal of Experimental Medicine. 2001;194(12):1861–74.

35. Lam LT, Davis RE, Pierce J, Hepperle M, Xu Y, Hottelet M, et al. Small molecule inhibitors of IκB kinase are selectively toxic for subgroups of diffuse large B-cell lymphoma defined by gene expression profiling. Clinical Cancer Research. 2005;11(1):28–40.

36. Iqbal J, Joshi S, Patel KN, Javed SI, Kucuk C, Aabida A, et al. Clinical implication of genome-wide profiling in diffuse large B-cell lymphoma and other subtypes of B-cell lymphoma. Indian J Cancer. 2007;44(2):72–86.

37. Lin Y, Wong KK, Calame K. Repression of c-myc transcription by Blimp-1, an inducer of terminal B cell differentiation. Science (1979). 1997;276(5312):596–9.

38. Silva CM. Role of STATs as downstream signal transducers in Src family kinase-mediated tumorigenesis. Oncogene [Internet]. 2004;23(48):8017–23. Available from: https://doi.org/10.1038/sj.onc.1208159

39. Lam LT, Wright G, Davis RE, Lenz G, Farinha P, Dang L, et al. Cooperative signaling through the signal transducer and activator of transcription 3 and nuclear factor-kκB pathways in subtypes of diffuse large B-cell lymphoma. Blood. 2008;111(7):3701–13.

40. Hardee J, Ouyang Z, Zhang Y, Kundaje A, Lacroute P, Snyder M. STAT3 targets suggest mechanisms of aggressive tumorigenesis in diffuse large B-cell lymphoma. G3: Genes, Genomes, Genetics. 2013;3(12):2173–85.

41. Zhang B, Calado DP, Wang Z, Fröhler S, Köchert K, Qian Y, et al. An Oncogenic Role for Alternative NF-κB Signaling in DLBCL Revealed upon Deregulated BCL6 Expression. Cell Rep. 2015;11(5):715–26.

42. Akira S, Takeda K. Toll-like receptor signalling. Nat Rev Immunol. 2004;4(7):499–511.

43. Loiarro M, Volpe E, Ruggiero V, Gallo G, Furlan R, Maiorino C, et al. Mutational analysis identifies residues crucial for homodimerization of myeloid differentiation factor 88 (MyD88) and for its function in immune cells. Journal of Biological Chemistry. 2013;288(42):30210–22.

44. Guy C a, Hoogendoorn B, Smith SK, Coleman S, O'Donovan MC, Buckland PR. Promoter polymorphisms in glutathione-S-transferase genes affect transcription. Pharmacogenetics. 2004;14(1):45–51.

45. Knittel G, Liedgens P, Korovkina D, Pallasch CP, Reinhardt HC. Rewired NFκB signaling as a potentially actionable feature of activated B-cell-like diffuse large B-cell lymphoma. Eur J Haematol. 2016;97(6):499–510.

46. Compagno M, Lim WK, Grunn A, Nandula S V., Brahmachary M, Shen Q, et al. Mutations of multiple genes cause deregulation of NF-B in diffuse large B-cell lymphoma. Nature. 2009;459(7247):717–21.

47. Maschera B, Ray K, Burns K, Volpe F. Overexpression of an enzymically inactive interleukin-1-receptor-associated kinase activates nuclear factor-κB. Biochemical Journal. 1999;339(2):227–31.

48. Puente XS, Pinyol M, Quesada V, Conde L, Ordóñez GR, Villamor N, et al. Europe PMC Funders Group Whole-genome sequencing identifies recurrent mutations in chronic lymphocytic leukaemia. 2012;475(7354):101–5.

49. Treon SP, Xu L, Yang G, Zhou Y, Liu X, Cao Y, et al. MYD88 L265P Somatic Mutation in Waldenström's Macroglobulinemia. New England Journal of Medicine. 2012;367(9):826–33.

50. Knittel G, Liedgens P, Korovkina D, Seeger JM, Al-Baldawi Y, Al-Maarri M, et al. B-cell-specific conditional expression of Myd88p.L252P leads to the development of diffuse large B-cell lymphoma in mice. Blood. 2016;127(22):2732–41.

51. Rowley RB, Burkhardt AL, Chao HG, Matsueda GR, Bolen JB. Syk protein-tyrosine kinase is regulated by tyrosine-phosphorylated Igα/Igβ immunoreceptor tyrosine activation motif binding and autophosphorylation. Journal of Biological Chemistry. 1995;270(19):11590–4.

52. Rawlings DJ, Scharenberg AM, Park H, Wahl M, Lin S, Kato RM, et al. 79. Rawlings1996. 1995;33372(November):1–4.

53. Dal Porto JM, Gauld SB, Merrell KT, Mills D, Pugh-Bernard AE, Cambier J. B cell antigen receptor signaling 101. Mol Immunol. 2004;41(6–7):599–613.

54. Young RM, Staudt LM. Targeting pathological B cell receptor signalling in lymphoid malignancies. Nat Rev Drug Discov. 2013;12(3):229–43.

55. Mahajan S, Ghosh S, Sudbeck EA, Zheng Y, Downs S, Hupke M, et al. Rational design and synthesis of a novel anti-leukemic agent targeting Bruton's tyrosine kinase (BTK), LFM-A13 [α-cyano-β-hydroxy-β-methyl-N- (2,5-dibromophenyl)propenamide. Journal of Biological Chemistry. 1999;274(14):9587–99.

56. Honigberg LA, Smith AM, Sirisawad M, Verner E, Loury D, Chang B, et al. The Bruton tyrosine kinase inhibitor PCI-32765 blocks B-cell activation and is efficacious in models of autoimmune disease and B-cell malignancy. Proc Natl Acad Sci U S A. 2010;107(29):13075–80.

57. da Cunha-Bang C, Niemann CU. Targeting Bruton's Tyrosine Kinase Across B-Cell Malignancies. Drugs. 2018;78(16):1653–63.

58. Syed YY. Zanubrutinib: First Approval. Drugs. 2020;80(1):91–7.

59. Kaptein A, de Bruin G, Emmelot-van Hoek M, van de Kar B, de Jong A, Gulrajani M, et al. Potency and Selectivity of BTK Inhibitors in Clinical Development for B-Cell Malignancies. Blood. 2018;132(Supplement 1):1871–1871.

60. Wilson WH, Young RM, Schmitz R, Yang Y, Pittaluga S, Wright G, et al. Targeting B cell receptor signaling with ibrutinib in diffuse large B cell lymphoma. Nat Med. 2015;21(8):922–6.

61. Mondello P, Brea EJ, de Stanchina E, Toska E, Chang AY, Fennell M, et al. Panobinostat acts synergistically with ibrutinib in diffuse large B cell lymphoma cells with MyD88 L265P mutations. JCI Insight. 2017;2(6).

62. Alizadeh AA, Elsen MB, Davis RE, Ma CL, Lossos IS, Rosenwald A, et al. Distinct types of diffuse large B-cell lymphoma identified by gene expression profiling. Nature. 2000;403(6769):503–11.

63. Coiffier B, Lepage E, Brière J, Herbrecht R, Tilly H, Bouabdallah R, et al. CHOP Chemotherapy plus Rituximab Compared with CHOP Alone in Elderly Patients with Diffuse Large-B-Cell Lymphoma. New England Journal of Medicine. 2002;346(4):235–42.

64. Susanibar-Adaniya S, Barta SK. 2021 Update on Diffuse large B cell lymphoma: A review of current data and potential applications on risk stratification and management. Am J Hematol. 2021;96(5):617–29.

65. Dlouhy I, Armengol M, Recasens-Zorzo C, Ribeiro ML, Pérez-Galán P, Bosch F, et al. Interleukin-1 receptor associated kinase 1/4 and bromodomain and extra-terminal inhibitions converge on NF-κB blockade and display synergistic antitumoral activity in activated B-cell subset of diffuse large B-cell lymphoma with MYD88 L265P mutation. Haematologica. 2021;106(10):2749–53.

66. Wang L, Li L rong, Young KH. New agents and regimens for diffuse large B cell lymphoma. J Hematol Oncol. 2020;13(1):1–23.

67. Recasens-Zorzo C, Cardesa-Salzmann T, Petazzi P, Ros-Blanco L, Esteve-Arenys A, Clot G, et al. Pharmacological modulation of CXCR4 cooperates with BET bromodomain inhibition in diffuse large B-cell lymphoma. Haematologica. 2019;104(4):778–88.

68. Sun T, Liu Z, Yang Q. The role of ubiquitination and deubiquitination in cancer metabolism. Mol Cancer. 2020;19(1):1–19.

69. Nath D, Shadan S. The ubiquitin system. Nature. 2009;458(7237):421.

70. Baur R, Rape M. Getting Close: Insight into the Structure and Function of K11/K48-Branched Ubiquitin Chains. Structure. 2020;28(1):1–3.

71. Montagut AM, Armengol M, de Pablo GG, Estrada-Tejedor R, Borrell JI, Roué G. Recent advances in the pharmacological targeting of ubiquitin-regulating enzymes in cancer. Vol. 132, Seminars in Cell and Developmental Biology. Elsevier Ltd; 2022. p. 213–29.

72. Antao AM, Tyagi A, Kim K seong, Ramakrishna S. Advances in Deubiquitinating Enzyme Inhibition. Cancers (Basel). 2020;1–34.

73. Montagut AM, Armengol M, de Pablo GG, Estrada-Tejedor R, Borrell JI, Roué G. Recent advances in the pharmacological targeting of ubiquitin-regulating enzymes in cancer. Semin Cell Dev Biol. 2022;132(February):213–29.

74. Hydbring P, Castell A, Larsson LG. MYC modulation around the CDK2/p27/SKP2 axis. Genes (Basel). 2017;8(7):1–4.

75. Yeh CH, Bellon M, Nicot C. FBXW7: A critical tumor suppressor of human cancers. Mol Cancer. 2018;17(1):1–19.

76. Feki A, Irminger-Finger I. Mutational spectrum of p53 mutations in primary breast and ovarian tumors. Crit Rev Oncol Hematol. 2004;52(2):103–16.

77. Yuan J, Luo K, Zhang L, Cheville JC, Lou Z. USP10 Regulates p53 Localization and Stability by Deubiquitinating p53. Cell. 2010;140(3):384–96.

78. Ren H, Koo J, Guan B, Yue P, Deng X, Chen M, et al. The E3 ubiquitin ligases β-TrCP and FBXW7 cooperatively mediates GSK3-dependent Mcl-1 degradation induced by the Akt inhibitor API-1, resulting in apoptosis. Mol Cancer. 2013;12(1):1–11.

79. Sancho M, Leiva D, Lucendo E, Orzáez M. Understanding MCL1: from cellular function and regulation to pharmacological inhibition. FEBS Journal. 2021;289:6209–34.

80. Maubach G, Schmädicke AC, Naumann M. NEMO Links Nuclear Factor-κB to Human Diseases. Trends Mol Med. 2017;23(12):1138–55.

81. Niu J, Shi Y, Iwai K, Wu ZH. LUBAC regulates NF-κB activation upon genotoxic stress by promoting linear ubiquitination of NEMO. EMBO Journal. 2011;30(18):3741–53.

82. Kirisako T, Kamei K, Murata S, Kato M, Fukumoto H, Kanie M, et al. A ubiquitin ligase complex assembles linear polyubiquitin chains. EMBO Journal. 2006;25(20):4877–87.

83. Tokunaga F, Iwai K. LUBAC, a novel ubiquitin ligase for linear ubiquitination, is crucial for inflammation and immune responses. Microbes Infect. 2012;14(7–8):563–72.

84. Vallabhapurapu S, Karin M. Regulation and function of NF-κB transcription factors in the immune system. Annu Rev Immunol. 2009;27:693–733.

85. Tokunaga F, Sakata SI, Saeki Y, Satomi Y, Kirisako T, Kamei K, et al. Involvement of linear polyubiquitylation of NEMO in NF-κB activation. Nat Cell Biol. 2009;11(2):123–32.

86. Jo T, Nishikori M, Kogure Y, Arima H, Sasaki K, Sasaki Y, et al. LUBAC accelerates B-cell lymphomagenesis by conferring resistance to genotoxic stress on B cells [Internet]. 2020. Available from: http://ashpublications.org/blood/article-pdf/136/6/684/1750775/bloodbld2019002654.pdf

87. Oikawa D, Sato Y, Ohtake F, Komakura K, Hanada K, Sugawara K, et al. Molecular bases for HOIPINs-mediated inhibition of LUBAC and innate immune responses. Commun Biol. 2020;3(1).

88. Strickson S, Campbell DG, Emmerich CH, Knebel A, Plater L, Ritorto MS, et al. The anti-inflammatory drug BAY 11-7082 suppresses the MyD88-dependent signalling network by targeting the ubiquitin system. Biochemical Journal. 2013;451(3):427–37.

89. cb500653y.pdf.

90. De Cesare V, Johnson C, Barlow V, Hastie J, Knebel A, Trost M. The MALDI-TOF E2/E3 Ligase Assay as Universal Tool for Drug Discovery in the Ubiquitin Pathway. Cell Chem Biol. 2018;25(9):1117-1127.e4.

91. Yanguas-Casás N, Pedrosa L, Fernández-Miranda I, Sánchez-Beato M. An overview on diffuse large b-cell lymphoma models: Towards a functional genomics approach. Cancers (Basel). 2021;13(12):1–22.

92. Domcke S, Sinha R, Levine DA, Sander C, Schultz N. Evaluating cell lines as tumour models by comparison of genomic profiles. Nat Commun. 2013;4:1–10.

93. Cox DBT, Platt RJ, Zhang F. Therapeutic genome editing: Prospects and challenges. Nat Med. 2015;21(2):121–31.

94. Ciavarella S, Vegliante MC, Fabbri M, De Summa S, Melle F, Motta G, et al. Dissection of DLBCL microenvironment provides a gene expression-based predictor of survival applicable to formalin-fixed paraffin-embedded tissue. Annals of Oncology. 2018;29(12):2363–70.

95. Foxall R, Narang P, Glaysher B, Hub E, Teal E, Coles MC, et al. Developing a 3D B Cell Lymphoma Culture System to Model Antibody Therapy. Front Immunol. 2021;11(February):1–20.

96. Sajjad H, Imtiaz S, Noor T, Siddiqui YH, Sajjad A, Zia M. Cancer models in preclinical research: A chronicle review of advancement in effective cancer research. Animal Model Exp Med. 2021;4(2):87–103.

97. Shah SB, Singh A. Creating artificial lymphoid tissues to study immunity and hematological malignancies. Curr Opin Hematol. 2017 Jul;24(4):377–83.

98. Apoorva FNU, Tian YF, Pierpont TM, Bassen DM, Cerchietti L, Butcher JT, et al. Lymph node stiffness-mimicking hydrogels regulate human B-cell lymphoma growth and cell surface receptor expression in a molecular subtype-specific manner. J Biomed Mater Res A. 2017 Jul;105(7):1833–44.

99. Gava F, Faria C, Gravelle P, Valero JG, Dobaño-López C, Morin R, et al. 3D Model Characterization by 2D and 3D Imaging in t(14;18)-Positive B-NHL: Perspectives for In Vitro Drug Screens in Follicular Lymphoma. Cancers (Basel). 2021 Mar;13(7).

100. Baarsma HA, Van der Veen CHTJ, Lobee D, Mones N, Oosterhout E, Cattani-Cavalieri I, et al. Epithelial 3D-spheroids as a tool to study air pollutant-induced lung pathology. SLAS Discov. 2022;27(3):185–90.

101. Sabhachandani P, Motwani V, Cohen N, Sarkar S, Torchilin V, Konry T. Generation and functional assessment of 3D multicellular spheroids in droplet based microfluidics platform. Lab Chip. 2016;16(3):497–505.

102. Aboulkheyr Es H, Montazeri L, Aref AR, Vosough M, Baharvand H. Personalized Cancer Medicine: An Organoid Approach. Trends Biotechnol. 2018 Apr;36(4):358–71.

103. Vidal-Crespo A, Matas-Céspedes A, Rodriguez V, Rossi C, Valero JG, Serrat N, et al. Daratumumab displays in vitro and in vivo anti-tumor activity in models of B-cell non-Hodgkin lymphoma and improves responses to standard chemo-immunotherapy regimens. Haematologica. 2020;105(4):1032–41.

104. Béguelin W, Rivas MA, Calvo Fernández MT, Teater M, Purwada A, Redmond D, et al. EZH2 enables germinal centre formation through epigenetic silencing of CDKN1A and an Rb-E2F1 feedback loop. Nat Commun. 2017;8(1):1–16.

105. Fontan L, Goldstein R, Casalena G, Durant M, Teater MR, Wilson J, et al. Identification of MALT1 feedback mechanisms enables rational design of potent antilymphoma regimens for ABC-DLBCL. Blood. 2021 Feb;137(6):788–800.

106. Harris AW, Pinkert CA, Crawford M, Langdon WY, Brinster RL, Adams JM. THE Et . -myc TRANSGENIC MOUSE A Model for High-incidence Spontaneous Lymphoma and Leukemia of Early B Cells Translocation of the c-myc protooncogene into or near one of the Ig loci is found in almost every case of Burkitt ' s B cell lymphoma in man and e. J Exp Med. 1988;167(February):353–71.

107. Greenwald RJ, Tumang JR, Sinha A, Currier N, Cardiff RD, Rothstein TL, et al. Eμ-BRD2 transgenic mice develop B-cell lymphoma and leukemia. Blood. 2004;103(4):1475–84.

108. Cattoretti G, Pasqualucci L, Ballon G, Tam W, Nandula S V., Shen Q, et al. Deregulated BCL6 expression recapitulates the pathogenesis of human diffuse large B cell lymphomas in mice. Cancer Cell. 2005;7(5):445–55.

109. Sindel A, McConnell I, Windle J, Sabo R, Chesney A, Lai G, et al. Role of the PI3K Pathway in the Pathogenesis of Marginal Zone Lymphoma. Blood. 2018 Nov 29;132(Supplement 1):4125.

110. Zhao Z, Chen L, Dawlaty MM, Pan F, Weeks O, Zhou Y, et al. Combined Loss of Tet1 and Tet2 Promotes B Cell, but Not Myeloid Malignancies, in Mice. Cell Rep. 2015;13(8):1692–704.

111. Day CP, Merlino G, Van Dyke T. Preclinical mouse cancer models: a maze of opportunities and challenges. Cell. 2015 Sep;163(1):39–53.

112. Cho SY, Kang W, Han JY, Min S, Kang J, Lee A, et al. An integrative approach to precision cancer medicine using patient-derived xenografts. Mol Cells. 2016;39(2):77–86.

113. Yin L, Wang XJ, Chen DX, Liu XN, Wang XJ. Humanized mouse model: a review on preclinical applications for cancer immunotherapy. Am J Cancer Res. 2020;10(12):4568–84.

114. Harper K, Yatsyna A, Charbonneau M, Brochu-Gaudreau K, Perreault A, Jeldres C, et al. The chicken chorioallantoic membrane tumor assay as a relevant in vivo model to study the impact of hypoxia on tumor progression and metastasis. Cancers (Basel). 2021;13(5):1–15.

115. Kue CS, Tan KY, Lam ML, Lee HB. Chick embryo chorioallantoic membrane (CAM): An alternative predictive model in acute toxicological studies for anti-cancer drugs. Exp Anim. 2014;64(2):129–38.

116. Ribatti D. The chick embryo chorioallantoic membrane (CAM). A multifaceted experimental model. Mech Dev. 2016;141:70–7.

117. Maeda Y, Noda M. Coordinated development of embryonic long bone on chorioallantoic membrane in ovo prevents perichondrium-derived suppressive signals against cartilage growth. Bone. 2003;32(1):27–34.

118. Seto F. Early development of the avian immune system. Poult Sci. 1981;60(9):1981–95.

119. Gitlin AD, Nussenzweig MC. Immunology: Fifty years of B lymphocytes. Nature. 2015;517(7533):139–41.

120. Leene W, Duyzings MJ, van Steeg C. Lymphoid stem cell identification in the developing thymus and bursa of Fabricius of the chick. Z Zellforsch Mikrosk Anat. 1973 Feb;136(4):521–33.

121. Marga Janse E, Jeurissen SHM. Ontogeny and Function of Two Non-Lymphoid Cell Populations in the Chicken Embryo. Immunobiology. 1991;182(5):472–81.

122. Power EA, Fernandez-Torres J, Zhang L, Yaun R, Lucien F, Daniels DJ. Chorioallantoic membrane (CAM) assay to study treatment effects in diffuse intrinsic pontine glioma. PLoS One. 2022;17(2):10–2.

123. Li L, Zhang X, Kovacic S, Long AJ, Bourque K, Wood CR, et al. Brief Definitive Report Identification of a Human Follicular Dendritic Cell Molecule That Stimulates Germinal Center B

Cell Growth [Internet]. Vol. 191, J. Exp. Med. 2000. Available from: http://www.jem.org/cgi/current/full/191/6/1077

124. Manfroi B, de Grandis M, Moreaux J, Tabruyn S, Mayol JF, Quintero M, et al. The microenvironment of DLBCL is characterized by noncanonical macrophages recruited by tumor-derived CCL5. Blood Adv. 2021 Nov 9;5(21):4338–51.

125. Verzella D, Cornice J, Arboretto P, Vecchiotti D, Di Vito Nolfi M, Capece D, et al. The NF-κB Pharmacopeia: Novel Strategies to Subdue an Intractable Target. Biomedicines. 2022;10(9):1–37.

126. Yu H, Lin L, Zhang Z, Zhang H, Hu H. Targeting NF-κB pathway for the therapy of diseases: mechanism and clinical study. Signal Transduct Target Ther. 2020;5(1).

127. Kelly PN, Romero DL, Yang Y, Shaffer AL, Chaudhary D, Robinson S, et al. Selective interleukin-1 receptor-associated kinase 4 inhibitors for the treatment of autoimmune disorders and lymphoid malignancy. Journal of Experimental Medicine. 2015;212(13):2189–201.

128. De Nardo D, Balka KR, Gloria YC, Rao VR, Latz E, Masters SL. Interleukin-1 receptor-associated kinase 4 (IRAK4) plays a dual role in myddosome formation and Toll-like receptor signaling. Journal of Biological Chemistry. 2018;293(39):15195–207.

129. Yang G, Hatcher JM, Wang J, Liu X, Munshi M, Chen JG, et al. A Novel, Highly Selective IRAK1 Inhibitor Jh-X-119-01 Shows Synergistic Tumor Cell Killing with Ibrutinib in MYD88 Mutated B-Cell Lymphoma Cells. Blood. 2017;130:719.

130. Boudesco C, Verhoeyen E, Martin L, Chassagne-Clement C, Salmi L, Mhaidly R, et al. HSP110 sustains chronic NF-kB signaling in activated B-cell diffuse large B-cell lymphoma through MyD88 stabilization. Blood. 2018;132(5):510–20.

131. Ni H, Shirazi F, Baladandayuthapani V, Lin H, Kuiatse I, Wang H, et al. Targeting Myddosome Signaling in Waldenström's Macroglobulinemia with the Interleukin-1 Receptor-Associated Kinase 1/4 Inhibitor R191. Clin Cancer Res. 2018 Dec;24(24):6408–20.

132. Dlouhy I, Filella X, Rovira J, Magnano L, Rivas-Delgado A, Baumann T, et al. High serum levels of soluble interleukin-2 receptor (sIL2-R), interleukin-6 (IL-6) and tumor necrosis factor alpha (TNF) are associated with adverse clinical features and predict poor outcome in diffuse large B-cell lymphoma. Leuk Res. 2017 Aug;59:20–5.

133. Ceribelli M, Kelly PN, Shaffer AL, Wright GW, Xiao W, Yang Y, et al. Blockade of oncogenic IκB kinase activity in diffuse large B-cell lymphoma by bromodomain and extraterminal domain protein inhibitors. Proc Natl Acad Sci U S A. 2014;111(31):11365–70.

134. Iwai K, Fujita H, Sasaki Y. Linear ubiquitin chains: NF-κB signalling, cell death and beyond. Nat Rev Mol Cell Biol [Internet]. 2014;15(8):503–8. Available from: https://doi.org/10.1038/nrm3836

135. Yang Y, Schmitz R, Mitala J, Whiting A, Xiao W, Ceribelli M, et al. Essential role of the linear ubiquitin chain assembly complex in lymphoma revealed by rare germline polymorphisms. Cancer Discov. 2014;4(4):480–93.

ACKNOLEDGEMENTS

ACKNOLEDGEMENTS

Esta tesis doctoral es la culminación de un sueño desde bien pequeño: dedicarme a uno de los campos más bonitos que existe, la ciencia. No solo porque nuestra intención última como científicos, y más en un campo como la biomedicina, sea ayudar a los demás con nuestros descubrimientos, sino además porque pocas cosas más bellas se me ocurren que el intentar desgranar los secretos del mundo que nos rodea. Un momento de *Eureka* como el de Arquímedes, a pesar de ser poco habitual en esta profesión en que la frustración suele estar bastante presente, es de las mejores sensaciones que uno puede tener. Ya sea porque un experimento funciona, por un resultado interesante, por un artículo aceptado o mejor aún, cuando ves el fruto de tantos años de esfuerzo y dedicación en forma de esta tesis doctoral. Al final, todo cobró sentido y estructura.

Si bien ha requerido de esfuerzo y mucha dedicación por parte del autor y su director de tesis, este momento no hubiese sido posible sin la amistad y el apoyo de todas y cada una de las personas que han estado conmigo durante esta montaña rusa de casi 4 años. Muchos de los que a continuación citaré han sido un apoyo más importante de lo que ellos creen.

Como no, empezaré por **mi familia**. Mi madre Rosa Maria, siempre has estado a mi lado apoyándome y animándome a ser mejor persona y muchas veces sin entender de lo que te hablaba me has escuchado y animado tanto como has podido. A mi padre Antoni, sin duda eres uno de los responsables de la persona que soy hoy y no me equivocaría al decir que eres quien sembró la semilla (y la ha ido regando) de la curiosidad y el pensamiento crítico que me ha llevado a perseguir esta carrera. A mi hermana mayor Ingrid, la segunda madre, el ejemplo a seguir. Que paciencia has tenido durante mis años académicos… A Thaïs, la pequeña. Empezaste aguantándome como profesor de biología, química y física y estas a punto de convertirte en una brillante médico (que no doctora jejejej…). Verte crecer ha sido uno de los privilegios de esta vida y ver tu crecimiento como médico un motor extra para tirar la tesis hacia delante. A Álvaro y Pau por hacerme feliz a mí y a mis hermanas. A Mauro y Damián, mis encantadores sobrinos, que a pesar de su corta edad cada día me enseñan lo maravillosa que es la vida y la belleza de la inocencia y la curiosidad.

A Ylenia, **compañera "predoc" y de vida**. En el momento de escribir estas palabras queda menos de un mes para casarme contigo. Probablemente para el momento de la defensa ya llevemos un par de meses de lo que, no tengo dudas, será una larga y preciosa vida a tu lado. Sin duda te has llevado lo mejor y lo peor de mi tesis. Sin tu voluntad de escuchar y ayudar no estaríamos aquí. Has sido EL pilar emocional de este candidato a doctor. Ya ves, al final todo llega a buen puerto. Sigue adelante con tus valores, tu valentía y tu entereza y sin darte cuenta, estarás escribiendo los agradecimientos de tu propia tesis.

A mis suegros, Joaquina y José Luis dos de las personas más maravillosas que he conocido. Me he sentido arropado por vosotros desde el primer momento y vuestro apoyo constante tanto a mi como a vuestra hija han sido y son un combustible más que necesario. Es un verdadero placer teneros en la vida y formar parte de vuestra familia.

A mis compañeros en el laboratorio durante todo este proceso. Al ser el primero en el grupo no hay un apartado de "los que estaban" así que vamos a los que llegaron.

A Diana, por tus enseñanzas, no solo a nivel científico, también personal. Te hemos echado mucho de menos por el lab a ti, a tus historias de Madrid y a tus espadas.

Marcelo, no me puedo imaginar estos años con otro senior (Senior senior jeje) postdoc que no seas tu. Creo que nunca he llegado a expresarte toda la admiración y el cariño que te tengo. Te deseo lo mejor en esta nueva etapa de tu vida profesional.

A Juliana, la investigadora más integra y entregada que he conocido. Tus consejos y tu optimismo son como un faro en la noche. Tu llegada fueron los mejores refuerzos que mi tesis podía pedir.

A Pau, que es una mente preclara y brillante. Tu futuro sí que me tiene intrigado porque puedes hacer lo que te propongas, y encima lo harás a lo grande, no me cabe duda.

Núria, no sé ni per on començar. No hi ha persona més dolça i agradable en tot el planeta. Ets una petita llum sempre encesa per qui la necessiti. Sempre has estat oberta a compartir tot el teu coneixement (que és infinit) amb paciència i carinyo. Resumint, ets una "locura" de postdoc <3.

A miss Miranda, porque no me imagino mejor compitrueno que tú. Ha sido una suerte inmensa compartir esta parte de nuestra formación juntos. Siempre que te he necesitado has

estado ahí (si no en citometría…) y espero haber podido ayudarte y apoyado como mínimo la mitad de lo que lo has hecho tu conmigo. La citometría no asusta tanto cuando te la saben explicar. A día de hoy, aún echo mucho de menos tenerte sentada al lado.

A la gente que he tenido el placer de formar en estos años.

Laia, tens un futur brillant al davant! No puc esperar a veure els teus futurs èxits! I sempre que ho necessitis, aquí tens el teu humil assessor.

A l'Alicia, entrar a les 6 del matí per fer un ADCC o un ADCP és menys dur si és amb tu. He rigut amb tu lo que no está escrito. Gràcies per ser com ets i endavant!

A Ana Maria por siempre estar dispuesta a aprender de un campo que no es el tuyo y por el reto extra de formar a una doctora.

A Gema, la jefaaa, la investigadora 360. Te hace un western blot como una síntesis química y además sabe pronunciar cosas tan complicadas como reacción de Schotten–Baumann (y sabe lo que significa). Mira hasta donde has llegado, así que aparca tus inseguridades y a brillar.

A Aitana, la más joven, haciendo su TDR con nosotros durante una semana. La satisfacción de saber que esa breve estancia te llevo a matricularte en la carrera de biotecnología no cabe en el pecho. A todos espero haberos inspirado o como mínimo haberos enseñado algo y dejado un buen recuerdo.

A los que nos han visitado como Anežka y Sam. Fue breve pero intenso. Toda la suerte del mundo con vuestro futuro (y esos esferoides). A Mélody, quien sin quererlo se ha convertido en una grandísima amiga. Gracias por todo lo que nos has enseñado. Siempre tendrás un amigo en Barcelona. A bientôt et bon chance ma chérie. To Babis (which is short for Charalampos, still don't know how or why…) The greatest visiting PhD student I've ever met. The only regret I have is that your stay had an ending. Wish you the best of luck with your thesis writing and defense, which will surely be amazing.

A Beatriz Berzosa, a pesar de tu brutal intento de asesinato hacia mi persona en tu primer día de trabajo. Sigue sorprendiéndome como empezó nuestra amistad, pero creo que eso le da un extra de belleza. Por tu paciencia y estar siempre dispuesta a escuchar. A Ruth Blanco, impactada al verme en su primer día vestido de dinosaurio. Por tus sabios consejos y naturalidad. Seguro que ninguna olvidará su primer día en el IJC.

A mi director de tesis, el Dr. Gaël Roué, sin quien nada de esto habría pasado. Por tu confianza hace ya muchos años, cuando te llegó el currículum de un joven graduado en biotecnología buscando unas prácticas mientras esperaba a empezar su Máster y decidiste creer en su potencial. Por el equipo tan maravilloso que conseguiste reunir y por todas las primeras veces que nos has regalado a tus estudiantes: nuestro primer artículo publicado, nuestro primer congreso, nuestro primer poster, nuestra primera presentación oral, nuestro primer trabajo como primer autor, etc…

A mis amigos, Pepo (después de 19 años de amistad sincera no me imagino la vida sin ti), Helen que es un pilar indispensable en mi vida desde hace 13 años y a Espe que en muy poco tiempo se ha ganado un sitio en este tándem (y en este corazoncito). A Alfredo Arbona y sus ideas de bombero. Buyse (Xavi…) fiel amigo desde la carrera y a su futura esposa Alexia, una mujer excepcional y fascinante. Marta Pellicer que a pesar de la distancia y el paso del tiempo siempre está conmigo. Por muchos más años. A María Fraile por tantos años de amistad llenos de música. A Borja Moreno y su incapacidad para pasar desapercibido. A su mujer María y sus hijas Elenita y Rocío. Por vosotras cobra sentido nuestro trabajo y aguanta nuestra vocación.

Arturo Vega (AKA Tachimon), el animal que defiende su tesis y a la semana empieza a preparase el MIR. Ole tú y tus asados. Paula Vázquez (AKA HitPau) mí trocito de corazón en Euskadi.

A mis profesores del colegio… imposible no estaros agradecido en este momento académico tan importante. A Carlos Mínguez por enseñarnos a pensar y enamorarnos de la filosofía. Gloria López-Barrena mi querida profesora de química y de cultura general. A Hortènsia Mallén, quien me enamoró de la biología. A Julie Connolly, Mark Paterson y Mr. David, los responsables de sembrar la semilla académica por las ciencias. A Anna Fuertes, por ser la mejor profesora que nunca he tenido, la responsable de que dudara durante dos años entre la física y la biología… porque cuando alguien se entrega a su trabajo en cuerpo y alma consigue inspirar. A Patricia Carranza por cuidarnos y guiarnos. A Ferran, nuestro encantador director. Y tantísimos otros como Rogelio, Mateu, José María, Stephen y a todos los demás porque soy, gracias a vosotros.

A mis actuales compañeros de trabajo. Àlex Cordero y Francesc Madriles, Tanit Devant y Chiara Corliano, que habéis vivido el final de esta. Vaya quinteto más estupendo formamos hermosos. A Timothy Cash por la confianza y enseñarme este otro mundo de la biotec.

A los Jesters, Juanito, Carlos Choquín y Lolo. **A los Jokers**. Dani Romera, Jose, Jordi, Juanra, Tibu, Floro, Crespo, Franky, Juanjo, Àlex, Joaquín y todos los demás. **A las Jokerinas y Jesterinas**: Coco, Merche, Sandra, Esther, Eva, Andrea, Claudia… No os nombro a todos y todas porque serían más largos los agradecimientos que la propia tesis. Por vuestro apoyo constante, por aguantar mis idas y venidas y por todo el cariño que me mostráis siempre.

Finalmente, a la Fundación Josep Carreras contra la leucemia por su esfuerzo constante en la lucha contra las enfermedades malignas de la sangre. A todo el personal del IJC, compañeros investigadores, y administración, en especial a Maribel cuya sonrisa y palabras amables hacen que cada día empiece de la mejor manera posible.

No pensaba que se alargarían tanto los agradecimientos. La verdad es que no era consciente de la cantidad de gente a la que le debo este momento. Deberíamos pararnos a pensar más a menudo en la gente tan estupenda que nos acompaña en la vida. Resumiendo…. Gracias, gracias y mil gracias a todos, por formar parte de mi vida y por estar. Una parte de este manuscrito es vuestro. Por siempre en el corazón y ahora en la última página de mi tesis. Ahora sí: **PUNTO FINAL.**

ANNEXES

frontiers | Frontiers in Immunology

TYPE Original Research
PUBLISHED 21 April 2023
DOI 10.3389/fimmu.2023.1130052

OPEN ACCESS

EDITED BY
Simone Ferrero,
University of Turin, Italy

REVIEWED BY
Maria Teresa Scupoli,
University of Verona, Italy
Ali Roghanian,
University of Southampton,
United Kingdom

*CORRESPONDENCE
Gael Roué
groue@carrerasresearch.org

†These authors have contributed equally to this work and share first authorship

SPECIALTY SECTION
This article was submitted to Cancer Immunity and Immunotherapy, a section of the journal Frontiers in Immunology

RECEIVED 22 December 2022
ACCEPTED 10 April 2023
PUBLISHED 21 April 2023

CITATION
Ribeiro ML, Profitós-Pelejà N, Santos JC, Blecua P, Reyes-Garau D, Armengol M, Fernández-Serrano M, Miskin HP, Bosch F, Esteller M, Normant E and Roué G (2023) G protein-coupled receptor 183 mediates the sensitization of Burkitt lymphoma tumors to CD47 immune checkpoint blockade by anti-CD20/PI3Kδi dual therapy.
Front. Immunol. 14:1130052.
doi: 10.3389/fimmu.2023.1130052

G protein-coupled receptor 183 mediates the sensitization of Burkitt lymphoma tumors to CD47 immune checkpoint blockade by anti-CD20/PI3Kδi dual therapy

Marcelo Lima Ribeiro[1,2†], Núria Profitós-Pelejà[1†], Juliana Carvalho Santos[1†], Pedro Blecua[3], Diana Reyes-Garau[1], Marc Armengol[1,4], Miranda Fernández-Serrano[1,4], Hari P. Miskin[5], Francesc Bosch[4,6,7], Manel Esteller[3,8,9], Emmanuel Normant[5] and Gael Roué[1,4,6,7*]

[1]Lymphoma Translational Group, Josep Carreras Leukemia Research Institute, Badalona, Spain, [2]Laboratory of Immunopharmacology and Molecular Biology, Sao Francisco University Medical School, Braganca Paulista, São Paulo, Brazil, [3]Cancer Epigenetics Group, Josep Carreras Leukemia Research Institute, Badalona, Spain, [4]Department of Biochemistry and Molecular Biology, Autonomous University of Barcelona, Barcelona, Spain, [5]TG Therapeutics, New York, NY, United States, [6]Department of Hematology, Vall d'Hebron University Hospital, Barcelona, Spain, [7]Experimental Hematology, Vall d'Hebron Institute of Oncology, Barcelona, Spain, [8]Centro de Investigación Biomédica en Red de Cáncer (CIBERONC), Instituto de Salud Carlos III, Barcelona, Spain, [9]Institució Catalana de Recerca i Estudis Avançats (ICREA), Barcelona, Spain

Background: Immunotherapy-based regimens have considerably improved the survival rate of B-cell non-Hodgkin lymphoma (B-NHL) patients in the last decades; however, most disease subtypes remain almost incurable. TG-1801, a bispecific antibody that targets CD47 selectively on CD19+ B-cells, is under clinical evaluation in relapsed/refractory (R/R) B-NHL patients either as a single-agent or in combination with ublituximab, a new generation CD20 antibody.

Methods: A set of eight B-NHL cell lines and primary samples were cultured *in vitro* in the presence of bone marrow-derived stromal cells, M2-polarized primary macrophages, and primary circulating PBMCs as a source of effector cells. Cell response to TG-1801 alone or combined with the U2 regimen associating ublituximab to the PI3Kδ inhibitor umbralisib, was analyzed by proliferation assay, western blot, transcriptomic analysis (qPCR array and RNA sequencing followed by gene set enrichment analysis) and/or quantification of antibody-dependent cell death (ADCC) and antibody-dependent cell phagocytosis (ADCP). CRISPR-Cas9 gene edition was used to selectively abrogate GPR183 gene expression in B-NHL cells. In vivo, drug efficacy was determined in immunodeficient (NSG mice) or immune-competent (chicken embryo chorioallantoic membrane (CAM)) B-NHL xenograft models.

Results: Using a panel of B-NHL co-cultures, we show that TG-1801, by disrupting the CD47-SIRPα axis, potentiates anti-CD20-mediated ADCC and

ADCP. This led to a remarkable and durable antitumor effect of the triplet therapy composed by TG-1801 and U2 regimen, *in vitro*, as well as in mice and CAM xenograft models of B-NHL. Transcriptomic analysis also uncovered the upregulation of the G protein-coupled and inflammatory receptor, GPR183, as a crucial event associated with the efficacy of the triplet combination. Genetic depletion and pharmacological inhibition of GPR183 impaired ADCP initiation, cytoskeleton remodeling and cell migration in 2D and 3D spheroid B-NHL co-cultures, and disrupted macrophage-mediated control of tumor growth in B-NHL CAM xenografts.

Conclusions: Altogether, our results support a crucial role for GPR183 in the recognition and elimination of malignant B cells upon concomitant targeting of CD20, CD47 and PI3Kδ, and warrant further clinical evaluation of this triplet regimen in B-NHL.

KEYWORDS

B-NHL, immune checkpoint blockade, drug combination, ADCP, M1 macrophage, 3D spheroid, CAM assay, inflammatory receptor

1 Introduction

Immunotherapy regimens based on checkpoint inhibitors, tumour vaccination, immune cell-based therapy and cytokines, utilize the power and specificity of the host's immune system against cancer and have become one of the most promising therapeutic interventions in oncology (1). This holds particularly true in B-cell lymphoma, with the considerable advances recently achieved by PD1/PD-L1, CAR-T cell therapies and CD3/CD20 bispecific antibodies, in heavily pre-treated patients (2). Prior to these new approaches, combining therapeutic (i.e. anti-CD20) antibodies with conventional chemotherapy have marked a milestone in the treatment of these diseases, although treatment toxicity and counteracting effects of the tumor-supportive microenvironment that affect the efficacy of immunotherapies, remained a challenge in a significant proportion of patients (3). Among the entities that benefited the most from the venue of anti-CD20 agents, Burkitt lymphoma (BL) is a rare and highly malignant type of B-cell lymphoma that accounts for approximately 50% of non-Hodgkin lymphoma (B-NHL) in children and adolescents (4). In 85% of the cases, BL is molecularly defined by the overexpression of the oncogene MYC caused by the translocation of 8q24 region to the immunoglobulin heavy chain locus (14q32) (5). Among the different immunological targets currently under evaluation on BL, cluster of differentiation 47 (CD47), also known as integrin-associated protein (IAP), is a cell surface receptor that is part of the immunoglobulin superfamily, and which interacts with the macrophage receptor signal regulatory protein-alpha (SIRPα). This interaction sends a "do-not-eat-me" signal to macrophages, which mediates immune evasion in several types of cancers, from both hematological and non-hematological origin (6). High levels of CD47 have indeed been observed in both lymphoid and myeloid neoplasms, in which this factor is both an adverse prognostic indicator and a valid anti-cancer target with several therapeutic antibodies currently being tested in clinical trials. In B-cell lymphoma, these trials frequently involve a combination with anti-CD20 therapy, to ensure a proper engagement of the Fc receptors at the surface of macrophages and natural killer (NK) effector cells. The anti-CD20 mAb rituximab has been the most common IgG1 antibody tested in this setting, and has demonstrated combinatorial activity in both indolent and aggressive entities (7, 8). However, as CD47 is widely expressed on the surface of a broad range of cell types, including erythrocytes and platelets, a major limitation of CD47 blocking agents is the target-mediated drug disposition and the potential side effects, which include anaemia or thrombocytopenia.

TG-1801 (also known as NI-1701) is a fully human IgG1 anti-CD47xCD19 bispecific antibody with the whole spectrum of Fc-mediated effector function, and that binds CD47 with sub-micromolar affinity and CD19 with a sub-nanomolar affinity. This thousand-fold difference between its affinity to these antigens allows TG-1801 to bind selectively to CD19-positive B cells *in vitro* and *in vivo*, including malignant B cells, but not CD19-negative red blood cells or platelets (9–11). TG-1801 is currently being tested clinically as a single agent and in combination with the glyco-engineered CD20 antibody, ublituximab, in patients with R/R B-cell lymphoma (NCT04806035).

In parallel, pre-clinical and clinical data have provided a rationale for the combination of anti-CD20 antibody with PI3Kδ antagonists in B-cell malignancies, mediated by the capacity of these latter to potentiate CD20-mediated direct cell death (12). Clinical efficacy and safety of this combinatorial approach has been confirmed in R/RB-NHL and chronic lymphocytic leukaemia (CLL) patients (13). Although the value of associating CD20 mAb therapy to CD47

modulating agents has been well established in aggressive B-cell lymphoma, both preclinically and clinically, two questions remained unanswered. First, we still don't known whether the addition of PI3K-targeting agents to those immunotherapeutic regimens that contain checkpoint blockers could impact the efficacy of these latter. Second, beside rituximab which mainly depletes B cell by complement fixation, it would be interesting to assess in these settings the efficacy of new generation anti-CD20 antibodies harbouring a glycoengineering Fc region and a higher capacity to elicit ADCC. To investigate these two issues, we studied the effect of the B-cell specific, CD47/CD19 immune checkpoint blocker, TG-1801, in association with anti-CD20/PI3Kδi dual therapy in different *in vitro* and *in vivo* models of BL, as a disease model of aggressive B-NHL.

2 Materials and methods

2.1 Cell lines

Three BL (Raji, Daudi, Ramos), two diffuse large B cell lymphoma (DLBCL) (Pfeiffer, and Karpas-422 (Karpas)), one follicular lymphoma (FL) (RL), and one T-cell acute lymphoblastic leukemia (Jurkat) cell lines were used in this study. Cells were grown in Advanced-RMPI 1640 medium supplemented with 5% heat-inactivated FBS, 2 mmol/L glutamine, and 50 µg/mL penicillin-streptomycin (Thermo Fisher). All cultures were routinely tested for mycoplasma infection by PCR and the identity of all cell lines was verified by using AmpFISTR identifier kit (Thermo Fisher).

2.2 Occupancy assay

Cytofluorimetric quantification of CD47 and CD19 membrane levels was carried out in a panel of 10 B-NHL cell lines. Cells were stained with phycoerythrin (PE)-labelled anti-CD47 or anti-CD19 antibodies (Becton Dickinson) and the absolute number of membrane-bound molecules of CD47 or CD19 was estimated using QuantiBRITE PE beads (BD Biosciences) on a FACSCanto II (Becton Dickinson). Data were analysed using FlowJo software package (TreeStar, USA).

For the detection of unbound surface CD47, Raji (CD19+), or Jurkat (CD19-) cells were stained with a PE-labelled anti-CD47 (B6H12 clone) or isotype control antibody (BD Biosciences). Cells were pre-treated for 1 h with TG-1801 or an anti-human CD47 (B6H12 clone) control antibody. For quantification, a total of 10.000 events were acquired on a FACSCanto II (Becton Dickinson). Relative median fluorescence intensity (RMFI) was calculated using FlowJo software package as the ratio between CD47 and control signal intensity. Shown are the percentages of occupancy, defined as the decreases in CD47 RMFI ratios evoked by anti-CD47-treatment, using untreated cells as a calibrator. B6H12 clone was used as a CD19-independent positive control of CD47 occupancy.

2.3 Peripheral blood mononuclear cells isolation and macrophage polarization

Peripheral blood mononuclear cells (PBMCs) were purified by standard Ficoll-Hypaque (GE Healthcare) gradient centrifugation from buffy coats of human healthy donors and cultured freshly in Advanced-RMPI 1640 medium supplemented with 5% heat-inactivated FBS, 2 mmol/L glutamine, 50 µg/mL penicillin-streptomycin (Thermo Fisher).

RosetteSep™ Human Monocyte Enrichment Cocktail (Stemcell Technologies) was used to purify human monocytes from buffy coats following manufacturer specifications. For M1 or M2 macrophage polarization, the selected monocytes were cultured in complete Advanced-RMPI 1640 supplemented with either 20 ng/mL human GM-CSF (PeproTech), for M1 differentiation, or 20 ng/mL human M-CSF (PeproTech), for M2 differentiation, and incubated for 6 days. On day 6 M0 macrophages were activated with 100 ng/mL human IFN-γ (PeproTech) and 50 ng/mL LPS, for M1 macrophage polarization for 24 h.

2.4 Antibody-dependent cell-mediated cytotoxicity and phagocytosis assays

ADCC activity was assessed in B-cell lymphoma cell lines co-cultured for 4 hours with freshly obtained PBMCs (1:10, target: effector), in the presence of 10 ng/mL TG-1801 +/- U2 dual assets (10 µg/mL ublituximab + 1 µM umbralisib), using and a lactate deshydrogenease (LDH) release assay (Roche). Relative ADCC was calculated using the following formula: ADCC percentage = [(sample release – spontaneous release)/(maximal release – spontaneous release)]*100.

Spontaneous release, corresponding to target cells incubated with effector cells without antibody, was defined as 0% cytotoxicity, with maximal release (target cells lysed with 1% Triton X-100) defined as 100% cytotoxicity. The average percentage of ADCC and standard deviations of the triplicates of each experiment were calculated.

ADCP activity was assessed in B-cell lymphoma cell lines co-cultured for 4 hours with M1-polarized macrophages (1:5, target: effector), in the presence of 10 ng/mL TG-1801 +/- U2 dual assets (10 µg/mL ublituximab + 1 µM umbralisib), using and the pHrodo-stained B cells (IncuCyte® pHrodo® Red Cell Labelling Kit for Phagocytosis, Sartorius). Following phagocytosis assay, the non-phagocytosed cells were removed by washing with PBS 2–3 times and phagocytosis was analysed by fluorescent microscopy on an EVOS M5000 Cell Imaging Systems (Thermo Fisher).

2.5 Xenograft mouse model and tumor immunophenotyping

Eight-week-old NOD/SCID IL2Rγ-null (NSG) male and female mice (Janvier Labs) were subcutaneously injected with Raji cells and after two weeks tumor-bearing mice were randomized using

GraphPad Prism 9.0 software (GraphPad Software, Inc) and assigned to one of the following treatment arms (8-6 mice per group): TG-1801 (5 mg/kg, qw), ublituximab (5 mg/kg, qw) + umbralisib (U2) (150 mg/kg, bid), or the triplet (TG-1801 + U2), or an equal volume of vehicle for 17 days. Tumour volumes were measured each 2-3 days with external callipers. The number of animals used in each of the experimental groups is based on the literature and previous results from the group (14). Immunohistochemical staining of representative tumor specimens (n=3 per group) was performed using anti-CD20 (Sigma), anti-GPR183 (Santa Cruz), anti-F4/80 (Abcam), anti-Histone H3-pSer10 (Abcam) and anti-CD56/NCAM-1 (Abcam) primary antibodies, as previously described (14). Preparations were evaluated using an Olympus BX53 microscope and MicroManager software (Fiji, Plugin).

Immunohistochemical signal intensity was quantified in at least 5 pictures of two representative tumor specimens from the Raji xenograft model, using QuPath v.0.2.3 software developed at Queen's University (Belfast, Northern Ireland) (15). Cell detection was conducted using QuPath's built-in "Positive cell detection" by calculating the percent of positively stained cells in each field.

2.6 Chicken embryo chorioallantoic membrane model

Fertilized white Leghorn chicken eggs were purchased from Granja Santa Isabel, S. L. (Córdoba, Spain) and incubated for 9 days at 37°C with 55% humidity. At day 9 of their embryonic development, eggs were cleaned with ethanol 70° and a window of an approximate 2 cm-diameter was drilled on top of the air chamber of the eggshell. Then, one million Raji-GPR183^{WT} (n=10) or Raji-GPR183^{KO} (n=10) Raji cells per egg were resuspended in 25 µL RPMI medium containing 10% FBS and 100 U/mL penicillin and streptomycin (Thermo Fisher) and 25 µL Matrigel (BD Biosciences). The mix was incubated for 15 min at 37°C and subsequently implanted into the CAM. The window was then covered with a sterile tape and the eggs were placed back in the incubator. At days 12 and 14 of their embryonic development, 10 ng/mL TG-1801 +/- U2 dual assets (10 µg/mL ublituximab + 1 µM umbralisib) or vehicle diluted in RPMI medium were administered topically on the tumor-bearing CAMs. On the 15th day of development (6 days post-implantation), chick embryos were sacrificed by decapitation. Tumors were excised and carefully weighed to determine their mass. Immunohistochemical detection and quantification of CD20 and GPR183 were carried out as above, in representative tumor specimens (n=3 per group).

2.7 RNA sequencing analysis

Two BL cell lines (Daudi and Raji) and two BL primary samples were co-cultured with the bone marrow stromal (BMSC) cell line, StromaNKterts, M2-polarized macrophages and PBMCs (4:1:1:1) in the presence of 10 ng/mL TG-1801 +/- U2. After a 24h incubation, CD20+ target cells were isolated using the EasySep Human Biotin Positive Selection Kit II (StemCell Technologies) and the biotinylated anti-CD20 antibody (BioLegend). Purified CD20+ cells, together with representative bulk Raji xenografts with > 95% tumor B cells were subjected to RNA-seq analysis according to previous procedures (14). Volcano plot showing the most relevant significantly differentially expressed genes between triplet and TG-1801 treatments, with |Log2 fold change| > 1.5 and p-adj value < 0.01 (red dots). Grey, green and blue dots identified genes with insignificant transcriptional and/or statistical variation. Briefly, the raw fastq RNAseq files of each condition were quality checked and gene expression was estimated using Salmon software (https://combine-lab.github.io/salmon/). Differential expression analysis was then carried out using the negative binomial distribution (DESeq2 software, https://bioconductor.org/packages/release/bioc/html/DESeq2.html), accounting for and filtering the effects of the respective controls. Sequencing data have been deposited at the Gene Expression Omnibus (GEO) of the National Center for Biotechnology Information and are accessible through GEO Series accession GSE199413 at (https://www.ncbi.nlm.nih.gov/geo/query/acc.cgi?acc=GSE199413).

Purified CD20+ cells, together with representative Raji xenografts were subjected to RNA extraction and qPCR validation. Briefly, total RNA was extracted using TRIZOL (Thermo Fisher) following manufacturer's instructions. One microgram of RNA was retrotranscribed to complementary DNA using Moloney murine leukemia virus reverse transcriptase (Thermo Fisher) and random hexamer primers (Roche). mRNA expression was analyzed in triplicate by quantitative real-time PCR and the relative expression of each gene was quantified by the comparative cycle threshold method ($\Delta\Delta C_t$) *β-actin* (Fw: GACGA CATGGAGAAAATCTG, Rv: ATGATCTGGGTCATCTTCTC) were used as an endogenous control. The sequences used for the primers are the following *GPR183* (Fw: GACTG GAGAATCGGAGATGC, Rv: CAGCAATGAAGCGGTCAATA), *CCL20* (Fw: CCAATGAAGGCTGTGACATCA, Rv: AGTCTGTTT TGGATTTGCGCA), *IL8* (Fw: AAGGAAAACTGGGTGCAGAG, Rv: GCTTGAAGTTTCACTGGCATC), *CD68* (Fw: CCTCCAGCAGAAGGTTGTCT, Rv: CGAAGGGATGCATTCT GAGC), *CCL4* (Fw: TTCCTCGCAATTTGTGGTA, Rv: GCTTGCTTCTTTTGGTTTGG), *CCL7* (Fw: TGG AGA GCTA CAGAAGGACCA, Rv: GGGTCAGCACAGATCTCCTT), *CXCL1* (Fw: CATCCAAAGTGTGAACGTGAA, Rv: CTATGGGGGATG CAGGATT), *CXCL3*, (Fw: CAAAGTGTGAATGTAAGGTCCCC, Rv: CGGGGTTGAGACAAGCTTTC) and *CXCL10* (Fw: CCTGCA AGCCAATTTTGTCCA, Rv: TGGCCTTCGATTCTGGATTCA).

2.8 Generation of Raji-GPR183^{KO} cells

The generation of a CRISPR-Cas9 gene-editing tool was employed to edit the Raji parental cells line to create GPR183 knockout. 0.5 x 10^6 cells were electroporated on a Nucleofector II device (program A032, Lonza) with 36 pmol SpCas9 Nuclease V3, 44 pmol CRISPR-Cas9 tracRNA ATTO 550, 44 pmol Alt-R CRISPR-Cas9 crRNA Hs.Cas9.GPR183.1.AA (GPR183^{KO} 5´-CAATGAAGCGGTCAATACTC AGG -3`) (IDT-Integrated

DNA Technologies). GPR183^{KO} cells were resuspended in 96-well plates with a limiting dilution of 0.3 cells per well. Two GPR183^{KO} biallelic clones were confirmed by Sanger Sequencing and western blot. Raji-GPR183^{KO} clones are available upon request.

2.9 Western blot analysis

Total protein extracts were obtained from cell lines and tumor specimens using RIPA (Sigma-Aldrich) buffer and subjected to SDS-PAGE. Membrane-transferred proteins were revealed by incubating with primary and secondary antibodies followed by chemiluminescence detection using the ECL system (Pierce) and a Fusion FX imaging system (Vilber Lourmat). Band intensity was quantified using Image J software and normalized to housekeeping protein (GAPDH). Values were referred to the indicated control and added below the corresponding band. If not otherwise specified, representative data from n=2 experiments are shown.

2.10 3D multicellular spheroid generation

One hundred thousand Raji-GPR183^{WT} or Raji-GPR183^{KO} (clone#1) cells were then stained with Hoechst 33342 blue dye (Invitrogen) and cultivated in a conditional medium with 25.000 StromaNKtert-GFP cells for 2 days to generate the BL 3D spheroids. Then, 25,000 M1-macrophages were stained with PKH26 red-fluorescent dye and added to 3D spheroid in the presence or absence of 10 ng/mL TG-1801 +/- U2 (10 μg/mL ublituximab + 1 μM umbralisib) for one more day. The M1-macrophages infiltration was evaluated by live-cell red fluorescence on the EVOS M5000 Cell Imaging Systems.

2.11 Transwell migration assay and F-actin staining

Briefly, Raji-GPR183^{WT}, Raji-GPR183^{KO} (clone#1) and Raji parental cells exposed to the GPR183 inhibitor NIBR189 (Sigma-Aldrich) were cultured for 1 h in culture medium w/o FBS but supplemented with 0.5% bovine serum albumin (Sigma-Aldrich), in the presence or absence of 10 ng/mL TG-1801 +/- U2 combination, and analyzed for CXCL12-dependent chemotaxis, as previously described (16). Values were referred to cells cultured without CXCL12. F-actin levels were assessed after exposure to TG-1801 +/- U2, followed by staining with a TRITC-labelled phalloidin and direct red fluorescence recording.

2.12 Ethics

Animals were handled following protocols approved by the Animal Ethics Committee of the University of Barcelona (registry num. 38/18). Institutional Review Board approvals for the study protocol (ref PI-20-040), amendments, and written informed consent documents from BL patients and healthy donors were obtained prior to study initiation. Study procedures were conducted in accordance with the Declaration of Helsinki. Buffy coats were provided by the Blood and Tissue Bank of Catalonia (agreement NE-A1-IJC).

2.13 Statistical analysis

Presented data are the mean ± SD or SEM of 3 independent experiments. All statistical analyses were done by using GraphPad Prism 9.0 software (GraphPad Software). Comparison between two groups of samples was evaluated by nonparametric Mann–Whitney test to determine how the response is affected by 2 factors. Pearson test was used to assess the statistical significance of correlation. Results were considered statistically significant when p-value < 0.05.

3 Results

3.1 Anti-CD20/PI3Kδi dual asset cooperates with CD47 blockade therapy in CD19+ B-cell tumors

The CD47/CD19 bispecific antibody TG-1801 has recently been shown to trigger *in vitro* response against CD19+ tumors; however these studies did not determine the lowest effective concentrations of this antibody, which may be further used in combination approaches (11). To determine the best working concentrations of TG-1801 *in vitro*, we developed a CD47 occupancy assay using the BL cell line Raji. In this assay, the bispecific CD47/CD19 antibody reached a similar CD47 occupancy compared with the first-in-class CD47 blocking mAb, B6H12 (17) (Figure 1A, right panel and Supplemental Figure S1A). This difference may potentially be explained by the lower level of expression of CD19 compared to CD47 in the BL cell line (data not shown). As expected, TG-1801, but not B6H12-mediated target occupancy, was highly dependent on CD19 expression, as shown when using the T-ALL-derived, CD19-negative, Jurkat cells, in which no significant CD47 blockade was detected with TG-1801 at doses as high as 2 μg/mL, contrasting with the sustained binding of B6H12 at the same concentration (Figure 1A, right and left panels). To evaluate the rationale for combining TG-1801 with ublituximab, a type 1 chimeric anti-CD20 IgG1κ mAb and the PI3Kδ inhibitor umbralisib (U2 dual asset), Raji cells were exposed to these agents either alone or in combination, and cultured in the presence of M1-polarized macrophages or primary circulating PBMCs from healthy donors as a source of effector cells, to assess ADCP or ADCC induction, respectively. As shown in Supplemental Figure S1B, the U2 combination triggered the highest levels of ADCC and ADCP, displaying a 3-fold increase over the control and a significant increase in antibody-dependent cell death compared to both umbralisib and ublituximab alone. Subsequently, U2 combo was directly tested in association with TG-1801 at the previously determined dose, and ADCP and ADCC levels were evaluated as above in a panel of n=6 human B-cell lymphoma cell lines from either BL (Raji, Daudi and Ramos; Figure 1B), DLBCL (Pfeiffer and

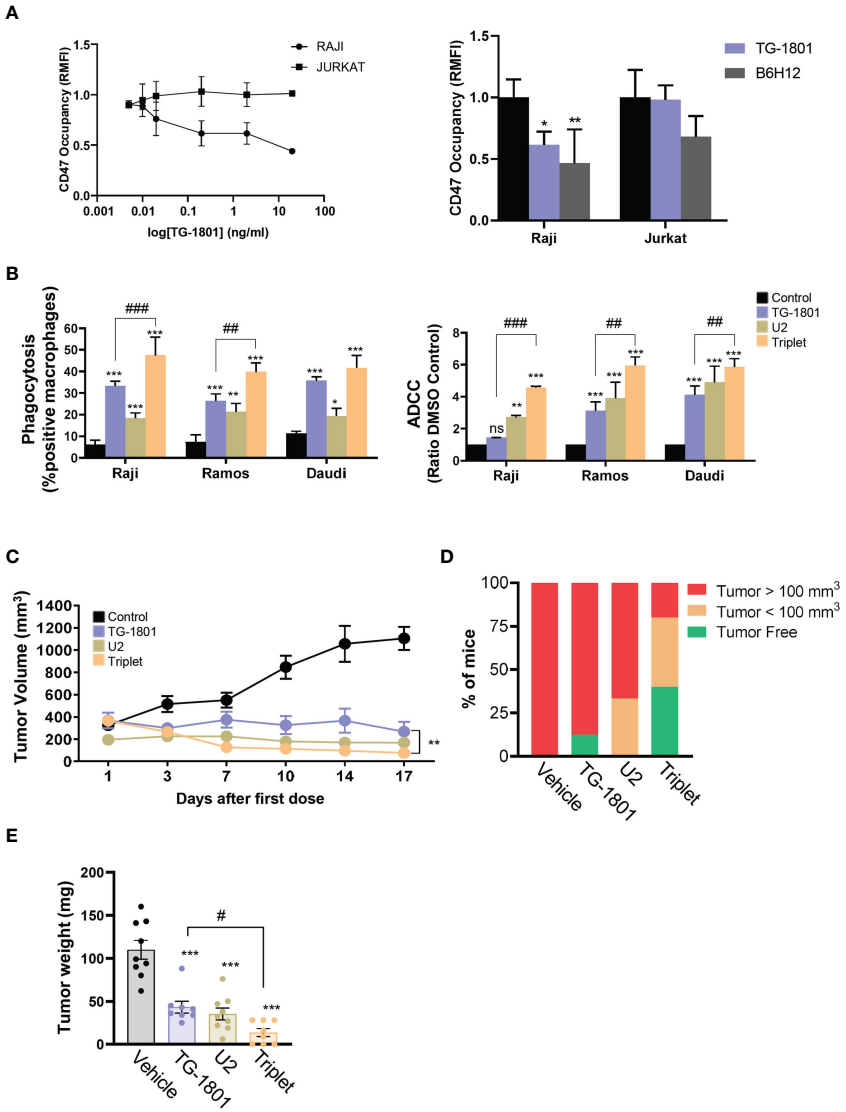

FIGURE 1
U2 regimen cooperates with CD47 blockade in *in vitro* and *in vivo* models of B-cell lymphoma. **(A)** FACS-mediated CD47 occupancy assay in the CD19+ Burkitt lymphoma cell line Raji, and in the CD19- T-ALL cells Jurkat, treated for 1h with different doses of TG-1801 or B6H12. Results are expressed in Relative median fluorescence intensity (RMFI) of the PE-labelled anti-CD47 antibody. Left panel is a dose-occupancy curve of Raji and Jurkat cell lines with different doses of TG-1801. Right panel is a comparison between TG-1801 and B6H12 at 2µg/ml (n=3). **(B)** ADCP (left panel) and ADCC (right panel) activities were assessed in three representative BL cell lines (N=3). Values are expressed as mean ± SD. **(C)** NOD/SCID IL2Rγ-null (NSG) mice were inoculated subcutaneously with 10^7 Raji cells and after 14 days, tumour-bearing animals (n=6-8 mice per group) were orally dosed for 17 days with TG-1801 (5 mg/kg, qw), ublituximab (5 mg/kg, qw) + umbralisib (U2) (150 mg/kg, bid), the triplet (TG-1801 + U2), or an equal volume of vehicle. Tumour volumes were measured each 2-3 days with external callipers. **(D)** Mice with no tumour or low tumour size were kept alive for another 35 days. At day 52 all the mice either tumour-free (green) or bearing a small tumour (orange, < 100 mm^3) were alive. The triplet combo group showed a higher number of tumour-free or low tumour burden-bearing mice. **(E)** Weight recording of Raji CAM-derived tumour at day 15 exposed to TG-1801, U2 or triplet combination (n=8-10 replicates per treatment group). * $p<0.05$, ** $p<0.01$, *** $p<0.001$, when compared to control group. # $p<0.05$, ## $p<0.01$ and ### $p<0.001$ when compared to TG-1801 alone. ns, non-significant.

Karpas-422; Supplemental Figure S1C), or FL (RL; Supplemental Figure S1C) origin. Although both biological processes were visibly potentiated in almost all of the cell lines exposed to the triplet treatment, a comparative analysis demonstrated that, in BL cell lines both TG-1801 pro-cytotoxic and pro-phagocytic activities were potentiated (1.4- to 3.2-fold) by U2 addition, whereas only a barely additive effect of the triplet combination on ADCC was observed in DLBCL- and FL-derived cell lines. Of note, this effect appeared to be related to neither the expression levels of CD47, nor to CD47/CD19 ratios (Supplemental Figure 1D), in accordance with previous reports (10). To carry out an *ad-hoc* drug-drug interaction analysis, a new ADCP analysis was performed in the 3 BL cell lines exposed to increasing doses of TG-1801 (5-10-20 ng/ml), ublituximab (1-2-4 ng/ml) and umbralisib (0.5-1-2 µM), and the drug combination indexes (CI) were calculated using the Chou and Talalay's algorithm. As shown on Supplemental figure S1E, for 20 out of the 27 different TG-1801/U2 combinations evaluated, the CI value was ≤ 0.8, indicative of synergistic drug interaction.

Based on these results, we evaluated the activity of the TG-1801 +U2 triplet combo in a BL (Raji-derived) mouse xenograft. In line with our abovementioned observation, in tumor-bearing mice TG-1801 and U2 exerted notable anti-lymphoma activities, with 76% and 89% tumor growth inhibition (TGI) at day 17 of treatment, respectively (Figure 1C). Nonetheless, the activity of the triplet was maximum as early as 7 days of treatment, reaching a 93% TGI at a time point where TG-1801 monotherapy was almost ineffective. This superior efficacy was maintained during the whole treatment schedule (Figure 1C), with no detectable toxicity (data not shown). Of special interest, 2 out of 5 mice (40%) remained tumor-free 35 days after the last dose in the triplet arm, compared to the reduced rate of prolonged remission (12.5%) in the TG-1801 group (Figure 1D).

To pinpoint the effect of the triple combination, an immunocompetent chicken chorioallantoic membrane (CAM)-derived xenograft Raji model (18) was carried out (see experimental workflow in Supplemental Figure S1F). Similarly, to the mouse model, in the Raji-derived CAM assay, both TG-1801 and U2 treatments inhibited 70% of tumor growth and the activity of the triplet was significantly higher (86% TGI, Figure 1E).

Altogether, these *in vitro* and *in vivo* data suggested that the combination of CD47 checkpoint blockade therapy to dual CD20/PI3K targeting evokes a mechanism that promotes a stronger and prolonged innate immune response when compared to each agent used separately.

3.2 GPR183 is upregulated in response to CD47/CD20/PI3Kδi triplet treatment

To uncover the mechanisms underlying the superior effect of the triplet *vs* anti-CD47/CD19 monotherapy, transcriptomic analyses were carried out on a set of six samples that included Raji mouse xenograft tumors (n=2) and CD20+ cells isolated from Raji, Daudi and two adult sporadic BL primary samples (one case with abdominal involvement and another case with bone marrow involvement), co-cultured with the bone marrow-derived stromal cell line, stromaNKtert (19), M2-polarized primary macrophages, primary circulating PBMCs, in the presence of either TG-1801 or TG-1801+U2 triplet. As shown in Figure 2A, a total of 20 genes were significantly up- or down-regulated in the triplet compared to TG-1801 monotherapy, in all six samples and in both *in vitro* and *in vivo* settings. A gene set enrichment analysis (GSEA) of the same data identified inflammatory (NES=2.43, FDR=0) and TNFα-driven signatures (NES=2.43, FDR=0) as predominantly expressed upon treatment with the triplet combination, when compared to TG-1801 single agent therapy, suggesting that the stronger activity of the triplet was based on the activation of an immune-related antitumor effect. In the heatmap showing a set of genes strongly activated in all six samples in the triplet group (Figure 2B), the highest up-regulated gene in both signatures was the G protein-coupled receptor 183 (GPR183, also known as Epstein-Barr virus (EBV)-induced G protein-coupled receptor 2, EBI2). An increase in *GPR183* mRNA was confirmed by qPCR after a 4-hour and a 24-hour incubation of the four cell lines with TG-1801/U2 combo (Figure 2C; Supplemental Figure S1G). A comparable increase in GPR183 protein levels was also shown using western blotting in the Raji and Daudi cell lines subjected to the same treatments (+49% and +43%, respectively; Figure 2D), and by immunohistochemistry (IHC) in representative tumors from the two Raji xenograft models (mouse and CAM) dosed with the triplet regimen (Figure 2E; Supplemental Figure S1H).

GPR183 was first identified by sequence similarity as a GPCR induced by Epstein-Barr virus (EBV) infection. The upregulation of this pro-inflammatory receptor is associated with a better prognosis of DLBCL patients treated with the standard immunochemotherapeutic (R-CHOP) regimen, according to published gene array database (gse10846; R2: Genomics Analysis and Visualization Platform (http://r2.amc.nl; http://r2platform.com)). In addition, GPR183 plays an important role in B-cell motility and positioning during the germinal center reaction (20, 21). The gradient of its natural ligand, oxysterol, acts as a chemoattractant of GPR183+ cells. Interestingly, among a panel of eight genes identified besides *GPR183* in the two inflammation gene signatures, the transcript of another chemoattractant gene, *CCL20*, was upregulated by the triplet combination in all *in vitro* and *in vivo* models (Figure 2C). In addition, increased tumor infiltration of mouse and chicken macrophages in BL tumors, as revealed by IHC detection of the mouse antigen F4/80 and qPCR quantification of the chicken antigen *MRCL1* (22), was accompanied by a loss of histone H3-pSer10 nuclear staining, suggestive of a consistent reduction in tumor mitotic index in animals subjected to triplet therapy, when compared to TG-1801 and U2 treatment arms (Figures 2E, F).

3.3 GPR183 is required for B-cell trafficking and macrophage-dependent phagocytosis after the triplet treatment

To investigate how the upregulation of GPR183 in cancer cells could impact their recognition and phagocytosis by M1 macrophages, two Raji-GPR183^{KO} single-clones (clone #1 and clone #2) were generated by CRISPR/Cas9 gene editing (Figure 3A) using previously described procedures (14). Cells from clone #1 were co-cultured for 24h with primary M1 macrophages and BMSCs in a conditioned medium to form functional 3D spheroids, as previously reported (23). Compared to their Raji-GPR183^{wt} counterparts, the Raji-GPR183^{KO} spheroids displayed a complete absence of M1 cell infiltration within the multicellular aggregates, both at basal levels and upon exposure to the triplet therapy (Figure 3B). Accordingly, ADCP activity was abrogated in the Raji-GPR183^{KO} cell cultures obtained from the two clones (Figure 3C, left panel) highlighting the critical role of GPR183 in the recruitment of macrophages after CD47/CD20/PI3Kδ triple targeting. ADCC was also compromised, although to a lower extent (Figure 3C, right panel). Supporting these results, global inflammatory signature, and especially *CCL20* gene overexpression, was not detected anymore in Raji-GPR183^{KO} (clone #1) co-cultures exposed to the triplet therapy (Figure 3D).

To evaluate whether a functional GPR183 was required for the triplet drug interaction, Raji cells were exposed for 1 hour to the

10.3389/fimmu.2023.1130052

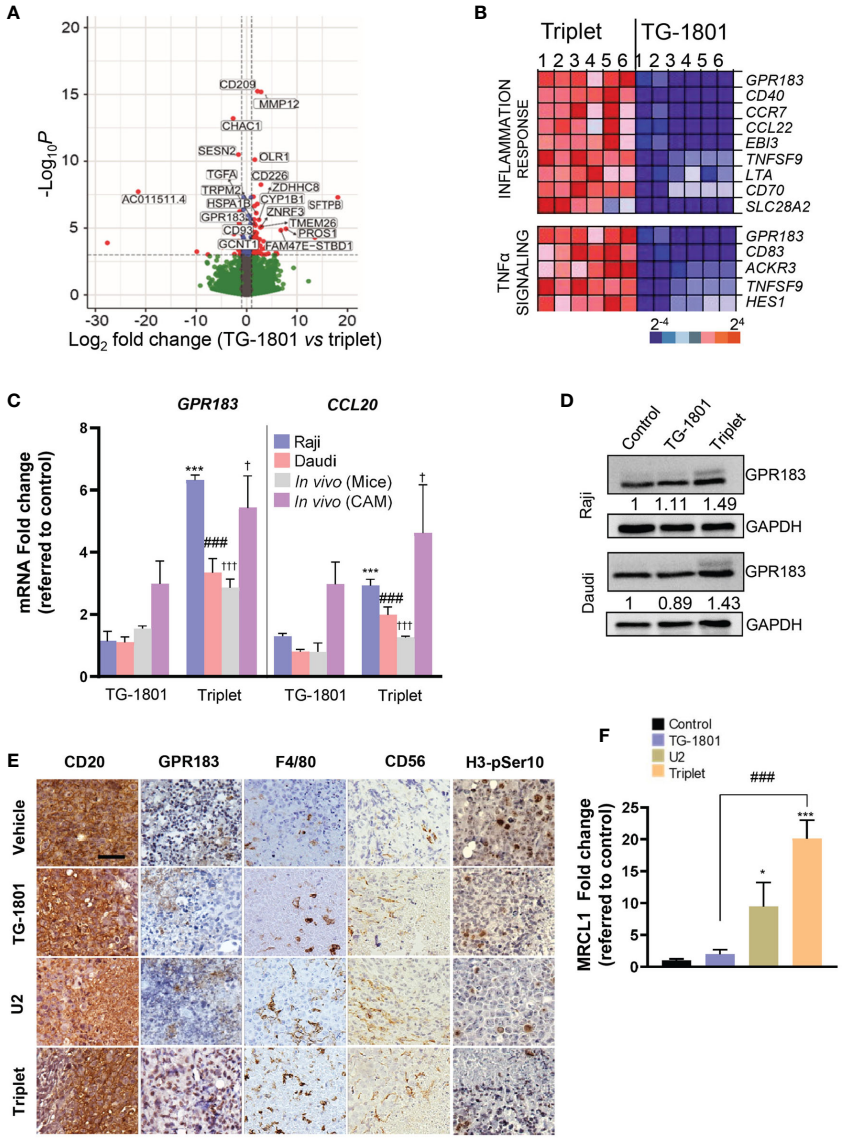

FIGURE 2
Upregulation of GPR183 is a hallmark of U2 and TG-1801 combinational effect *in vitro* and *in vivo*. **(A)** Volcano plot showing the most relevant significantly differentially expressed genes between triplet and TG-1801 treatments in n=6 BL samples (two cell lines, two primary samples and two representative Raji xenografts specimens). Genes undergoing a similar modulation in all the *in vitro* and *in vivo* models (n=20) have been labelled. **(B)** GSEA-mediated identification of the main enriched gene sets in the triplet-treated samples compared to the samples treated with TG-1801. Samples were sorted from left to right: 1-Raji, 2-Daudi, 3-4- BL primary samples and 5-6- CD20+ cells sorted from 2 representative Raji xenograft specimens. **(C)** qPCR determination of *GPR183* and *CCL20* transcript levels in Raji and Daudi cell lines exposed to TG-1801 or to the triplet therapy as previously, and in the two Raji *in vivo* (mouse and CAM) models dosed with the different agents. Values are referred to untreated Raji cultures. **(D)** Immunoblot detection and densitometric quantification of GPR183 protein levels (SantaCruz, #sc-514342) in BL cell lines exposed to TG-1801 +/- U2 dual asset, using GAPDH as a loading control. Values are normalized to control untreated cells. For each cell line, shown is a representative experiments out of three. **(E)** Immunohistochemistry (IHC) labelling of CD20 (Clone L26, Sigma-Aldrich), GPR183 (Clone G-12, Santa Cruz), F4/80 (Clone SP115, Abcam), Histone H3-pSer10 (Clone E173, Abcam) and CD56/NCAM-1 (Clone EPR1827, Abcam) in tissue sections from tumour specimens (shown are pictures from 1 out of 3 representative specimens) Scale bar: 50 µm. **(F)** *MRCL1* transcript levels in the Raji-derived CAM model. Data are presented in fold-change related to the control (N=8-10) according to the different treatment regimens. * $p<0.05$, *** $p<0.001$, ### $p<0.001$, and † $p<0.05$ and ††† $p<0.001$ when compared to control group in Raji (*in vitro*), Daudi (*in vitro*) and Raji (*in vivo*) models, respectively. ns, non-significant.

GPR183 inhibitor NIBR189 (24), washed out, and co-cultured for 4 hours with M1-polarized macrophages, in the presence of U2 +/- TG-1801, and ADCP induction was quantified as described above. As shown in Figure 3E, the relative levels of phagocytosis were decreased by 3-fold after GPR183 pharmacological blockade in triplet-treated co-cultures, thus confirming the requirement of an active GPR183 receptor for the full activation of macrophage function.

Since GPR183 is a known antagonist of chemokine-mediated B cell migration (25), a transwell migration assay using recombinant CXCL12 as a chemoattractant was set up. The chemotaxis

10.3389/fimmu.2023.1130052

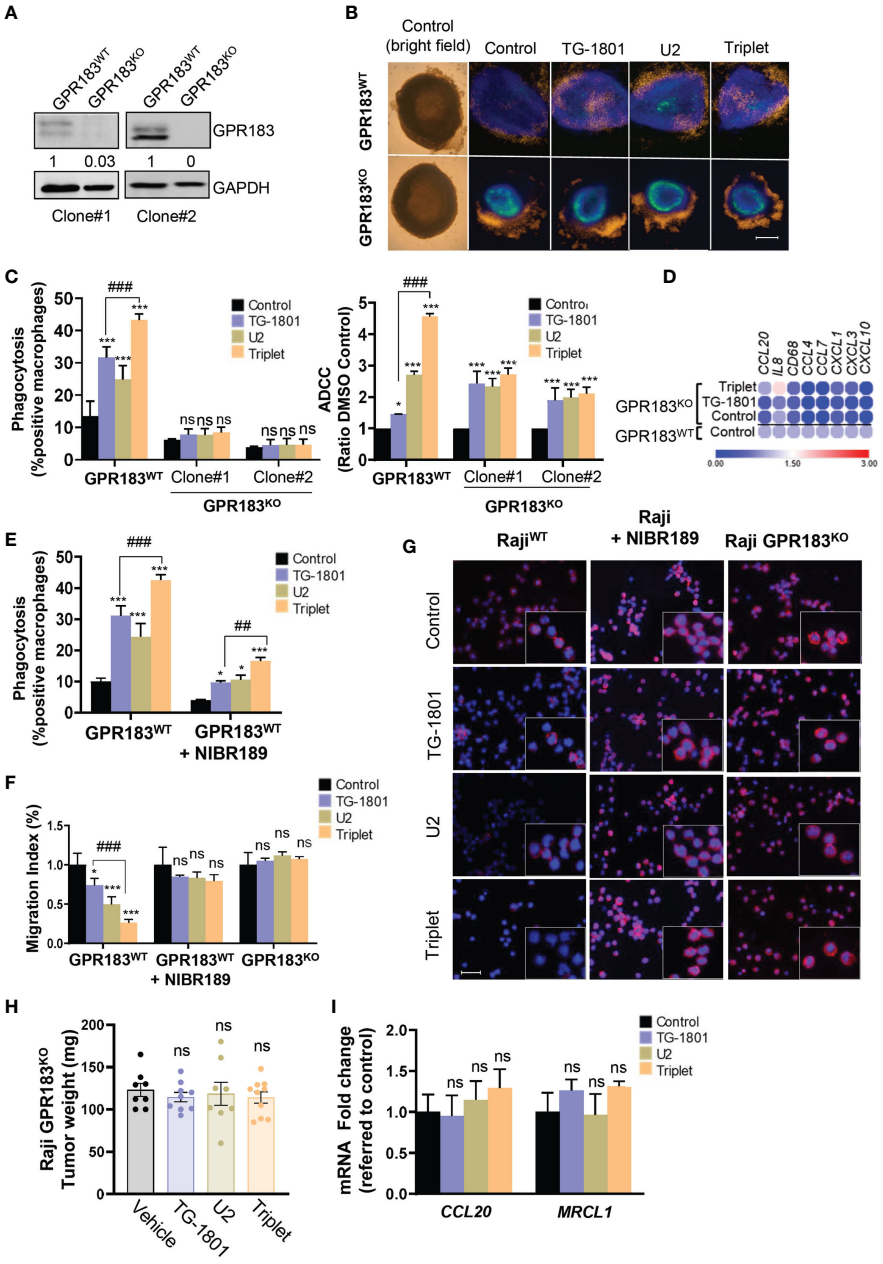

FIGURE 3
GPR183 is required for impaired B cell trafficking and tumour cell phagocytosis upon TG-1801/U2 triple combination therapy. **(A)** Immunoblot detection and densitometric quantification of GPR183 in both Raji-GPR183^{WT} and Raji-GPR183^{KO} cells, using GAPDH expression as a loading control. Values are referred to control, wild type cells. **(B)** Raji-GPR183^{WT} or Raji-GPR183^{KO} 3D spheroid in presence or absence of 10 ng/mL TG-1801 +/- U2 (10 µg/mL ublituximab + 1 µM umbralisib) for one more day. The infiltration of M1 macrophages was evaluated by live-cell red fluorescence. Scale bar: 500 µm. **(C)** Triggering of phagocytosis (left panel) and cell-mediated cytotoxicity (right panel) was assessed in Raji-GPR183^{WT} and Raji-GPR183^{KO} cultures upon quantification of engulfed B cell red fluorescence with pHrodo and LDH release assay, respectively. For each assay, shown are average values obtained from three independent replicates. **(D)** Raji-GPR183^{WT} and Raji-GPR183^{KO} were co-cultured with BMSCs, M2-polarized primary macrophages and PBMCs (4:1:1:1) and treated with vehicle, TG-1801 or the triplet combination for 24h. Then, purified CD20+ cells were subjected to RNA extraction and qPCR. Data are presented in fold-change related to the Raji-GPR183^{WT} control. **(E)** ADCP activities were assessed in Raji cells with or without the GPR183 inhibitor NIBR189 prior to treatment with 10 ng/mL TG-1801 +/- U2. Shown are average values from n=3 replicates. **(F)** The cell migration index of Raji-GPR183^{WT}, Raji-GPR183^{KO} (clone #1) cells exposed to the GPR183 inhibitor NIBR189, in presence or absence of 10 ng/mL TG-1801 +/- U2 combination. Shown are average values from n=3 replicates. **(G)** F-actin levels were assessed in the different cultures exposed to TG-1801 +/- U2 as in **(E)**, followed by staining with a TRITC-labelled phalloidin and direct red fluorescence recording. Nuclei were counterstained with DAPI (blue) (shown are representative pictures from 1 out of 3 fields). Scale bar: 50 µm. **(H)** Tumour weights at day 15 for Raji GPR183^{KO} (N=8-10) exposed to TG-1801, U2 or triplet combination. **(I)** *CCL20* and *MRCL1* transcript levels in GPR183^{KO} tumours. Data are presented in fold-change related to the control (shown are median values from 8-10 replicates) according to the different treatment regimens. Values are expressed as mean ± SD. * p<0.05, *** p<0.001, when compared to control group. $^{\#\#}$ p<0.01 and $^{\#\#\#}$ p<0.001 when compared to TG-1801 alone. ns, non-significant.

properties of CXCL12 were tested on the Raji parental cells, the Raji-GPR183^{KO} cells, and the NIBR189-pretreated cultures. Figure 3F shows that BL cell migration was significantly impaired by both U2 and TG-1801 treatments, and that the combination led to an accentuated (75%) inhibition of cell mobility. This effect was completely lost either after GPR183 pharmacological inhibition by NIBR189 or upon the genetic deletion of the receptor. Accordingly, F-actin polymerization was decreased by 70% in Raji cells exposed to the triplet treatment and this effect was counteracted by the absence of GPR183 (clone #1) or by its pharmacological blockade (Figures 3G, S1I), in agreement with previous studies highlighting the relevance of F-actin disruption in the anti-lymphoma effect of anti-CD47 antibodies (26). Finally, the crucial role of GPR183 in BL response to the triplet was confirmed *in vivo* in a Raji-GPR183^{KO} CAM model, in which TG-1801, U2, and the combination treatment failed to impact tumoral growth, with no modulation of *CCL20* expression and failed intratumoral infiltration of MRCL1 + macrophages (Figures 3H, I).

Altogether, these data strongly support that GPR183 upregulation is a prerequisite to the recruitment of macrophages and to the initiation of the inflammatory response, in Raji xenografts subjected to the triplet treatment.

4 Discussion

CD47 immune checkpoint inhibitors have emerged as promising immunotherapy in cancer treatment thanks to their ability to facilitate the concomitant inhibition of the "do-not-eat-me" signal and to boost antitumor T-cell response. Indeed, although CD47/SIRPα axis blockade was initially believed to lead to antitumor activity exclusively through ADCP (27), it was further demonstrated that targeting CD47 also promotes T cell–mediated elimination of immunogenic tumors (28, 29). Considering the relevance of the CD47/SIRPα axis in tumor progression, including under (chemo)-therapeutic pressure, several novel studies have demonstrated the potential of CD47-based combination therapies in different types of cancer (30). Among the most promising combinations, the synergistic FcR-dependent activation of phagocytosis by the anti-CD47 mAb Hu5F9-G4 associated to rituximab signaling has demonstrated great effectivity in B-NHL cell lines and primary samples (31), and has further shown promising clinical activity with few side effect in the phase Ib clinical trial NCT02953509 involving R/R DLBCL and FL patients (32). Similarly, bispecific antibodies that co-target CD47 and CD20 can induce selective phagocytosis of B-NHL cells, and prolong the survival time of mice transplanted with these tumors (33). This dual anti-CD20/anti-CD47 approach has provided convincing clinical results and is still being extensively evaluated, both pre-clinically and clinically, in B-cell lymphoma (7). Here, we present a new set of data that propose for the first time a biological rationale for the combination of the first-in-kind anti-CD47/CD19 bispecific antibody, TG-1801, with the clinically tested pair of the anti-CD20 antibody ublituximab with umbralisib, a PI3K inhibitor.

PI3Ks are a key component of cell machinery controlling cellular key pathways such as growth, proliferation, survival, migration and differentiation. Dysregulation of this pathway have been described in several types of cancer, including BL (34, 35). Expression of the PI3Kδ subunit is generally restricted to hematopoietic cells, and is essential for the development and expansion of normal and malignant B-cells (36). Preclinical data with different class-specific PI3K inhibitors have suggested that part of their antitumor activity relies on the modulation of the tumor microenvironment (TME) and to an enhancement of adaptive immunity, including an improved intratumoral macrophage infiltration, thereby increasing the efficacy of immune checkpoint blockade therapy (37–39). Our present data support for the first time the use of a PI3Kδ inhibitor to promote the remodeling of the tumor microenvironment *in vitro* and *in vivo*, for a better anti-CD47-mediated activation of macrophages. Indeed, we observed that the TG-1801/ublituximab/umbralisib triplet, when compared to TG-1801 monotherapy, significantly improved innate immunity *in vitro* and *in vivo*, with the potentiation of both macrophages and cytotoxic cell activity, although this latter at a lower extent. Unsurprisingly, most of this effect was due to TG-1801, which was already known to exert its antitumor effect by eliciting ADCP and ADCC (10) and to increase the phagocytosis of tumor cells by the macrophage and monocyte populations present in lymphoid TME (11). Of special interest, the superior antitumor activity of the triplet combination in mice resulted in a prolonged response with a higher number of tumor-free animals 35 days after the last dose. Transcriptomic and immunophenotypic analyses revealed that this sustained effect was closely linked to an enrichment in inflammatory gene signatures and an enhanced recruitment of macrophages and NK cells at the tumor site, being these two phenomena known prerequisites for full activity of immune checkpoint blockers (40).

By coupling phenotypic characterization to gene edition, we further propose that among the main pro-inflammatory genes activated in a set of *in vitro* and *in vivo* models of B-NHL that reconstitute most features of the lymphoid TME and the main aspects of B-NHL architecture, the GPR183 receptor represents a crucial regulator involved in the efficacy of the drug combination. GPR183 belongs to the rhodopsin family and is widely expressed in B, T, and dendritic cells (20, 40). This factor is responsible for regulating the positioning and migration of immune cells within secondary lymphoid organs (41, 42) and its deregulated activity or expression has been found in germinal center B-like DLBCL, FL, CLL and acute myeloid leukemia (43). Accordingly, we found that treatment-induced upregulation of GRP183 in BL tumors strongly affect F-actin polymerization in B cells, with the consequent impairment of CXCL12-dependent chemotaxis, a phenomenon that possibly render these latter more accessible to pro-inflammatory macrophages with the capacity to limit tumor growth (42). Finally, and in agreement with our finding although in another cellular context, loss-of-function mutation of *GPR183* or treatment with a GPR183 antagonist, have recently been associated with a reduced macrophage infiltration and a lower inflammatory cytokine production in the lungs of mice infected by respiratory viruses (44).

PI3K/Akt signaling was recently identified as the main downstream axis synergistically affected by co-exposure of

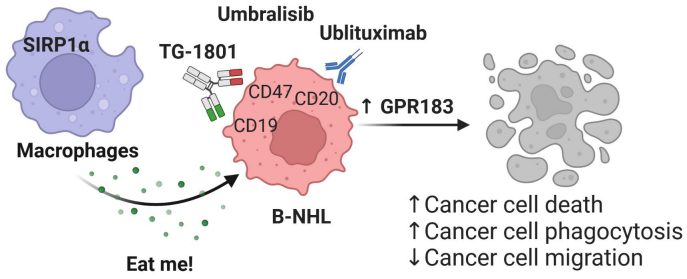

FIGURE 4
Mechanism of action of the TG-1801/U2 triplet combination therapy in BL. The novel CD47-CD19 bispecific antibody potentiates the anti-tumour activity of the ublituximab-umbralisib regimen through activation of the pro-inflammatory GPR183, thus promoting macrophage-dependent phagocytosis, B-cell cytoskeleton remodelling and B-cell motility.

malignant B cells to different anti-CD20 mAbs and to the PI3Kδ inhibitor idelalisib (45). However, in the case of BL and under determined experimental settings (i.e. upon exposure to immunomodulatory drugs), the anti-CD20 mAb rituximab was shown to promote EBV reactivation, thereby stimulating PI3K signaling (46). Although EBV intracellular signaling hasn't been challenged here, one may hypothesize that, as a bona fide EBV-responsive gene, GPR183 may be upregulated by the simultaneous ligation of CD47 and CD20 by TG-1801 and ublituximab, rending at the same time these cells more susceptible to PI3Kδ blockade by umbralisib.

In summary, our results support a role for GPR183 in the recognition and elimination *in vitro* and *in vivo* of malignant B cells by activated macrophages, upon concomitant targeting of CD20, CD47 and PI3Kδ in tumor cells (Figure 4). Future studies will be aimed at understanding whether GPR183 could constitute a *bona fide* biomarker for the activity of anti-CD47-based therapeutic regimens. Testing whether this discovery can be generalized to other agents from the same classes than those used here, is currently underway.

Data availability statement

The datasets presented in this study can be found in online repositories. The names of the repository/repositories and accession number(s) can be found in the article/Supplementary Material.

Author contributions

MR, NP-P and JS: Resources, investigation, methodology, writing–original draft. PB: Data curation, software, visualization. DR-G: Investigation, methodology. MA: Investigation. MF-S: Investigation. HM: Validation, writing review and editing. FB: Writing–review and editing. ME: Data curation, writing review and editing. EN: Conceptualization, resources, supervision, validation, writing–original draft, writing–review and editing. GR: Conceptualization, resources, supervision, funding acquisition, validation, investigation, visualization, writing–original draft, project administration, writing–review and editing. All authors contributed to the article and approved the submitted version.

Funding

This study was financially supported by TG Therapeutics, Fondo de Investigación Sanitaria PI18/01383, European Regional Development Fund (ERDF) "Una manera de hacer Europa" (to GR). JS and MF-S were recipients of a Sara Borrell research contract (CD19/00228) and a predoctoral fellowship (FI19/00338) from Instituto de Salud Carlos III, respectively. MA was a fellow of PROTEOblood, a project co-financed by the European Regional Development Fund (ERDF) through the Interreg V-A Spain-France-Andorra (POCTEFA) program (EFA360/19). This work was carried out under the CERCA Program (Generalitat de Catalunya).

Acknowledgments

We are very grateful to Salvador Sánchez Vinces, at Sao Francisco University/Brazil, for his support in bioinformatics analysis. Samples included in this study were provided by "Colección de muestras biológicas del Institut de Recerca contra la Leucèmia Josep Carreras" and were processed following standard operating procedures with the approval of the Ethics and Scientific Committees of the Germans Trias I Pujol University Hospital (Badalona, Spain).

Conflict of interest

Authors HP and EN were employed by company TG Therapeutics.

The authors declare that this study received funding from TG Therapeutics. The funder had the following involvement in the study: study design, data validation and manuscript preparation. HM reports personal fees from TG Therapeutics, Inc. during the conduct of the study. EN reports employment and ownership of stock with TG Therapeutics. GR reports grants from TG Therapeutics and Instituto de Salud Carlos III during the conduct of the study.

The remaining authors declare that the research was conducted in the absence of any commercial or financial relationships that could be construed as a potential conflict of interest.

Publisher's note

All claims expressed in this article are solely those of the authors and do not necessarily represent those of their affiliated organizations, or those of the publisher, the editors and the reviewers. Any product that may be evaluated in this article, or claim that may be made by its manufacturer, is not guaranteed or endorsed by the publisher.

Supplementary material

The Supplementary Material for this article can be found online at: https://www.frontiersin.org/articles/10.3389/fimmu.2023.1130052/full#supplementary-material

References

1. Blattman JN, Greenberg PD. Cancer immunotherapy: a treatment for the masses. *Science* (2004) 305:200–5. doi: 10.1126/science.1100369

2. Banerjee T, Vallurupalli A. Emerging new cell therapies/immune therapies in b-cell non-hodgkin's lymphoma. *Curr Probl Canc* (2022) 46(1):100825. doi: 10.1016/j.currproblcancer.2021.100825

3. Rushton CK, Arthur SE, Alcaide M, Cheung M, Jiang A, Coyle KM, et al. Genetic and evolutionary patterns of treatment resistance in relapsed b-cell lymphoma. *Blood Adv [Internet]* (2020) 4(13):2886–98. doi: 10.1182/bloodadvances.2020001696

4. Miles RR, Arnold S, Cairo MS. Risk factors and treatment of childhood and adolescent burkitt lymphoma/leukaemia. *Br J Haematol* (2012) 156:730–43. doi: 10.1111/j.1365-2141.2011.09024.x

5. Hecht JL, Aster JC. Molecular biology of burkitt's lymphoma. *J Clin Oncol* (2000) 18(21):3707–21. doi: 10.1200/JCO.2000.18.21.3707

6. Barclay A, Van den Berg T. The interaction between signal regulatory protein alpha (SIRPα) and CD47: structure, function, and therapeutic target. *Annu Rev Immunol* (2014) 32:25–50. doi: 10.1146/annurev-immunol-032713-120142

7. Armengol M, Santos JC, Fernández-Serrano M, Profitós-Pelejà N, Ribeiro ML, Roué G. Immune-checkpoint inhibitors in b-cell lymphoma. *Cancers (Basel)* (2021) 13 (2):1–41. doi: 10.3390/cancers13020214

8. Matlung HL, Szilagyi K, Barclay NA, van den Berg TK. The CD47-SIRPα signaling axis as an innate immune checkpoint in cancer. *Immunol Rev* (2017) 276 (1):145–64. doi: 10.1111/imr.12527

9. Hatterer E, Chauchet X, Richard F, Barba L, Moine V, Chatel L, et al. Targeting a membrane-proximal epitope on mesothelin increases the tumoricidal activity of a bispecific antibody blocking CD47 on mesothelin-positive tumors. *MAbs [Internet]* (2020) 12(1):1739408. doi: 10.1080/19420862.2020.1739408

10. Buatois V, Johnson Z, Salgado-Pires S, Papaioannou A, Hatterer E, Chauchet X, et al. Preclinical development of a bispecific antibody that safely and effectively targets CD19 and CD47 for the treatment of b-cell lymphoma and leukemia. *Mol Cancer Ther* (2018) 17(8):1739–51. doi: 10.1158/1535-7163.MCT-17-1095

11. Chauchet X, Cons L, Chatel L, Daubeuf B, Didelot G, Moine V, et al. CD47xCD19 bispecific antibody triggers recruitment and activation of innate immune effector cells in a b-cell lymphoma xenograft model. *Exp Hematol Oncol* (2022) 11(1):1–13. doi: 10.1186/s40164-022-00279-w

12. Palazzo A, Herter S, Grosmaire L, Jones R, Frey CR, Limani F, et al. The PI3Kδ-selective inhibitor idelalisib minimally interferes with immune effector function mediated by rituximab or obinutuzumab and significantly augments b cell depletion in vivo. *J Immunol* (2018) 200(7):2304–12. doi: 10.4049/jimmunol.1700323

13. Lunning M, Vose J, Nastoupil L, Fowler N, Burger JA, Wierda WG, et al. Ublituximab and umbralisib in relapsed/refractory b-cell non-Hodgkin lymphoma and chronic lymphocytic leukemia. *Blood [Internet]* (2019) 134(21):1811–20. doi: 10.1182/blood.2019002118

14. Ribeiro ML, Reyes-Garau D, Vinyoles M, Profitos-Peleja N, Santos JC, Armengol M, et al. Antitumor activity of the novel BTK inhibitor TG-1701 is associated with disruption of ikaros signaling in patients with b-cell non-Hodgkin lymphoma. *Clin Cancer Res* (2021) 27(23):6591–601. doi: 10.1158/1078-0432.CCR-21-1067

15. Bankhead P, Loughrey MB, Fernández JA, Dombrowski Y, McArt DG, Dunne PD, et al. QuPath: open source software for digital pathology image analysis. *Sci Rep* (2017) 7(1):1–7. doi: 10.1038/s41598-017-17204-5

16. Balsas P, Esteve-Arenys A, Roldán J, Jiménez L, Rodríguez V, Valero JG, et al. Activity of the novel BCR kinase inhibitor IQS019 in preclinical models of b-cell non-Hodgkin lymphoma. *J Hematol Oncol* (2017) 10(1):1–14. doi: 10.1186/s13045-017-0447-6

17. Mateo V, Lagneaux L, Bron D, Biron G, Armant M, Delespesse G, et al. CD47 ligation induces caspase-independent cell death in chronic lymphocytic leukemia. *Nat Med* (1999) 5(11):1277–84. doi: 10.1038/15233

18. Klingenberg M, Becker J, Eberth S, Kube D, Wilting J. The chick chorioallantoic membrane as an in vivo xenograft model for burkitt lymphoma. *BMC Cancer* (2014) 14 (1):1–12. doi: 10.1186/1471-2407-14-339

19. Dlouhy I, Armengol M, Recasens-Zorzo C, Ribeiro ML, Pérez-Galán P, Bosch F, et al. Interleukin-1 receptor associated kinase 1/4 and bromodomain and extraterminal inhibitions converge on NF-κB blockade and display synergistic antitumoral activity in activated b-cell subset of diffuse large b-cell lymphoma with $MYD88^{L265P}$ mutation. *Haematologica* (2020) 106:2749. doi: 10.3324/haematol.2022.281988

20. Liu C, Yang XV, Wu J, Kuei C, Mani NS, Zhang L, et al. Oxysterols direct b-cell migration through EBI2. *Nat* (2011) 475(7357):519–23. doi: 10.1038/nature10226

21. Pereira JP, Kelly LM, Xu Y, Cyster JG. EBV induced molecule-2 mediates b cell segregation between outer and center follicle. *Nature* (2009) 460(7259):1122. doi: 10.1038/nature08226

22. Hu T, Wu Z, Bush SJ, Freem L, Vervelde L, Summers KM, et al. Characterization of subpopulations of chicken mononuclear phagocytes that express TIM4 and CSF1R. *J Immunol* (2019) 202(4):1186–99. doi: 10.4049/jimmunol.1800504

23. Souza GR, Molina JR, Raphael RM, Ozawa MG, Stark DJ, Levin CS, et al. Three-dimensional tissue culture based on magnetic cell levitation. *Nat Nanotechnol* (2010) 5 (4):291–6. doi: 10.1038/nnano.2010.23

24. Gessier F, Preuss I, Yin H, Rosenkilde MM, Laurent S, Endres R, et al. Identification and characterization of small molecule modulators of the Epstein–Barr virus-induced gene 2 (EBI2) receptor. *J Med Chem* (2014) 57(8):3358–68. doi: 10.1021/jm4019355

25. Barroso R, Martínez Muñoz L, Barrondo S, Vega B, Holgado BL, Lucas P, et al. EBI2 regulates CXCL13-mediated responses by heterodimerization with CXCR5. *FASEB J* (2012) 26(12):4841–54. doi: 10.1096/fj.12-208876

26. Barbier S, Chatre L, Bras M, Sancho P, Roué G, Virely C, et al. Caspase-independent type III programmed cell death in chronic lymphocytic leukemia: the key role of the f-actin cytoskeleton. *Haematologica* (2009) 94(4):507–17. doi: 10.3324/haematol.13690

27. Majeti R, Chao MP, Alizadeh AA, Pang WW, Jaiswal S, Gibbs KD, et al. CD47 is an adverse prognostic factor and therapeutic antibody target on human acute myeloid leukemia stem cells. *Cell* (2009) 138(2):286–99. doi: 10.1016/j.cell.2009.05.045

28. Liu X, Pu Y, Cron K, Deng L, Kline J, Frazier WA, et al. CD47 blockade triggers T cell-mediated destruction of immunogenic tumors. *Nat Med* (2015) 21(10):1209. doi: 10.1038/nm.3931

29. Tseng D, Volkmer JP, Willingham SB, Contreras-Trujillo H, Fathman JW, Fernhoff NB, et al. Anti-CD47 antibody-mediated phagocytosis of cancer by macrophages primes an effective antitumor T-cell response. *Proc Natl Acad Sci USA* (2013) 110(27):11103–8. doi: 10.1073/pnas.1305569110

30. Veillette A, Chen J. SIRPα–CD47 immune checkpoint blockade in anticancer therapy. *Trends Immunol* (2018) 39(3):173–84. doi: 10.1016/j.it.2017.12.005

31. Chao MP, Alizadeh AA, Tang C, Myklebust JH, Varghese B, Gill S, et al. Anti-CD47 antibody synergizes with rituximab to promote phagocytosis and eradicate non-Hodgkin lymphoma. *Cell* (2010) 142(5):699–713. doi: 10.1016/j.cell.2010.07.044

32. Advani R, Flinn I, Popplewell L, Forero A, Bartlett NL, Ghosh N, et al. CD47 blockade by Hu5F9-G4 and rituximab in non-hodgkin's lymphoma. *N Engl J Med* (2018) 379(18):1711–21. doi: 10.1056/NEJMoa1807315

33. Piccione EC, Juarez S, Liu J, Tseng S, Ryan CE, Narayanan C, et al. A bispecific antibody targeting CD47 and CD20 selectively binds and eliminates dual antigen expressing lymphoma cells. *MAbs* (2015) 7(5):946–56. doi: 10.1080/19420862.2015.1062192

34. Cantrell DA. Phosphoinositide 3-kinase signalling pathways. *J Cell Sci [Internet]* (2001) 114(8):1439–45. doi: 10.1242/jcs.114.8.1439

35. Lawrence MS, Stojanov P, Mermel CH, Robinson JT, Garraway LA, Golub TR, et al. Discovery and saturation analysis of cancer genes across 21 tumour types. *Nat [Internet]* (2014) 505(7484):495–501. doi: 10.1038/nature12912

36. Srinivasan L, Sasaki Y, Calado DP, Zhang B, Paik JH, DePinho RA, et al. PI3 kinase signals BCR-dependent mature b cell survival. *Cell* (2009) 139(3):573–86. doi: 10.1016/j.cell.2009.08.041

37. Gouni S, Marques-Piubelli ML, Strati P. Follicular lymphoma and macrophages: impact of approved and novel therapies. *Blood Adv [Internet]* (2021) 5(20):4303–12. doi: 10.1182/bloodadvances.2021005722

38. Zheng W, Pollard JW. Inhibiting macrophage PI3Kγ to enhance immunotherapy. *Cell Res* (2016) 26(12):1267–8. doi: 10.1038/cr.2016.132

39. Kaneda MM, Messer KS, Ralainirina N, Li H, Leem CJ, Gorjestani S, et al. PI3Kγ is a molecular switch that controls immune suppression. *Nat [Internet]* (2016) 539 (7629):437–42. doi: 10.1038/nature19834

40. Wang C, Cui A, Bukenya M, Aung A, Pradhan D, Whittaker CA, et al. Reprogramming NK cells and macrophages via combined antibody and cytokine therapy primes tumors for elimination by checkpoint blockade. *Cell Rep* (2021) 37 (8):110021. doi: 10.1016/j.celrep.2021.110021

41. Sun S, Liu C. 7a, 25-dihydroxycholesterol-mediated activation of EBI2 in immune regulation and diseases [Internet]. *Front Pharmacol* (2015) 6:60. doi: 10.3389/fphar.2015.00060

42. Gatto D, Wood K, Caminschi I, Murphy-Durland D, Schofield P, Christ D, et al. The chemotactic receptor EBI2 regulates the homeostasis, localization and immunological function of splenic dendritic cells. *Nat Immunol [Internet]* (2013) 14 (5):446–53. doi: 10.1038/ni.2555

43. Gatto D, Brink R. B cell localization: regulation by EBI2 and its oxysterol ligand. *Trends Immunol [Internet]* (2013) 34(7):336–41. doi: 10.1016/j.it.2013.01.007

44. Foo CX, Bartlett S, Chew KY, Ngo MD, Bielefeldt-Ohmann H, Arachchige BJ, et al. GPR183 antagonism reduces macrophage infiltration in influenza and SARS-CoV-2 infection. *Eur Respir J* (2022) 61(3):2201306. doi: 10.1183/13993003.01306-2022

45. Cavallini C, Galasso M, Pozza ED, Chignola R, Lovato O, Dando I, et al. Effects of CD20 antibodies and kinase inhibitors on b-cell receptor signalling and survival of chronic lymphocytic leukaemia cells. *Br J Haematol* (2021) 192(2):333–42. doi: 10.1111/bjh.17139

46. Jones RJ, Iempridee T, Wang X, Lee HC, Mertz JE, Kenney SC, et al. Lenalidomide, thalidomide, and pomalidomide reactivate the Epstein-Barr virus lytic cycle through phosphoinositide 3-kinase signaling and ikaros expression. *Clin Cancer Res* (2016) 22(19):4901–12. doi: 10.1158/1078-0432.CCR-15-2242

Antitumor Activity of the Novel BTK Inhibitor TG-1701 Is Associated with Disruption of Ikaros Signaling in Patients with B-cell Non–Hodgkin Lymphoma

Marcelo Lima Ribeiro[1,2], Diana Reyes-Garau[1], Meritxell Vinyoles[3,4,5], Núria Profitós Pelejà[1], Juliana Carvalho Santos[1], Marc Armengol[1,6], Miranda Fernández-Serrano[1,6], Alícia Sedó Mor[1,6], Joan J. Bech-Serra[7], Pedro Blecua[8], Eva Musulen[8,9], Carolina De La Torre[7], Hari Miskin[10], Manel Esteller[5,8,11], Francesc Bosch[6,12,13], Pablo Menéndez[3,4,5,11], Emmanuel Normant[10], and Gaël Roué[1,6,12,13]

ABSTRACT

Purpose: Despite the remarkable activity of BTK inhibitors (BTKi) in relapsed B-cell non–Hodgkin lymphoma (B-NHL), no clinically-relevant biomarker has been associated to these agents so far. The relevance of phosphoproteomic profiling for the early identification of BTKi responders remains underexplored.

Experimental Design: A set of six clinical samples from an ongoing phase I trial dosing patients with chronic lymphocytic leukemia (CLL) with TG-1701, a novel irreversible and highly specific BTKi, were characterized by phosphoproteomic and RNA sequencing (RNA-seq) analysis. The activity of TG-1701 was evaluated in a panel of 11 B-NHL cell lines and mouse xenografts, including two NF-κB- and BTK^{C481S}-driven BTKi-resistant models. Biomarker validation and signal transduction analysis were conducted through real-time PCR, Western blot analysis, immunostaining, and gene knockout (KO) experiments.

Results: A nonsupervised, phosphoproteomic-based clustering did match the early clinical outcomes of patients with CLL and separated a group of "early-responders" from a group of "late-responders." This clustering was based on a selected list of 96 phosphosites with Ikaros-pSer442/445 as a potential biomarker for TG-1701 efficacy. TG-1701 treatment was further shown to blunt Ikaros gene signature, including *YES1* and *MYC*, in early-responder patients as well as in BTKi-sensitive B-NHL cell lines and xenografts. In contrast, Ikaros nuclear activity and signaling remained unaffected by the drug *in vitro* and *in vivo* in late-responder patients and in BTK^{C481S}, BTK^{KO}, and noncanonical NF-κB models.

Conclusions: These data validate phosphoproteomic as a valuable tool for the early detection of response to BTK inhibition in the clinic, and for the determination of drug mechanism of action.

Introduction

B-cell non–Hodgkin lymphomas (B-NHL) account for up to 4% of globally diagnosed cancers (1). They are divided into low and high grades, typically corresponding to indolent (slow-growing) lymphomas, like chronic lymphocytic leukemia (CLL), and aggressive lymphomas, like diffuse large B-cell lymphoma (DLBCL), respectively (2). Targeting of the B-cell receptor (BCR) pathway through inhibition of Bruton tyrosine kinase (BTK) with the first-in-class irreversible inhibitor ibrutinib has demonstrated exceptional clinical activity as a monotherapy for various subtypes of B-NHL, most notably CLL (3) and mantle cell lymphoma (MCL; ref. 4), but also Waldenström macroglobulinemia (WM; ref. 5) and activated B-cell-like DLBCL (ABC-DLBCL; ref. 6). Nonetheless, resistance to ibrutinib has been observed due in part to the acquisition of mutations that either affect the irreversible binding of BTK inhibitors (BTKi) or activate the phospholipase C gamma 2 (PLCγ2) enzyme, a downstream enzyme in the BTK pathway (7). In the case of BTK, a cysteine-to-serine mutation (BTK^{C481S}) abrogates the covalent binding of ibrutinib to BTK and has been detected in up to 86% of relapsing patients with CLL, but only anecdotally in MCL relapsing patients (7–9). Additional intrinsic mechanisms of resistance involve activation of the noncanonical Nuclear factor κB (NF-κB)-inducible kinase (NIK)-NF-κB signaling in MCL (10, 11).

The use of distinct next-generation sequencing (NGS)-based genomic techniques including whole exome and targeted deep sequencing have been instrumental in identifying BTK^{C481S} mutation as a genetic cause of BTKi resistance (12, 13). More recently, global drug profiling using MS-based phosphoproteomics has been successfully employed to characterize drug mechanisms of action in single-agent therapy or

[1]Lymphoma Translational Group, Josep Carreras Leukaemia Research Institute, Badalona, Spain. [2]Laboratory of Immunopharmacology and Molecular Biology, Sao Francisco University Medical School, Braganca Paulista, São Paulo, Brazil. [3]Stem Cell Biology, Developmental Leukemia and Immunotherapy Group, Josep Carreras Leukaemia Research Institute, Badalona, Spain. [4]Department of Biomedicine, School of Medicine, University of Barcelona, Barcelona, Spain. [5]Centro de Investigación Biomédica en Red de Cáncer (CIBERONC), Instituto de Salud Carlos III, Barcelona, Spain. [6]Autonomous University of Barcelona, Barcelona, Spain. [7]Proteomics Unit, Josep Carreras Leukaemia Research Institute, Badalona, Spain. [8]Cancer Epigenetics Group, Josep Carreras Leukaemia Research Institute, Badalona, Spain. [9]Department of Pathology, Hospital Universitari General de Catalunya-Grupo Quironsalud, Sant Cugat del Vallès, Spain. [10]TG Therapeutics, New York, New York. [11]Institució Catalana de Recerca i Estudis Avançats (ICREA), Barcelona, Spain. [12]Department of Hematology, Vall d'Hebron University Hospital, Barcelona, Spain. [13]Experimental Hematology, Vall d'Hebron Institute of Oncology, Barcelona, Spain.

Note: Supplementary data for this article are available at Clinical Cancer Research Online (http://clincancerres.aacrjournals.org/).

E. Normant and G. Roué contributed equally as the co-senior authors of this article.

Corresponding Authors: Gaël Roué, Lymphoma Translational Group, Josep Carreras Leukaemia Research Institute, Badalona, 08916, Spain. E-mail: groue@carrerasresearch.org; and Emmanuel Normant, VP Preclinical Sciences, TG Therapeutics, 2 Gansevoort Street, New York, NY 10014. E-mail: enormant@tgtxinc.com

Clin Cancer Res 2021;27:6591–601

doi: 10.1158/1078-0432.CCR-21-1067

Translational Relevance

Covalent Bruton tyrosine kinase inhibitors (BTKi) have transformed the treatment of B-cell non–Hodgkin lymphoma (B-NHL), but their activities have been limited by off-target toxicity and acquired resistance. TG-1701 is a novel irreversible and highly specific BTKi currently under study in relapsed/refractory patients. Here we show that TG-1701 exerts similar activity than the first-in-class BTKi ibrutinib, although with greater selectivity, in *in vitro* and *in vivo* models of B-NHL. We also report for the first time that a phosphoproteomic-based approach can discriminate between TG-1701 early-responder and TG-1701 late-responder patients with B-NHL. Furthermore, the coupling of proteomic profiling and transcriptomic analysis allowed the identification of Ikaros signaling disruption as an event commonly found in early-responder patients, and a crucial determinant of TG-1701 efficacy in BTKi-sensitive and BTKi-resistant B-NHL cell lines and mouse xenografts.

multidrug combinations in solid cancers (14). In addition, a recent publication also showed that phosphoproteomic profiling can help to understand the role of BTKi in patients with CLL. In this study, CLL cells from patients with an unmutated immunoglobulin heavy chain gene (*IGVH*) status showed higher basal phosphorylation than patients with *IGVH*-mutated status (15).

Here, we present TG-1701, a novel, orally available, irreversible BTKi that exhibits improved selectivity when compared with ibrutinib (16), and shows activity in various models of B-NHL. A MS-based phosphoproteomic platform used to interrogate the effects of TG-1701 on patients with CLL enrolled in the phase I dose-escalation study (NCT03671590; refs. 17–19) pointed to the transcription factor Ikaros as both a potential biomarker of clinical activity and an important node downstream of BTK in the BCR pathway.

Materials and Methods

Patients

Blood samples were obtained from 6 patients with CLL treated on the NCT03671590 clinical trial (**Table 1**). Briefly, patients with relapsed or refractory histologically confirmed B-cell lymphoma or CLL were eligible and treated with TG-1701 orally once daily until disease progression or the occurrence of intolerable side effects. Patients received either 200, 300, or 400 mg TG-1701 daily (**Table 1**). On the first day of treatment, white blood cells were counted, the absolute lymphocyte count (ALC) calculated, and the normal lowest and normal highest ALC established (Supplementary Table S1). The percentage of CLL cells in each sample was the ratio of ALC subtracted from highest normal ALC and divided by total ALC. All patients provided written informed consent. Institutional Review Board approvals for the study protocol, amendments, and informed consent documents were obtained prior to study initiation; study procedures were conducted in accordance with the Declaration of Helsinki.

Cell lines

Seven MCL (REC-1$^{GFP+LUC+}$, JEKO-1, UPN-1, UPN-IbruR, GRANTA-519, Z-138, and MINO), two ABC-DLBCL (OCI-LY3 and HBL-1), and two follicular lymphoma (DoHH2 and RL) cell lines were cultured as described elsewhere (20, 21). JEKO-1, MINO, and REC-1 parental cells were obtained from ATCC cell bank (LGC Standards). DoHH-2, GRANTA-519, and RL cell lines were purchased at DSMZ. UPN-1 and Z-138 cells were provided by Dr. B. Sola (University of Caen). HBL-1 was provided by Dr. E. Valls (IDIBAPS). OCI-Ly3 was kindly provided by Dr. A. Staiger (Dr. Margarete Fischer-Bosch Institute of Clinical Pharmacology). Cell-line authentication was performed upon reception by short tandem repeat (STR) profiling, using AmpFlSTR Identifier Kit (Thermo Fisher Scientific), and based on available STR profiles. This analysis was then repeated every 6 months and up to 4 months prior to the submission of the present manuscript. Mycoplasm infection was routinely tested by PCR.

Drugs

TG-1701 was provided by TG Therapeutics, Inc. Ibrutinib was purchased from Selleckchem.

Xenograft mouse model and IHC staining

The MINO MCL xenograft model was generated by inoculating subcutaneously 6- to 7-week-old nude mice (Shanghai Ling Chang Experimental Animal Co., Ltd.) with 5×10^6 MINO cells. When tumor volume reached 100 to 200 mm^3, animals were randomized into five groups of 8 to10 mice each, and were dosed orally with TG-1701 (25, 50, or 100 mg/kg, orally, twice a day), ibrutinib (100 mg/kg, orally, twice a day), or vehicle for 21 days. The tumor volume (V) was calculated as: $V = 1/2 \times a \times b^2$, where a and b represent the length and width, respectively. In REC-1 and UPN-IbruR xenografts, CB17-SCID mice (Janvier labs) were inoculated subcutaneously with 10^7 REC-1$^{GFP+Luc+}$ cells or UPN-IbruR cells and monitored for tumor growth, bioluminescence signal, and vital parameters as described previously (21), in compliance with the Animal Ethics Committee of the autonomous University of Barcelona (registry number 38/18). Tumor-bearing mice received either TG-1701 (25 mg/kg, every day) or ibrutinib (25 mg/kg, every day) for 17 days. Tumor samples were snap-frozen in OCT medium (Sakura Tissue Tek) or formalin-fixed and paraffin-embedded prior to immunohistochemical (IHC) staining with primary antibodies against Ikaros (Cell Signaling Technology) and CD20 (Beckman Coulter). Preparations were evaluated using an Olympus microscope and MicroManager software.

Western blot analysis

Total and nuclear protein extracts were obtained from MCL cell lines and tumor specimens using RIPA (Sigma-Aldrich), the Nuclear/Cytosol Fractionation Kit (BioVision), and T-PER (Thermo Fisher Scientific) buffers, respectively, and subjected to SDS-PAGE, as described previously (22, 23). Membrane-transferred proteins were revealed by incubating with primary and secondary antibodies (Supplementary Materials and Methods) followed by chemiluminescence detection using the ECL system (Pierce) and a Fusion FX imaging system (Vilber Lourmat). Band intensity was quantified using Image J software and normalized to housekeeping protein (GAPDH or TUBULIN). Values were referred to the indicated control (i.e., predose sample or DMSO-treated cells) and added below the corresponding band. If not otherwise specified, representative data from $n = 2$ experiments are shown.

Proteomic and phosphoproteomic profiling

Peripheral blood mononuclear cells (PBMC) were obtained from a total of 6 patients with CLL before and after 4-hour treatment with TG-1701 (**Table 1**), using standard Ficoll-Hypaque density gradient. Proteins were extracted using a Urea-based buffer (6 M Urea, 100 mmol/L Tris-HCl pH 7.5) on a Bioruptor sonicator, followed by standard Lys-C and trypsin-mediated digestion. Proteomic quantitative analyses were performed using 13 of the 16 channels of a 16plex - Tandem Mass Tag (TMT) system, according to

Table 1. Clinical and biological characteristics of patients with CLL.

Patient	Age	Gender	Cytogenetic alterations	IGVH status	TG-1701 daily dose (mg)	Clinical outcome (% reduction)	% CLL cells
AII-0011	61	F	Trisomy 12	UM	400–300	PR (87%)	16
AIJ-0015	64	M	11q del, trisomy 12	M	400	PR (86%)	62
AIJ-0001	57	M	17p del, trisomy 12	M	200	SD (38%)	74
AIJ-0005	60	F	—	M	300	SD-PR (56%)	93
AII-0006	83	M	17p del, trisomy 12	UM	200	PR (66%)	98
AIK-0003	80	M	17p del	M	200	SD (lymphocytosis)	80

Abbreviations: PR, partial response; SD, stable disease.

manufacturer's instructions (Thermo Fisher Scientific). A small part of the sample (260 μg) was used for total proteome analysis, and remaining proteins were subjected to phosphoproteome enrichment using the High-Select TiO2 Phosphopeptide Enrichment Kit (Thermo Fisher Scientific). Total proteome and phosphopeptide fractions were fractionated in 24 and 9 fractions using a Zorbax Extent-C18 and the High pH Reversed-Phase Peptide Fractionation Kit (Thermo Fisher Scientific), respectively, with prior analysis on an Orbitrap Fusion Lumos Tribrid mass spectrometer. REC-1 and REC-BTK^{C481S} protein extracts were labeled in triplicates with two TMT10plex, using a single channel (131N) to label a pool of all the samples. TMT fractionation and MS analysis were performed as above. Raw data were processed in MaxQuant (RRID:SCR_014485) and analyzed as described in Supplementary Materials and Methods. Data have been deposited to the ProteomeXchange Consortium (http://proteomecentral.proteomexchange.org) via the PRIDE partner repository (PXD023231; ref. 24).

RNA sequencing (RNA-seq) analysis and real-time qPCR

Total RNA was extracted using TRizol (Thermo Fisher Scientific) following manufacturer's instructions and poly-A-tailed enriched mRNA selected. Paired-end stranded RNA libraries with 51 read-inward facing paired mates were prepared, following sequencing with Illumina's NovaSeq6000 at the Centro Nacional de Analisis Genomico (CNAG). Data analysis was performed as described in Supplementary Materials and Methods.

The reverse transcription reaction was performed using a High-Capacity cDNA Reverse Transcription Kit (Applied Biosystems). The mRNA expression was analyzed in triplicate by quantitative real-time PCR. Amplification was performed using SYBR Green-based detection (GoTaqPCR Master Mix; Promega). The relative expression of each gene was quantified by the comparative cycle threshold method (ΔΔCt). β-Actin, GAPDH, and B2M were used as endogenous controls.

Immunofluorescence

BTKi-treated REC-1 and JEKO-1 cells (2–3 × 10^5) were seeded on poly-L-lysine-coated glass coverslips and stained as previously (23) with anti-Ikaros antibody (Cell Signaling Technology). Fluorescence signal was acquired on a Leica microscope and quantified using the LAS X (Leica) and Image J (RRID:SCR_003070) softwares.

Generation of BTK^{C481S} and BTK^{KO} cell lines

CRISPR-Cas9 gene editing tool were used to generate REC-BTK^{C481S} and REC-BTK^{KO} cells. Briefly, REC-1$^{GFP+LUC+}$ cells were electroporated with SpCas9 nuclease and BTK-specific gRNA using a Neon Transfection System (Thermo Fisher Scientific). After 30 days, single clones obtained by limit dilution were checked for BTK protein levels and analyzed by Sanger sequencing. Complete gene edition protocol can be found in Supplementary Data.

Statistical analysis

Presented data are the means ± Standard Deviation or SEM of three independent experiments. All statistical analyses were done by using GraphPad Prism 4.0 software (RRID:SCR_002798). Comparison between two groups of samples was evaluated by nonparametric Mann–Whitney test to determine how response is affected by two factors. Pearson test was used to assess statistical significance of correlation. Results were considered statistically significant when P value < 0.05.

Results

TG-1701 is a novel irreversible BTK inhibitor, more selective than ibrutinib

In a binding assay on a panel of 441 human kinases, TG-1701 was more selective than ibrutinib, with a comparable BTK Kd (3 nmol/L vs. 1.5 nmol/L, respectively) and a lower binding to EGFR, ITK, TXK, and JAK3 (Kd 135-, >48-, 68-, and >94-fold higher than those of ibrutinib, respectively; **Fig. 1A** and Supplementary Table S2). A BTK kinase activity assay revealed a TG-1701 EC_{50} of 6.70 nmol/L, slightly higher than ibrutinib IC_{50} (1.65 nmol/L; **Fig. 1B** and Supplementary Table S3). Accordingly, in an *in vitro* BTK occupancy assay, TG-1701 and ibrutinib showed a similar dose-dependent capacity to displace a BTK-specific fluorescent probe in the BTKi-sensitive follicular lymphoma cell line DoHH-2 (20), with complete BTK occupancy at 30 and 10 nmol/L, respectively (**Fig. 1C**). Consistently, BCR downstream signaling was impaired in a concentration-dependent manner in IgM-stimulated cells, with maximal effects observed at 100 nmol/L for TG-1701 and 10 nmol/L for ibrutinib (**Fig. 1D**). These effects were associated with a mean TG-1701 GI_{50} of 6.4 μmol/L at 72 hours, in a set of 10 parental B-NHL cell lines, which was slightly inferior to mean ibrutinib GI_{50} (14.1 μmol/L), especially in MCL cell lines (4.3 μmol/L vs. 10.8 μmol/L, respectively; Supplementary Table S3). Given that the activity of both BTK inhibitors in MINO cells was similar to these mean values, the tumor growth inhibition (TGI) of TG-1701 was evaluated *in vivo* in the corresponding xenograft model. A 16-day treatment of mice bearing MINO-derived tumors with 25, 50, and 100 mg/kg TG-1701 achieved a 56%, 72%, and 78% TGI, respectively, comparable with the 70% TGI observed in the ibrutinib (100 mg/kg) arm (**Fig. 1E**). A single oral gavage with 50 mg/kg TG-1701 further confirmed a rapid dephosphorylation of BTK and AKT as early as 2 and 4 hours, respectively, which was maintained for at least 24 hours due to the irreversible nature of TG-1701–mediated BTK inhibition (**Fig. 1F**).

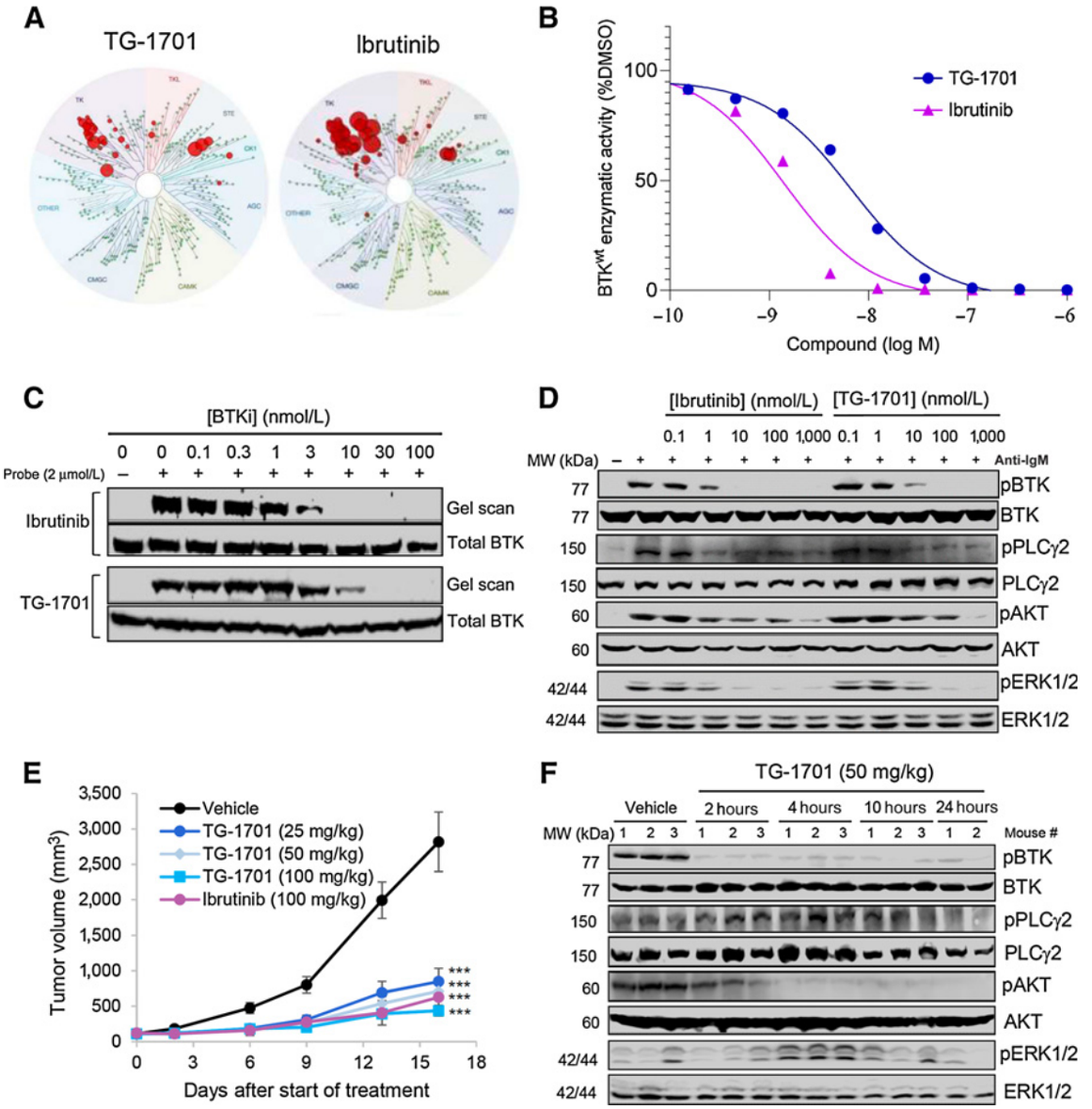

Figure 1.

TG-1701 is a novel irreversible BTK inhibitor as active as ibrutinib in *in vitro* and *in vivo* models of B-NHL. **A,** Binding of TG-1701 and ibrutinib 1 µmol/L was tested in a panel of 441 kinases using the DiscoverX technology. The size of each red circle is proportional to the strength of the binding. **B,** TG-1701 and ibrutinib BTK^{wt} anti-kinase activities were tested using a ^{33}P-ATP filtration assay. Shown are the average of two measurements. **C,** DoHH2 BTK-expressing cells were incubated with ibrutinib or TG-1701, lysed, and lysates were incubated with a fluorescent ibrutinib probe. Total BTK was assessed by Western blot analysis. **D,** Increasing concentrations of ibrutinib or TG-1701 were incubated with DoHH-2 cells for 20 minutes. BCR pathway was then activated with 10 µg/mL soluble goat F(ab')2 anti-IgM for 18 hours and levels of different downstream enzymes were assessed using Western blot analysis. **E,** TG-1701 or ibrutinib were dosed orally in the MINO MCL xenograft model and (**F**) intratumor levels of several BCR-related kinases were assessed by Western blot analysis.

Phosphoproteomic analysis differentiates early clinical outcomes and points to the inhibition of the Ikaros pathway as an important mechanism of TG-1701 activity

To identify potential biomarkers of TG-1701 activity in B-NHL, PBMCs from 6 patients with CLL enrolled in the TG-1701–101 phase I trial were isolated at different time points for omics analysis. In all patient samples but one, the percentage of circulating cancer cells was comprised between 60% and 98% (**Table 1**; Supplementary Table S1). All the patient samples harbored a wild-type BTK gene, as confirmed by Sanger sequencing of *BTK* exon 11 (data not shown).

Near-complete BTK occupancy was obtained in all samples tested (**Fig. 2A**) and linear kinetics was observed with approximately dose-proportional increases in C_{max} and $AUC_{0-8\ hours}$ from 100 to 300 mg (Supplementary Fig. S2; ref. 18), with a positive correlation between the daily dose and TG-1701 C_{max} for the

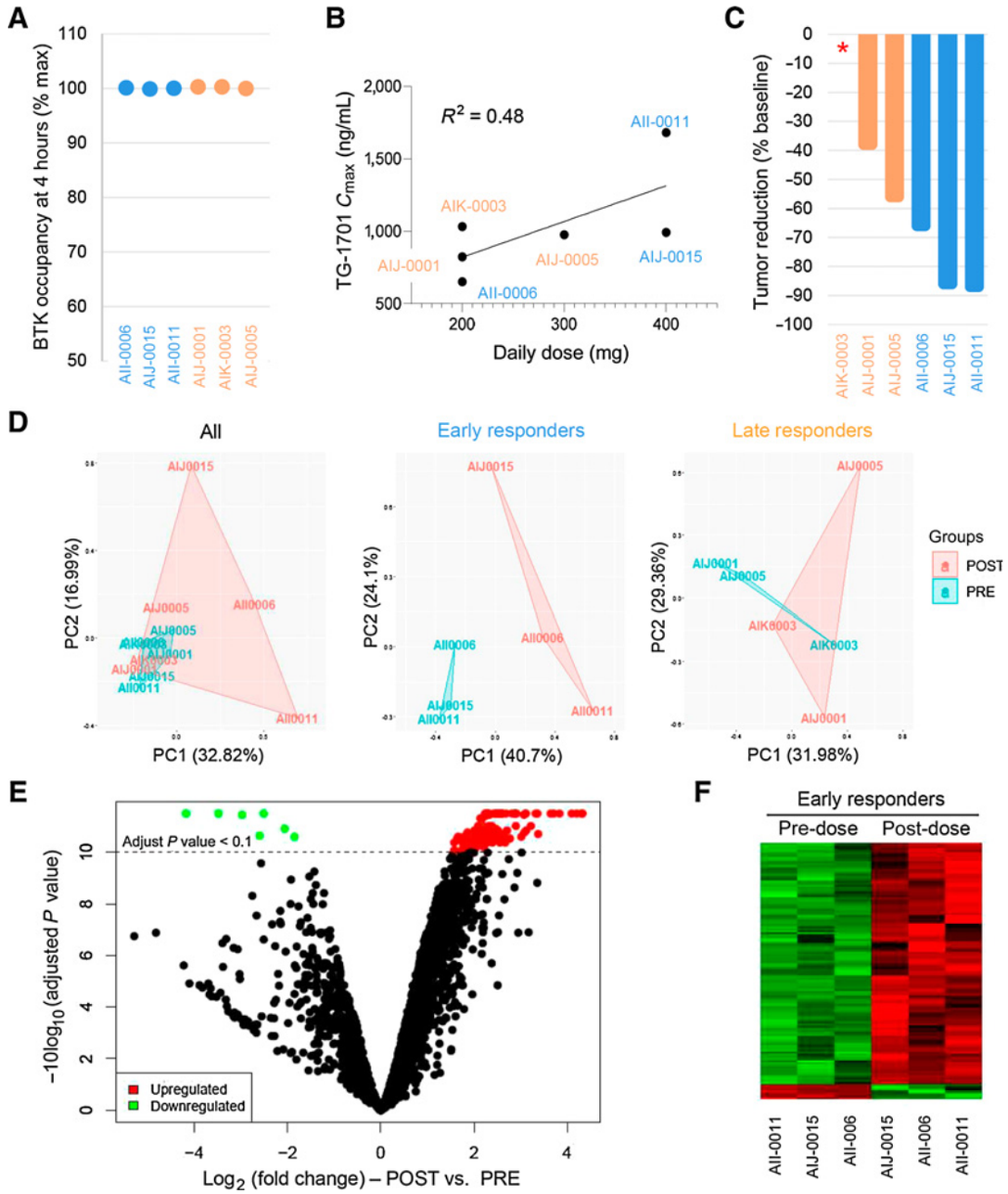

Figure 2.

Phosphoproteomic analysis of 6 patients with CLL treated with TG-1701 can segregate early and late responders. **A,** BTK occupancy was assessed in all patients in the study at nine different time points. Here the occupancy of the 6 patients with CLL are shown at 4 hours after treatment. The occupancy assay was run using a MSD method (as depicted in Supplementary Fig. S1) at Bioagilytix. **B,** Correlation of TG-1701 C_{max} and the daily dose received by the 6 patients. **C,** Best tumor reduction in all 6 patients at C3D1. *AIK-003 lymphocytosis at C3D1 rank the response as a stable disease. **D,** Phosphoproteomic profiling and principal components analysis were performed on all 6 patients with CLL (left), 3 early responders (middle), and 3 late responders (right). Pretreatment samples are shown in blue and the 4-hour posttreatment samples in red. Percentages refer to the total variance explained for each component. **E,** Quantified phosphopeptides in early responders. Volcano plot of the early responders–only samples. The late responders do not exhibit any TG-1701–driven changes. **F,** The phosphosites that are up- or downregulated are shown for 3 single patients.

6 patients studied (**Fig. 2B**). After three cycles of treatment, the best change in tumor burden as assessed by CT scan ranged from 38% to 87%, with 1 tumor-free patient with a lymphocytosis that defined his best response as a stable disease (**Fig. 2C**).

In PBMC protein extracts from the six predose and the six 4-hour postdose samples, a total of 5,585 proteins and 2,438 phosphosites were identified. An initial principal component analysis (PCA) did not discriminate the pretreatment (PRE) from the posttreatment (POST)

profiles. However, a specific unsupervised clustering of the data into two subgroups of 3 patients allowed a clear differentiation between the PRE and POST samples (**Fig. 2D**). These two subgroups, blindly selected to uncover changes due to TG-1701 treatment, clearly fitted the clinical outcome of the patients (**Fig. 2C**), separating *de facto* a group encompassing the 3 best responses (called the early responders) and a group gathering the 3 other patients with lower responses (called the late responders). Supporting this partition of the patients, the early responders exhibited a stronger *IL10* de-repression and a stronger, although not significant, decrease in *IL2* and *IL6* expression (Supplementary Fig. S3A), suggesting that they developed a more potent early anti-inflammatory response, a common feature of BTKi activity (25). In addition, *CCL3* and *CCL4* chemokine genes, two *bona fide* biomarkers for BCR pathway activation (26), were more downregulated in early-responder patients (Supplementary Fig. S3A). A set of 118 phosphopeptides were differentially phosphorylated (7 down- and 111 upregulated) after TG-1701 treatment in the early-responder subgroup only (adjusted P value < 0.1; **Fig. 2E**). These sites corresponded to the putative modulation of 14 protein kinases (Supplementary Tables S4 and S5). Importantly, these quantitative phosphoproteomic changes showed a strong homogeneity in the 3 early-responder patients and enabled a clear distinction between PRE and POST samples (**Fig. 2F**). Only one single phosphosite (UBA1-pSer4) was found significantly upregulated in the late-responder patients after TG-1701 treatment.

Beside the 118 phosphosites mentioned above and depicted in **Fig. 2E**, another set of 96 phosphopeptides were present in pretreatment samples and totally dephosphorylated upon treatment with TG-1701. The total absence of phosphorylation preempted the statistical analysis and incorporation of these 96 samples in the volcano plot, even though these sites were the most impacted by TG-1701 treatment. Of special interest, the corresponding list of phosphosites comprised the p-Ser442/445 residue of Ikaros, a zinc finger-containing DNA-binding protein that plays a pivotal role in B-cell homeostasis. Ikaros-Ser442/445 dephosphorylation was indeed the strongest event associated with TG-1701 activity (Supplementary Table S6). Because Ikaros nuclear localization and transcriptional activity both depend on BTK-mediated phosphorylation at Ser214/215 residues (27), we investigated whether, analogously, Ikaros function was differentially affected by TG-1701 in early-responder versus late-responder CLL patient samples. Using previously validated Ikaros-repressed and Ikaros-enhanced gene signatures (28), we identified 21 proteins of the repressed signature that were upregulated, whereas another set of 17 factors from the Ikaros-enhanced gene signature were depleted only in early responders, suggesting that Ikaros was functionally impaired after TG-1701 treatment (**Fig. 3A**). Although a comparative multidimensional (MDS) analysis of RNA-seq data obtained from the same subset of samples failed to show a clear difference between early-responsive and late-responsive patient clusters (Supplementary Fig. S3B), a clear trend in the upregulation of Ikaros-repressed genes and downregulation of Ikaros-enhanced genes was seen in TG-1701 early-responsive patients only (**Fig. 3B**). Accordingly, the IKZF1-repressed gene, *YES1*, was significantly upregulated, whereas the IKZF1-enhanced gene *MYC* was downregulated in early responders but not in late responders (**Fig. 3C**). Importantly, this effect was not due to Ikaros protein destabilization, as its level of expression did not vary upon TG-1701 treatment in early-responder patients, whereas the expression of p-BTK and MYC proteins underwent a 70% and 48% downregulation, respectively, and the levels of YES1 increased by almost 5-fold (**Fig. 3D**; Supplementary Fig. S3C). Such modifications were not seen in late-responder patients, although BTK was notably dephosphorylated (**Fig. 3D**; Supplementary Fig. S3C). These data were confirmed *in vitro* using the ibrutinib-sensitive MCL cell line REC-1 characterized by ibrutinib and TG-1701 GI_{50} values of 5.82 and 3.83 μmol/L at 72 hours, respectively (Supplementary Table S3). In these cells, as observed in early-responder patients with CLL, TG-1701 treatment led to efficient BTK dephosphorylation, *YES1* upregulation, and *MYC* downregulation both at mRNA and protein levels (**Fig. 3E** and **F**). Of note, among the *IKZF1*-target genes studied here, *YES1* reactivation was significantly higher in TG-1701–treated than in ibrutinib-exposed cells (**Fig. 3E**). Finally, **Fig. 3G** shows that ibrutinib and TG-1701 elicited a 67% to 83% and a 80% to 85% reduction in nuclear Ikaros, consistent with a nearly 50% to 70% decrease of Ikaros in REC-1 and JEKO-1 nuclear protein fraction (**Fig. 3H**), suggesting that dual dephosphorylation of Ikaros at Ser442 and Ser445 was associated with the nuclear exclusion of this factor.

Ikaros signature is a *bona fide* hallmark of BTKi mechanism of action

To further explore TG-1701 mechanisms of action and potential mechanisms of resistance, we CRISPR-engineered the REC-$1^{GFP+LUC+}$ cell line to express the BTK^{C481S}. This mutation was associated with a 10.3- and a 54.8-fold decrease in ibrutinib and TG-1701 inhibitory kinase activity, respectively (Supplementary Fig. S4A; Supplementary Table S3). The REC-1–BTK^{C481S} cell line was 4.2- and 2.8-fold less sensitive to ibrutinib and TG-1701 respectively, compared with parental REC-1 cells (**Fig. 4A**; Supplementary Table S3). A washout experiment further showed that irreversible BTK inhibition—illustrated by kinase phosphorylation over 24 hours after BTKi removal in REC-1 cells—was mostly lost in REC-1–BTK^{C481S} cells (**Fig. 4B**). Although total proteome composition was modified solely in the parental cells treated with either ibrutinib or TG-1701 as assessed by PCA analysis (Supplementary Fig. S4B), a set of 16 Ikaros-repressed proteins were upregulated and another set of 14 Ikaros-upregulated proteins were downregulated in REC-1, but not in REC-1–BTK^{C481S} cells exposed to TG-1701 (**Fig. 4C**). Despite the short drug exposure, transcriptional upregulation of *YES1*, and repression of *MYC* were observed in BTK^{wt} cells treated with both BTKis. In REC-1–BTK^{C481S} cells, a pronounced basal Ikaros-repressed gene signature was observed in the absence of any treatment (black bars, **Fig. 4D**), including *YES1* expression, and this pattern was not modified upon BTKi exposure (**Fig. 4D**; Supplementary Fig. S4C).

To confirm the role of BTK as an upstream regulator of Ikaros signaling in BTKi-exposed cells, we generated a BTK knockout (KO) model derived from the REC-1 cell line, using a CRISPR-Cas9 method, as described above. The obtained REC-BTK^{KO} derivative, characterized by an almost complete depletion of BTK (**Fig. 4E**) was refractory to both ibrutinib and TG-1701 (Supplementary Table S3) and did not undergo significant modulation of *YES1* and *MYC* expression after exposure to TG-1701 (**Fig. 4E** and **F**). To validate the relevance of the BTK-Ikaros signaling axis in the regulation of YES1 and MYC upon BTK inhibition, two CRISPR-Cas9–engineered cell lines either devoid of Ikaros (REC-$IKZF1^{KO}$) or with *de novo* expression of BTK after BTK gene knockout (REC-$BTK^{KO\text{-}OE}$) were generated (see Supplementary Materials and Methods). Supplementary Figure S5A and S5B shows that Ikaros depletion was accompanied by a 2- to 3-fold increase in YES1 expression in REC-1 cells, and that no further upregulation of this gene could be achieved after BTK inhibition. MYC expression did not undergo significant variation upon treatment with either TG-1701 or ibrutinib. Most interestingly, the re-introduction of an IgM-responsive form of BTK within REC-BTK^{KO} cells, restored the capacity of TG-1701, and in a lesser extent ibrutinib, to suppress the Ikaros-

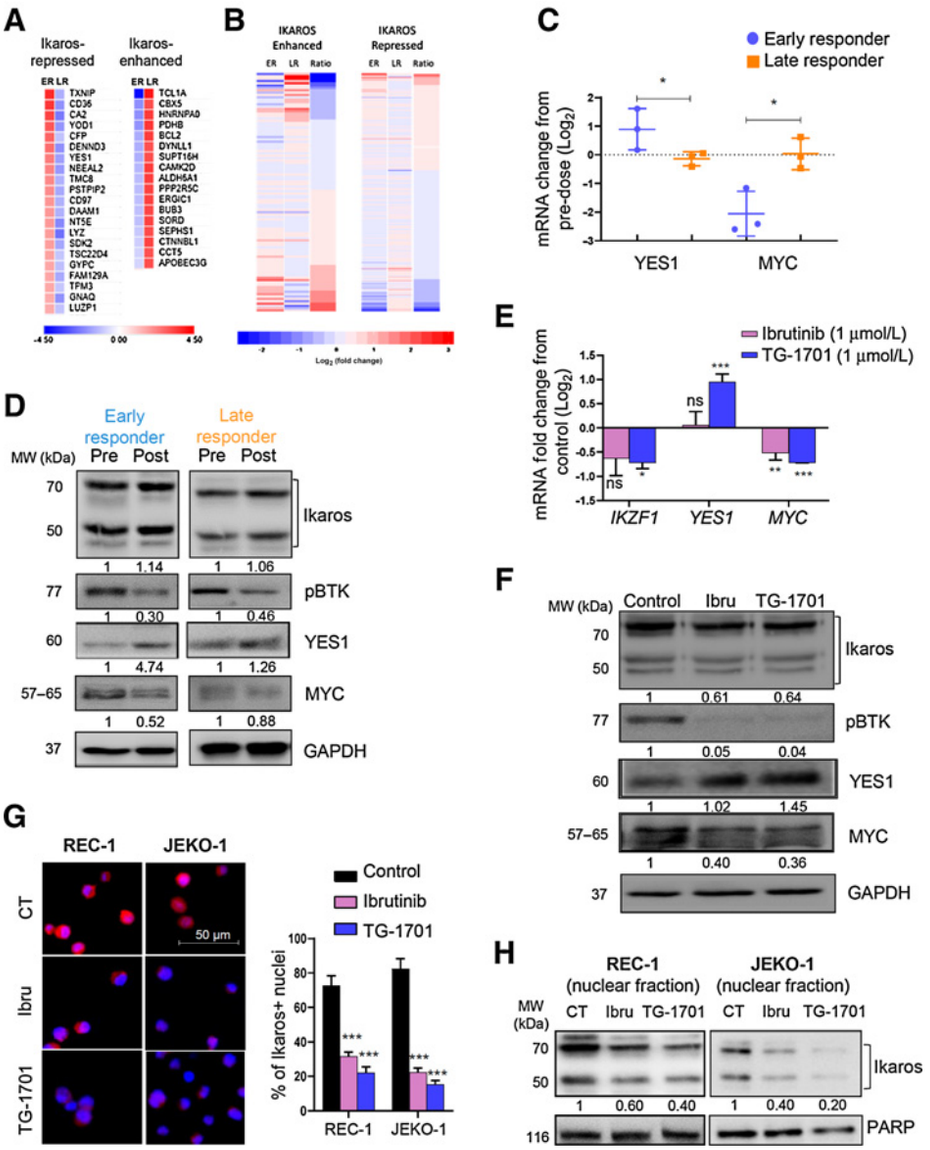

Figure 3.

Impairment of Ikaros signaling is associated with B-NHL response to TG-1701 in both clinical and preclinical settings. Change of Ikaros-regulated factors upon TG-1701 treatment in early responders (ER) and late responders (LR), according to (**A**) total proteome data and (**B**) RNA-seq analysis of the same samples. For each category, the average of the 3 patients is displayed. **C,** *YES1* (an Ikaros-repressed gene) and *MYC* (an Ikaros-enhanced gene) mRNA changes after TG-1701 treatment. **D,** Immunoblot evaluation of p-BTK, Ikaros, and Ikaros downstream factors, MYC and YES1, using one representative early- and one late-responder PBMC lysates. P-BTK detection was assessed to confirm on-target activity at 4 hours posttreatment. MCL REC-1 cells were treated for 24 hours with 1 μmol/L ibrutinib or TG-1701, and variations in Ikaros-regulated factors were quantified using (**E**) qPCR and (**F**) Western blot analysis. Subcellular localization of Ikaros was determined by (**G**) immunofluorescence staining (red signal, counterstained by DAPI nuclear labelling in blue) and (**H**) immunoblot analysis of nuclear protein fraction, in REC-1 and JEKO-1 cells treated as above with ibrutinib or TG-1701 (*, $P < 0.05$; **, $P < 0.01$; ***, $P < 0.001$; ns, nonsignificant).

dependent repression of YES1 and upregulation of MYC (Supplementary Fig. S5C and S5D). Altogether, these data strongly suggest that TG-1701–dependent impairment of Ikaros signaling in MCL cells is a BTK-dependent process.

Given the low recurrence of BTK^{C481S} mutation in patients with MCL (9), the UPN-IbruR noncanonical NF-κB–driven ibrutinib resistance model was also studied (20). This subclone is characterized by the absence of mutations in the *BTK* and *PLCG2* genes and the constitutive activation of p52-dependent signaling, driving a 2- to 3-fold increase in ibrutinib and TG-1701 GI_{50} at 72 hours (Supplementary Fig. S4D; Supplementary Table S3; ref. 20). When compared with the BTKi-sensitive REC-1 xenograft model in which a 17-day dosing with TG-1701 achieved a 53% tumor TGI versus vehicle, UPN-IbruR tumors were almost insensitive to TG-1701 (**Fig. 5A**). Accordingly, p-BTK was efficiently downregulated in representative REC-1 tumor specimens, but not in UPN-IbruR xenografts treated with TG-1701 (**Fig. 5B**). In agreement with *in vitro* results, MYC was downregulated, and YES1 upregulated at protein and/or mRNA levels, in association with Ikaros nuclear exclusion and a decrease in $CD20^{+}$ malignant B cells, in BTKi-sensitive, but not in BTK-insensitive MCL xenografts (**Fig. 5B–D**).

Discussion

During the past decade, BTK inhibitors have increasingly replaced chemotherapy-based regimens in patients with CLL and MCL. TG-1701 is a novel second-generation BTKi currently under clinical development. TG-1701 is more selective than ibrutinib, with a comparable BTK Kd and similar *in vitro* and *in vivo* characteristics. TG-1701 is currently being tested in a phase I trial comprised of a single-agent arm and a combination arm with ublituximab (a novel CD20 antibody) and umbralisib (a dual PI3Kδ and CKIε inhibitor). With a median follow-up of 7 months in a 200 mg daily monotherapy expansion cohort, preliminary overall response rates (ORR) are 95%

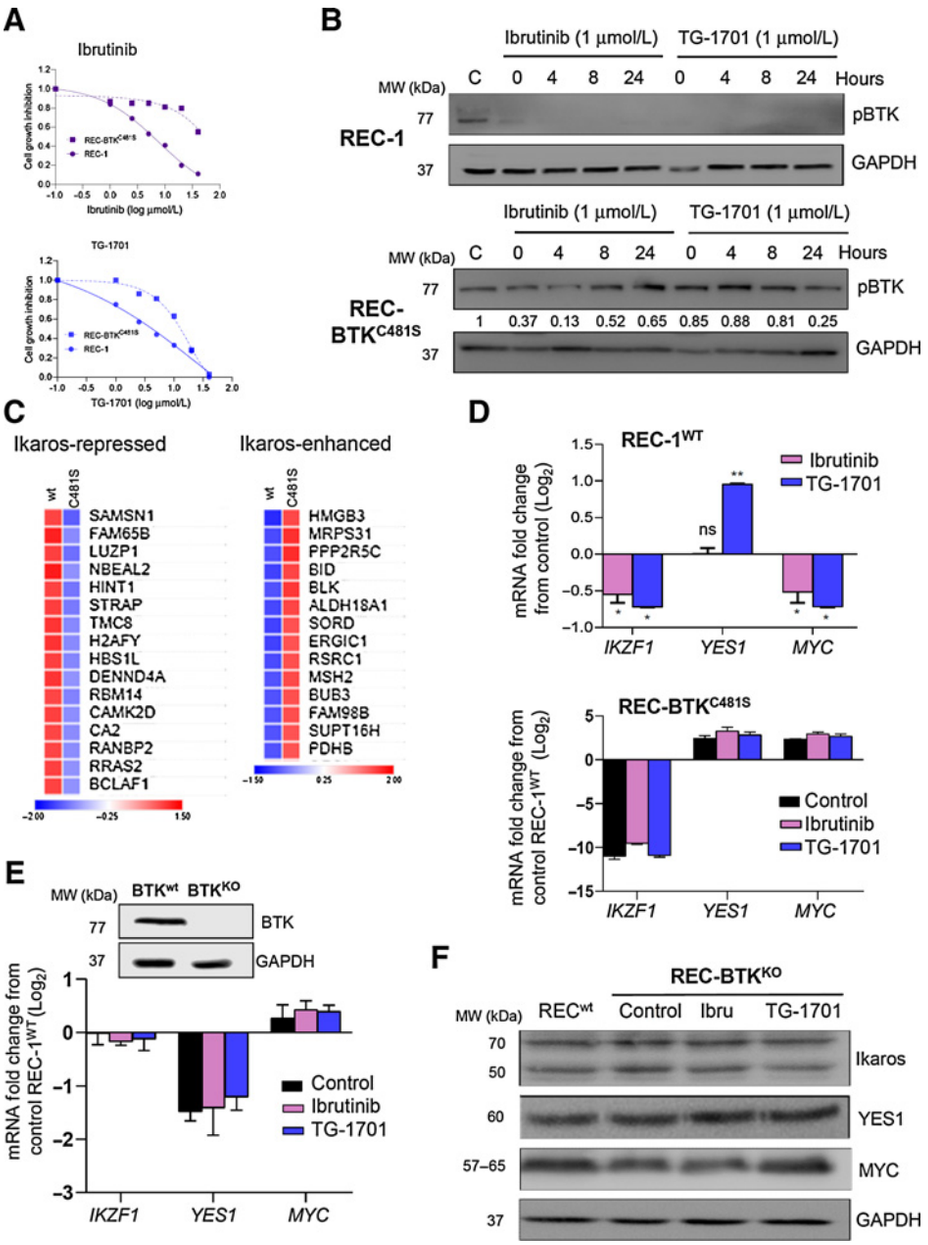

Figure 4.

Ikaros modulation is associated with TG-1701 efficacy in distinct *in vitro* and *in vivo* MCL models of ibrutinib resistance. **A,** Viability of BTK^{wt} and BTK^{C481S} REC-1 cells exposed to increasing doses of ibrutinib and TG-1701 was evaluated by CellTiter Glo assay. **B,** REC-1 and REC-1–BTK^{C481S} cells were exposed for 1 hour to 1 µmol/L TG-1701, washed-out for the indicated times, and levels of phospho- and total BTK were assessed using immunoblotting. Values below immunoblot correspond to the densitometric quantification of p-BTK/GADPH ratio. **C,** Regulation of Ikaros-regulated factors after 4 hours of treatment with TG-1701 or ibrutinib (1 µmol/L) in REC-1 and REC-1–BTK^{C481S} cells according to total proteome data. **D,** Ikaros gene signatures were evaluated by qPCR in REC-1 and REC-1–BTK^{C481S} cells exposed for 24 hours to 1 µmol/L ibrutinib or TG-1701. In REC-1–BTK^{C481S} cells, values were referred to untreated REC-1 cells (control). Ikaros transcriptional (**E**) and protein (**F**) signatures were evaluated in REC-1–BTK^{KO} cells as previously, using untreated REC-1 cells as a reference control.

(19/20) in CLL, 50% (9/18) in MCL, and 95% (18/19) in WM. No complete responses (CR) are confirmed on TG-1701 monotherapy (17). In this study, we show that phosphoproteomic analysis of pre- and posttreatment samples clustered patients with CLL according to their early clinical responses (early responders vs. late responders) and helped decipher the mechanisms underlying drug responsiveness. According to the results, the response from these patients did not depend on the pharmacokinetic or pharmacodynamic properties of TG-1701, but rather on differences in BTK downstream signaling. In early-responder patients, Ikaros-p-Ser442/445 was the phosphopeptide most impacted (dephosphorylated) by TG-1701 treatment and several Ikaros-dependent factors were transcriptionally deregulated, suggesting that Ikaros may represent a biomarker for early response, and/or an important new node downstream BTK inhibition. Interestingly, a recent study in acalabrutinib-treated patients with CLL (15) has shown that the unmutated *IGVH* cells displayed a higher basal phosphorylation level compared with the mutated *IGVH* cells, showing that the phosphoproteomic profile of BTKi-treated patients can cluster specific subgroups of patients.

Ikaros is a zinc finger protein involved in gene regulation and chromatin remodeling. Its nuclear localization, stability, and transcriptional activity depend on its phosphorylation status, which is regulated by BTK, casein kinase II (CKII), and protein phosphatase 1 (PP1) interplay (27, 29). Although the exact role of serine residues at position 442 and 445 is still unknown, their juxtaposition to the conserved PP1 binding motif in the C-terminal end of Ikaros protein (30) might confer them a role in the PP1-mediated regulation of Ikaros stability and pericentromeric localization (29).

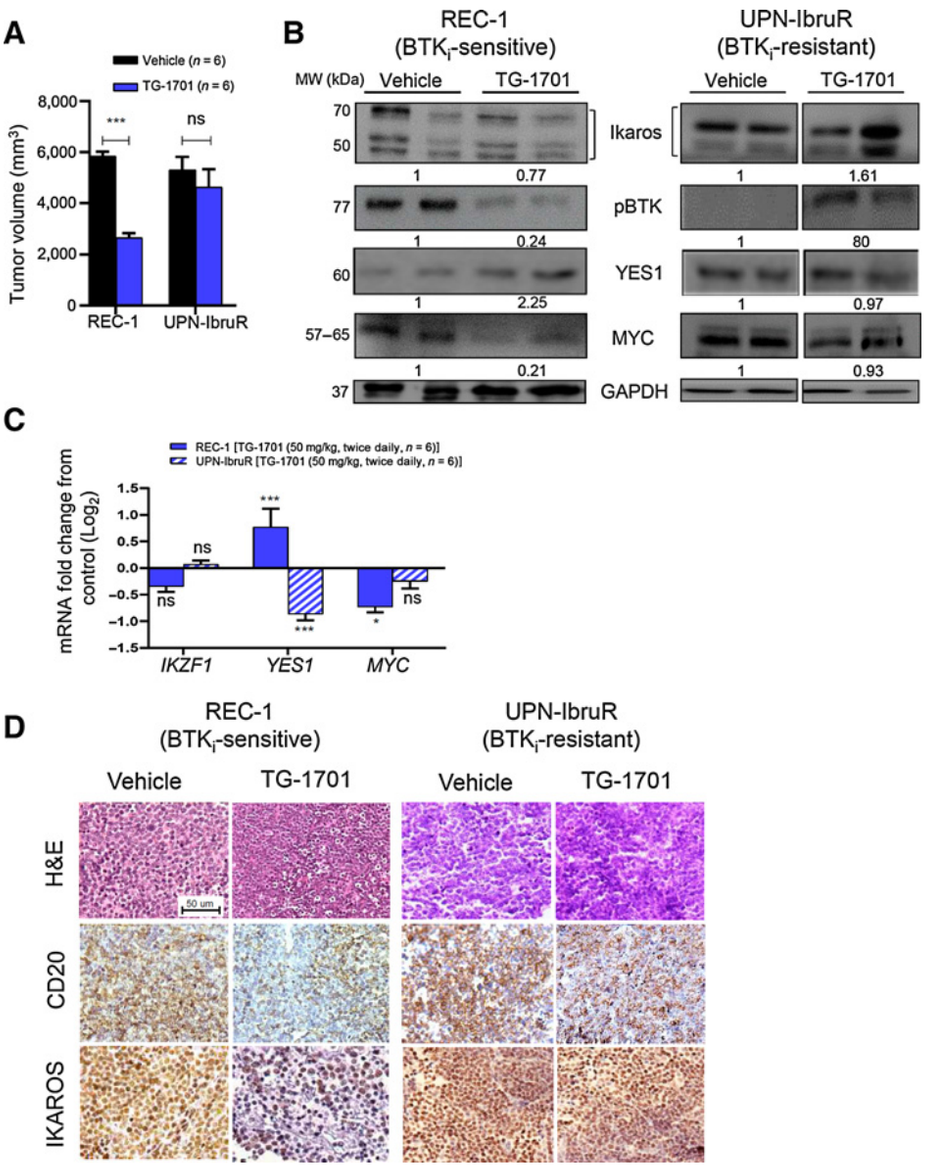

Figure 5.

In vivo activity of TG-1701 on BTKi-sensitive and BTKi-resistant MCL mouse models. **A,** TG-1701 was dosed orally in BKT_i-sensitive (REC-$1^{GFP+LUC+}$) and BTK_i-resistant (UPN-IbruR) MCL xenograft models and tumor volumes were recorded at the endpoint (17 days) by bioluminescence signal recording (REC-1) or external calipers (UPN-IbruR). Ikaros signature was evaluated by (**B**) Western blot analysis and (**C**) qPCR in 2/3 representative tumors from each treatment group. Densitometric quantification of Ikaros, phospho-BTK, and MYC protein levels were normalized to GAPDH levels and referred to vehicle-treated tumors. For each treatment group, the average of the two tumors is shown. **D,** IHC labeling of CD20 and Ikaros in tissue sections from four representative BTKi-sensitive (REC-1) and BTKi-resistant (UPN-IbruR) tumor specimens (scale bar: 25 µm; *, $P < 0.05$; **, $P < 0.01$; ***, $P < 0.001$; ns, nonsignificant).

Interestingly, CKII was ranked #4 in the list of kinases with reduced activity in TG-1701 early-responder patients, whereas phosphorylation of the PP1 inhibitory subunit, PPP1R14A, and dephosphorylation of the PP1 inhibitor, PPP1R2, both associated with reduced PP1 activity (31), were among the top four modifications detected in TG-1701 early-responder patients (Supplementary Tables S4 and S5). Ikaros expression was affected by TG-1701 treatment, neither in CLL primary cells nor in BTKi-sensitive REC-1 models, indicating that the inhibition of Ikaros signature in early responders was more likely due to a nuclear exclusion of the transcription factor. Importantly, our results obtained in REC-1–BTK^{C481S} and REC-1–BTK^{KO} subclones demonstrated that both the cell proliferation blockade and the modulation of Ikaros activity upon TG-1701 treatment are tightly dependent on the presence of a wild-type BTK protein, supporting the idea that Ikaros phosphorylation at Ser442/445 is controlled by the kinase, and discarding a potential off-target effect of the compound. Downregulation of the Ikaros program in BTK^{C481S} cell line is not understood at that point. One possible explanation is that the C481S mutation does not only abrogate the irreversibility of ibrutinib or TG-1701 binding but also modifies the substrate specificity of the newly formed substrate pocket that would not phosphorylate Ikaros anymore. Further studies involving the production of a phospho-specific Ikaros-Ser442/445 antibody will be required to confirm this hypothesis.

The number of samples tested in this study is too small to draw definitive conclusions, and because responses to BTKis continue to deepen over time (as long as 2 years), the early (C3D1) timepoint may not fully represent the overall drug efficacy. However, the differences presented here between "early-responders" and "late-responders" are clear enough to warrant future studies, for example testing an enlarged pool of patient samples treated with BTKis or exploring other NHLs. In addition, other (non-Ikaros) potential biomarkers for which an existing phospho-antibody is commercially available could be evaluated. In the study presented here, the assessment of the clinical

outcome available at the time of analysis was the first CT scan, after two cycles of treatment. Assessing the phosphorylation status of the biomarkers presented here in patients who progressed under, or become resistant to BTKi treatment, might also help understand the underlying mechanisms of activity or resistance.

Authors' Disclosures

H. Miskin reports personal fees from TG Therapeutics, Inc. during the conduct of the study. P. Menéndez reports personal fees from OneChain Immunotherapeutics outside the submitted work. E. Normant reports employment and ownership of stock with TG Therapeutics. G. Roué reports grants from TG Therapeutics and Instituto de Salud Carlos III during the conduct of the study. No disclosures were reported by the other authors.

Authors' Contributions

M.L. Ribeiro: Resources, investigation, methodology, writing–original draft. **D. Reyes-Garau:** Investigation, methodology. **M. Vinyoles:** Resources, validation, investigation, writing–review and editing. **N. Profitós Pelejà:** Investigation, methodology. **J.C. Santos:** Investigation, methodology. **M. Armengol:** Investigation. **M. Fernàndez-Serrano:** Investigation. **A. Sedó Mor:** Investigation, methodology. **J.J. Bech-Serra:** Data curation, software, visualization. **P. Blecua:** Data curation, software, visualization. **E. Musulen:** Investigation, methodology. **C. De La Torre:** Formal analysis, investigation, methodology. **H. Miskin:** Validation, writing–review and editing. **M. Esteller:** Data curation, writing–review and editing. **F. Bosch:** Writing–review and editing. **P. Menéndez:** Validation, investigation, methodology, writing–review and editing. **E. Normant:** Conceptualization, resources, supervision, validation, writing–original draft, writing–review and editing. **G. Roué:** Conceptualization, resources, supervision, funding acquisition, validation, investigation, visualization, writing–original draft, project administration, writing–review and editing.

Acknowledgments

We are very grateful to Dr. Chan Cheah at Linear Clinical Research, Dr. Constantine Tam at St. Vincents private hospital in Melbourne, and Dr. Nick Wickham at Adelaide Cancer Center in Ashford, as well as the TG Therapeutics clinical team led by Dr. Alejandro Ricart for their precious help. The authors would like to thank the CNAG-CRG for assistance with RNA sequencing. This study was financially supported by Fondo de Investigación Sanitaria PI18/01383, European Regional Development Fund (ERDF) "Una manera de hacer Europa" (to G. Roué), and TG Therapeutics. J.C. Santos and M. Fernández-Serrano were recipients of a Sara Borrell research contract (CD19/00228) and a predoctoral fellowship (FI19/00338) from Instituto de Salud Carlos III, respectively. M. Armengol was a fellow of PROTEOblood (EFA360/19), a project co-financed by the ERDF through the Interreg V-A Spain-France-Andorra (POCTEFA) program. This work was carried out under the CERCA Program (Generalitat de Catalunya).

The costs of publication of this article were defrayed in part by the payment of page charges. This article must therefore be hereby marked *advertisement* in accordance with 18 U.S.C. Section 1734 solely to indicate this fact.

Received March 24, 2021; revised July 7, 2021; accepted September 17, 2021; published first September 22, 2021.

References

1. Fisher SG, Fisher RI. The epidemiology of non-Hodgkin's lymphoma. Oncogene 2004;23:6524–34.
2. Quintanilla-Martinez L. The 2016 updated WHO classification of lymphoid neoplasias. Hematol Oncol 2017;35:37–45.
3. Byrd JC, Furman RR, Coutre SE, Flinn IW, Burger JA, Blum KA, et al. Targeting BTK with ibrutinib in relapsed chronic lymphocytic leukemia. N Engl J Med 2013;369:32–42.
4. Wang ML, Rule S, Martin P, Goy A, Auer R, Kahl BS, et al. Targeting BTK with ibrutinib in relapsed or refractory mantle-cell lymphoma. N Engl J Med 2013; 369:507–16.
5. Treon SP, Tripsas CK, Meid K, Warren D, Varma G, Green R, et al. Ibrutinib in previously treated Waldenström's macroglobulinemia. N Engl J Med 2015;372: 1430–40.
6. Wilson WH, Young RM, Schmitz R, Yang Y, Pittaluga S, Wright G, et al. Targeting B cell receptor signaling with ibrutinib in diffuse large B cell lymphoma. Nat Med 2015;21:922–6.
7. Woyach JA, Furman RR, Liu T-M, Ozer HG, Zapatka M, Ruppert AS, et al. Resistance mechanisms for the Bruton's tyrosine kinase inhibitor ibrutinib. N Engl J Med 2014;370:2286–94.
8. Furman RR, Cheng S, Lu P, Setty M, Perez AR, Guo A, et al. Ibrutinib resistance in chronic lymphocytic leukemia. N Engl J Med 2014;370:2352–4.
9. Chiron D, Di Liberto M, Martin P, Huang X, Sharman J, Blecua P, et al. Cell-cycle reprogramming for PI3K inhibition overrides a relapse-specific C481S BTK mutation revealed by longitudinal functional genomics in mantle cell lymphoma. Cancer Discov 2014;4:1022–35.
10. Wu J, Liu C, Tsui ST, Liu D. Second-generation inhibitors of Bruton tyrosine kinase. J Hematol Oncol 2016;9:80.
11. Rahal R, Frick M, Romero R, Korn JM, Kridel R, Chan FC, et al. Pharmacological and genomic profiling identifies NF-kappaB-targeted treatment strategies for mantle cell lymphoma. Nat Med 2013;20:87–92.
12. Doostparast Torshizi A, Wang K. Next-generation sequencing in drug development: target identification and genetically stratified clinical trials. Drug Discov 2018;23:1776–83.
13. Wacker SA, Houghtaling BR, Elemento O, Kapoor TM. Using transcriptome sequencing to identify mechanisms of drug action and resistance. Nat Chem Biol 2012;8:235–7.
14. Carvalho AS, Matthiesen R. Global MS-based proteomics drug profiling. Methods Mol Biol 2016;1449:469–79.
15. Beckmann L, Berg V, Dickhut C, Sun C, Merkel O, Bloehdorn J, et al. MARCKS affects cell motility and response to BTK inhibitors in CLL. Blood 2021;138: 544–56.
16. Normant E, Gorelik L, Shmeis R, Le H, Nisch R, Miskin HP, et al. TG-1701 a novel, orally available, and covalently-bound BTK inhibitor. EHA Library. 2018 [Internet]. [cited 2020 Oct 31]. Available from: https://library.ehaweb.org/eha/2018/stockholm/215080/emmanuel.normant.phd.tg-1701.a.novel.orally.available.and.covalentlybound.btk.html?f=listing%3D0%2Abrowseby%3D8%2Asortby%3D1%2Asearch%3Dtg-1701.
17. Cheah CY, Wickham N, Jurczak W, Lasica M, Wróbel T, Walewski J, et al. Clinical activity of TG-1701, as monotherapy and in combination with ublituximab and umbralisib (U2), in patients with B-cell malignancies [ASH abstract 1130]. Blood 2020;136(suppl 1).
18. Cheah CY, Wickham N, Yannakou CK, Lewis KL, Hui C-H, Tang PS, et al. Safety and activity of the once daily selective Bruton kinase (BTK) inhibitor TG-1701 in patients with chronic lymphocytic leukemia (CLL) and lymphoma. HemaSphere 2020;4:309.
19. Cheah CY, Wickham N, Yannakou CK, Lewis KL, Hui C-H, Tang PS, et al. Phase 1 study of TG-1701, a selective irreversible inhibitor of Bruton's tyrosine kinase (BTK), in patients with relapsed/refractory B-cell malignancies. Blood 2019;134:4001.
20. Balsas P, Esteve-Arenys A, Roldán J, Jiménez L, Rodríguez V, Valero JG, et al. Activity of the novel BCR kinase inhibitor IQS019 in preclinical models of B-cell non-Hodgkin lymphoma. J Hematol Oncol 2017;10:80.
21. Body S, Esteve-Arenys A, Miloudi H, Recasens-Zorzo C, Tchakarska G, Moros A, et al. Cytoplasmic cyclin D1 controls the migration and invasiveness of mantle lymphoma cells. Sci Rep 2017;7:13946.
22. Pérez-Galán P, Mora-Jensen H, Weniger MA, Shaffer AL, Rizzatti EG, Chapman CM, et al. Bortezomib resistance in mantle cell lymphoma is associated with plasmacytic differentiation. Blood 2011;117:542–52.
23. Esteve-Arenys A, Valero JG, Chamorro-Jorganes A, Gonzalez D, Rodriguez V, Dlouhy I, et al. The BET bromodomain inhibitor CPI203 overcomes resistance to ABT-199 (venetoclax) by downregulation of BFL-1/A1 in in vitro and in vivo models of MYC+/BCL2+ double hit lymphoma. Oncogene 2018;37:1830–44.

24. Perez-Riverol Y, Csordas A, Bai J, Bernal-Llinares M, Hewapathirana S, Kundu DJ, et al. The PRIDE database and related tools and resources in 2019: improving support for quantification data. Nucleic Acids Res 2019;47:D442–50.
25. Purvis GSD, Collino M, Aranda-Tavio H, Chiazza F, O'Riordan CE, Zeboudj L, et al. Inhibition of Bruton's TK regulates macrophage NF-κB and NLRP3 inflammasome activation in metabolic inflammation. Br J Pharmacol 2020; 177:4416–32.
26. Takahashi K, Sivina M, Hoellenriegel J, Oki Y, Hagemeister FB, Fayad L, et al. CCL3 and CCL4 are biomarkers for B cell receptor pathway activation and prognostic serum markers in diffuse large B cell lymphoma. Br J Haematol 2015; 171:726–35.
27. Ma H, Qazi S, Ozer Z, Zhang J, Ishkhanian R, Uckun FM. Regulatory phosphorylation of Ikaros by Bruton's tyrosine kinase. PLoS One 2013;8:e71302.
28. Díaz T, Rodríguez V, Lozano E, Mena M-P, Calderón M, Rosiñol L, et al. The BET bromodomain inhibitor CPI203 improves lenalidomide and dexamethasone activity in in vitro and in vivo models of multiple myeloma by blockade of ikaros and MYC signaling. Haematologica 2017;102:1776–84.
29. Popescu M, Gurel Z, Ronni T, Song C, Hung KY, Payne KJ, et al. Ikaros stability and pericentromeric localization are regulated by protein phosphatase 1. J Biol Chem 2009;284:13869–80.
30. Georgopoulos K. The making of a lymphocyte: the choice among disparate cell fates and the IKAROS enigma. Genes Dev 2017;31: 439–50.
31. Verbinnen I, Ferreira M, Bollen M. Biogenesis and activity regulation of protein phosphatase 1. Biochem Soc Trans 2017;45:89–99.

Interleukin-1 receptor associated kinase 1/4 and bromodomain and extra-terminal inhibitions converge on NF-κB blockade and display synergistic antitumoral activity in activated B-cell subset of diffuse large B-cell lymphoma with *MYD88* L265P mutation

The outcome of patients with diffuse large B-cell lymphoma (DLBCL) is very heterogeneous and is most likely dictated by their cell of origin (COO), defining two main molecular subtypes, i.e., germinal center B-cell (GCB) and activated B-cell (ABC).[1] Upon treatment with multi-agent chemotherapy (cyclophosphamide, doxorubicin, vincristine and prednisone) combined with the monoclonal anti-CD20 antibody rituximab (R-CHOP), almost a third of the patients, corresponding mainly to the ABC subtype of the disease, does not achieve complete remission (CR) or relapses shortly after CR.[2] However, the COO does not fully account for the different outcomes. Massive sequencing analyses recently uncovered molecular subtypes of DLBCL with distinct outcomes. In this regard, Chapuy *et al*. have described five different molecular subtypes with distinct pathogenic mechanisms and prognosis, independently of the COO. Interestingly, the C5 cluster (mostly ABC subtypes), enriched in *MYD88* L265P and *CD79B* mutations, maintained a shorter survival compared to the other ABC cluster.[3]

ABC-DLBCL tumors rely almost exclusively on constitutive nuclear transcription factor κB (NF-κB) signaling for their survival, a phenomenon that has been linked to a variety of genetic alterations that aberrantly activate the B-cell receptor (BCR) and the Toll-like receptor (TLR) signaling pathways.[1] Within the TLR axis, mutations in the gene codifying for the adaptor protein myeloid differentiation primary response gene 88 (*MYD88*) enhance interleukin-1 receptor-associated kinase 1 and 4 (IRAK1 and IRAK1) activity, providing sustained activation of NF-κB through most of the TLR. The p.L265P mutation, characterized by a change from leucine (CTC) to proline (CCG) in the MYD88 Toll/interleukin (IL)-1 receptor domain, recruits MYD88 to the cytoplasmic tail of TLR to form an active complex. Beside NF-κB, this complex promotes Janus kinase-signal transducer and activator of transcription 3 (JAK-STAT3) signaling through a pathway involving interleukin (IL)-6 and IL-10 secretion.[4]

Preclinical data have indicated that *MYD88*-mutant ABC-DLBCL cells were sensitive to pharmacological blockade of IRAK4 kinase activity, being IRAK4-compromised cells especially responsive to the Bruton's tyrosine kinase (BTK) inhibitor ibrutinib or the BCL-2 antagonist venetoclax, as almost all ABC-DLBCL display BCL2 amplification/overexpression.[5,6] Considering that both IRAK1 and IRAK4 are required for ABC-DLBCL cell survival,[4] we investigated the effect of a 24-72 hour treatment with a selective and orally bioavailable IRAK1/4 inhibitor (IRAKi, Merck),[7] in three well-characterized *MYD88*-mutated cell lines, OCI-LY3, OCI-LY10, HBL-1, using proliferation as a read out. Three germinal center B-cell (GCB)-DLBCL cell lines (SUDHL-4, SUDHL-8 and OCI-LY8) with wild-type MYD88 *($MYD88^{wt}$)* were analyzed in the same settings, as a control. We observed a partial and transitory response to IRAKi in ABC-DLBCL cells only, when using the compound at the physiological dose of 50 μM (Figure 1A). Treatment-related cytotoxicity decreased from 25.5% at 24 hours to 19% at 72 hours, respectively, despite an efficient blockade of IRAK1 and IRAK4 phosphorylation at Thr209 and Thr345 residues, in the three *MYD88*-mutated cell lines (Figure 1B). Interestingly, the destabilization of the anti-apoptotic protein and key mediator of IRAKi activity, MCL-1,[8] was not sufficient to confer a significant cytotoxicity to the compound (Figure 1B). A gene expression profiling (GEP) analysis in the three *MYD88*-mutated cell lines exposed for 6 hours to the inhibitor, further showed that IRAK1/4 blockade significantly altered the expression of the top NF-κB gene signatures associated to B-cell lymphoma,[9] namely *NFKB_ALL_OCI_LY10* and *NFKB_BOTH OCILY3ANDLY10*, with normalized enrichment score (NES) values reaching 1.8, while in contrast a third gene set, *NFKB_OCILY10_ONLY*, was slightly upregulated (NES: -1.20), according to GSEA analysis (Figure 1C; *Online Supplementary Table S1*). In agreement, the transcription of several NF-κB-regulated genes known to promote ABC-DLBCL pathogenesis, including *IL6, IL10, IRF4* and *CCL3*, were either unaffected or even increased after treatment with IRAKi (Figure 1D, *Online Supplementary Table S1*). Consistently, in an OCI-LY3 mouse xenograft model the compound failed to elicit a significant tumor growth inhibition (*Online Supplementary Figure S1A*).

We then considered the possibility to enhance IRAKi activity in *MYD88* L265P ABC-DLBCL by combining the compound with the BET bromodomain inhibitor CPI203 (kindly provided by Constellation Pharmaceuticals), as this BRD4 antagonist has been shown to effectively suppress a NF-κB gene signature that includes *IL6, IL10* and *IRF4*, in ABC-DLBCL.[10] After exposing the same ABC-DLBCL cell lines as above to a 50 μM dose of IRAKi, followed by a 24-hour treatment with 0.5 μM CPI203, a new GEP analysis was performed. As shown in Figure 2A, IRAKi-CPI203 combination induced a significant downregulation of NF-κB-related genes when compared to IRAKi single agent, with NES comprised between 1.46 and 1.99. Of note, the combination therapy allowed to a significant disruption of *NFKB_OCILY10_ONLY* gene signature with a NES of 1.89. Among the genes included in the *NFKB_ALL_OCILY3_LY10* gene set, a selected list of nineteen factors underwent a ≥2-fold increase in their rank metric score between this analysis and the previous one (*Online Supplementary Table S2*), suggesting that their improved modulation may be associated with the combinational effect of IRAKi and CPI203. From this list, we identified only four genes (*LTA, MARCKS, CD44* and *HEATR1*) that were not included in the core component of the NF-κB target genes affected by either IRAKi or CPI203 as single agents, but which underwent a significant downregulation upon treatment with the drug combination. Among these genes, we were unable to detect significant levels of *LTA* and *HEATR1* transcripts in the three ABC-DLBCL cell lines (*data not shown*). In contrast, upon exposure of the three *MYD88*-mutated cell lines to the IRAKi we observed a 1.2- to 2-fold transcriptional increase of *MARCKS* and *CD44*, together with *IL6* and *IL10* used here as hallmarks of NF-kB activation. These genes were all reduced down to 0.5-fold in cells treated with the drug combination (Figure 2B). Accordingly, IRAKi-CPI203 treatment led to the accumulation of the intracellular inhibitor of NF-κB, IκB, and to the consequent reduction in CD44 and MARCKS protein levels, while IRAKi and CPI203 single agents slightly affected the expression of these factors (Figure 2C). As expected, in two out of the three cell lines, CPI203-based treatments led to the decrease in MYC protein and mRNA, used here as hallmarks of BRD4 inhibition (Figures 2B and C). Also confirming a previous report linking bromodomain inhibitor therapy with IRAK1 downregulation in B-cell lymphoma,[11] IRAK1-pThr209 levels underwent a slight downregulation after CPI203 treatment and this effect was remarkably potentiated upon addition of

IRAKi to the cell cultures (Figure 2C). In line with the increased blockade of NF-κB signaling, the addition of CPI203 synergistically improved IRAKi cytostatic effect in the three cell lines, as attested by an 86% blockade in cell proliferation, significantly higher than the 19% activity achieved by IRAKi alone (combination index [CI]: 0.52, Figure 2D). Importantly, the co-operation between the IRAKi and CPI203 involved a remarkable downregulation of MCL-1 (Figure 2C), which was accompanied by a 36% increase in the relative apoptosis rate when compared with IRAKi and CPI203 used separately (Figure 2F).

In order to further validate the activity of the drug combination, primary lymph node biopsies from DLBCL patients with either *MYD88*^{wt} or *MYD88* L265P were co-cultured in the presence of a feeding stromal monolayer as previously reported,[12] and treated with the different drugs as above. While IRAKi-CPI203 was almost inactive in *MYD88*^{wt} cells, the combination induced a 16% augmentation in relative apoptotic cell death in the *MYD88* L265P primary co-culture (Figure 3A, left panel), which was accompanied by a 12% decrease in the fraction of cells with high contents of *IL6* mRNA, a percentage superior to what observed upon treatment with each drug alone (Figure 3B, right panel).

Among the above mentioned genes, CD44 expression and IL-6 serum levels have been described as prognostic markers in DLBCL.[13,14] In order to investigate the role of these two factors in the response of ABC-DLBCL cell lines to IRAKi-based treatment, HBL-1 and OCI-LY3 cells were stimulated with 0.5 μM of the CD44 ligand, hyaluronic acid (HA), or exposed to a 5 μg/mL dose of the IL-6 blocking antibody tocilizumab, prior to a 72-hour treatment with the drugs. In the case of HA, cells were exposed to IRAKi (50 μM) +/- CPI203 (0.5 μM), while effect of tocilizumab pretreatment was evaluated in IRAKi-treated cells. Cell response was determined by fluorescence microscopy recounting of cells with high contents in F-actin and by MTT assay, respectively. As shown on Figure 3B, both IRAKi and CPI203 were able to block actin polymerization by 50.4% and 54.5%, respectively, while the drug combination achieved a total 77.9% decrease in cells with high contents in F-actin following stimulation of

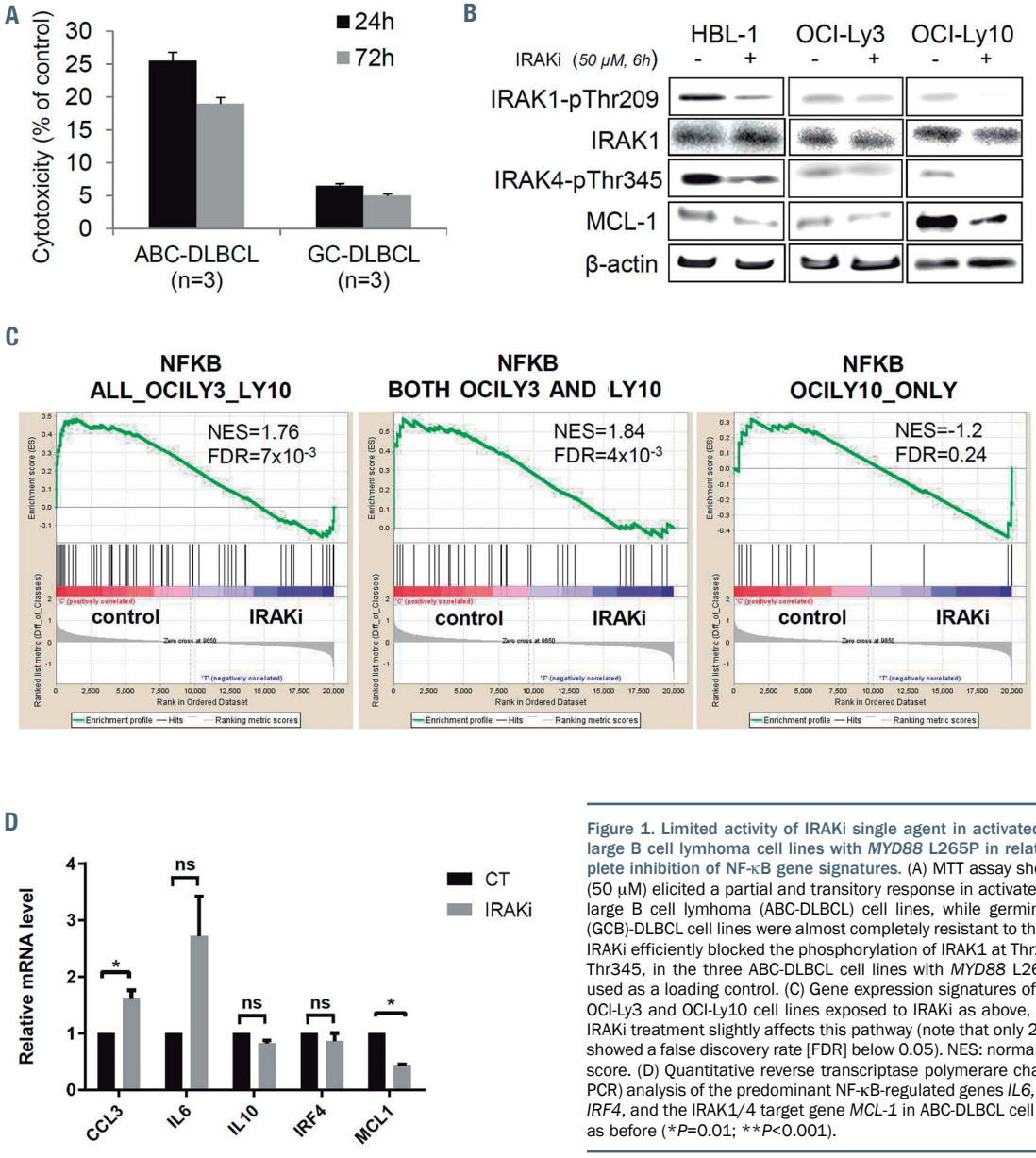

Figure 1. Limited activity of IRAKi single agent in activated B-cell - diffuse large B cell lymhoma cell lines with *MYD88* L265P in relation with incomplete inhibition of NF-κB gene signatures. (A) MTT assay showing that IRAKi (50 μM) elicited a partial and transitory response in activated B-cell - diffuse large B cell lymhoma (ABC-DLBCL) cell lines, while germinal center B-cell (GCB)-DLBCL cell lines were almost completely resistant to the compound. (B) IRAKi efficiently blocked the phosphorylation of IRAK1 at Thr29 and IRAK4 at Thr345, in the three ABC-DLBCL cell lines with *MYD88* L265P. β-actin was used as a loading control. (C) Gene expression signatures of NF-κB in HBL-1, OCI-Ly3 and OCI-Ly10 cell lines exposed to IRAKi as above, highlighting that IRAKi treatment slightly affects this pathway (note that only 2 out 3 gene sets showed a false discovery rate [FDR] below 0.05). NES: normalized enrichment score. (D) Quantitative reverse transcriptase polymerare chain reaction (RQ-PCR) analysis of the predominant NF-κB-regulated genes *IL6, IL10, CCL3*, and *IRF4*, and the IRAK1/4 target gene *MCL-1* in ABC-DLBCL cell treated by IRAKi as before (*P=0.01; **P<0.001).

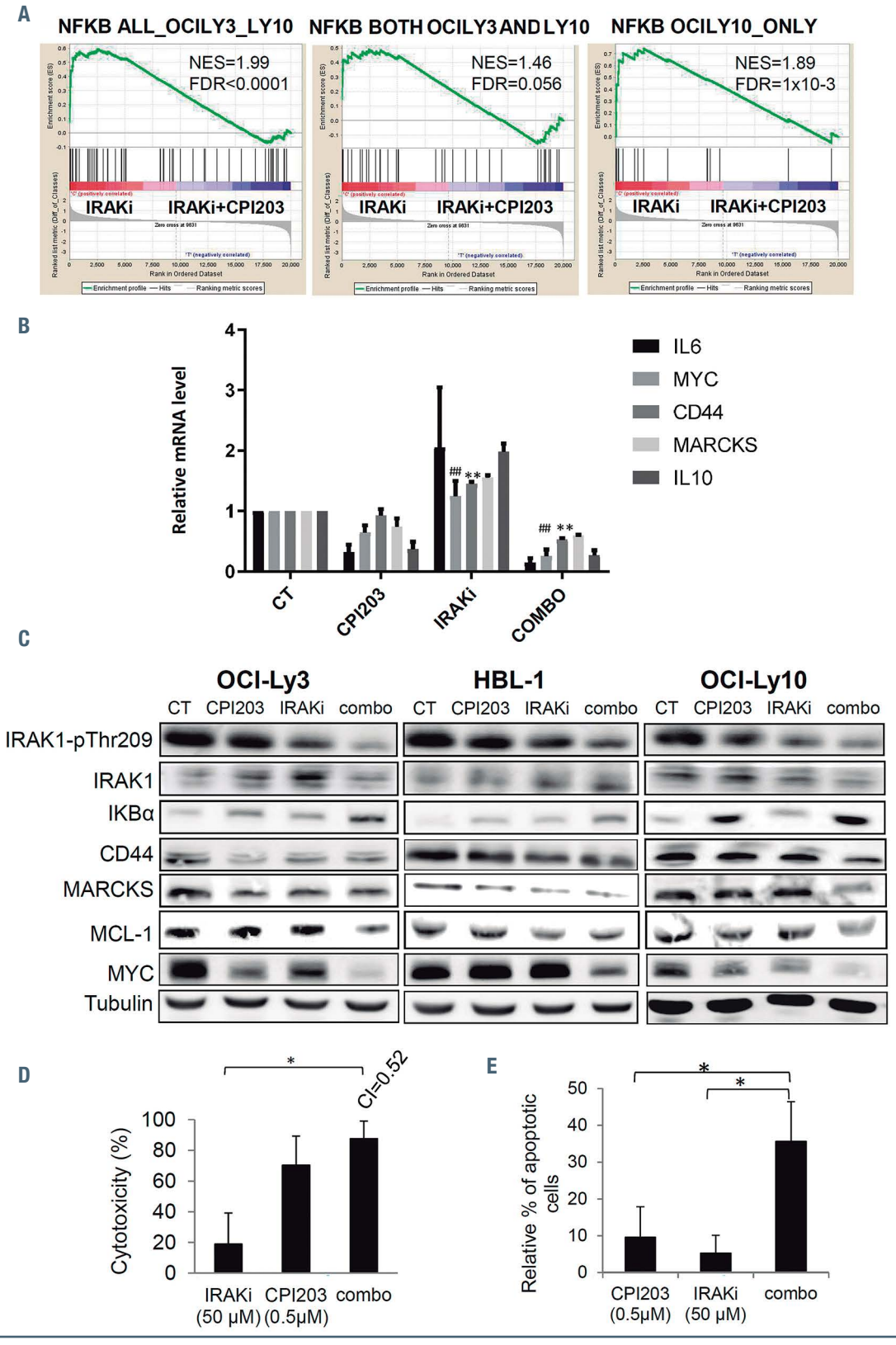

Figure 2. The BETi CPI203 synergizes with IRAKi in activated B-cell - diffuse large B cell lymphoma mediated by the inhibition of NF-κB downstream pathways. (A) Enrichment plots from gene set enrichment analysis (GSEA) analysis comparing IRAKi single agent *vs.* IRAKi-CPI203 combo in the 3 cell lines treated for 6 hours (Affymetrix HG-U219; GSEA), showing a significant improvement of NF-κB signature decrease by the addition of CPI203 to IRAKi. (B) Quantitative reverse transcriptase polymerare chain reaction (RQ-PRC) analysis of NF-κB downstream genes in the three cell lines exposed to IRAKi, CPI203 or CPI203-IRAKi combo as before. (*P=0.01; **P<0.001). (C) CPI203-IRAKi combination led to intracellular accumulation of IκB, and subsequent downregulation of IRAK1, MYC, CD44, MARCKS and MCL-1 proteins in activated B-cell - diffuse large B cell lymphoma (ABC-DLBCL) cells with *MYD88*^{L265P}. (D) OCI-Ly3, OCI-Ly10, HBL-1 cells were exposed for 24 hours to 0.1-0.5 μM CPI203 and/or 50-500 μM IRAKi. Cytotoxicity was evaluated by MTT assay and combination index (CI) was determined using the Calcusyn software. Shown are the cytotoxicity and the mean CI value calculated for cell treatment with 0.5 μM CPI203 and 50 μM IRAKi. (E) The drug combination led to a synergistic antitumoral effect *in vitro* in these 3 cell lines, inducing a median 36% increase in apoptosis rate when compared to single agent treatments (*P<0.04).

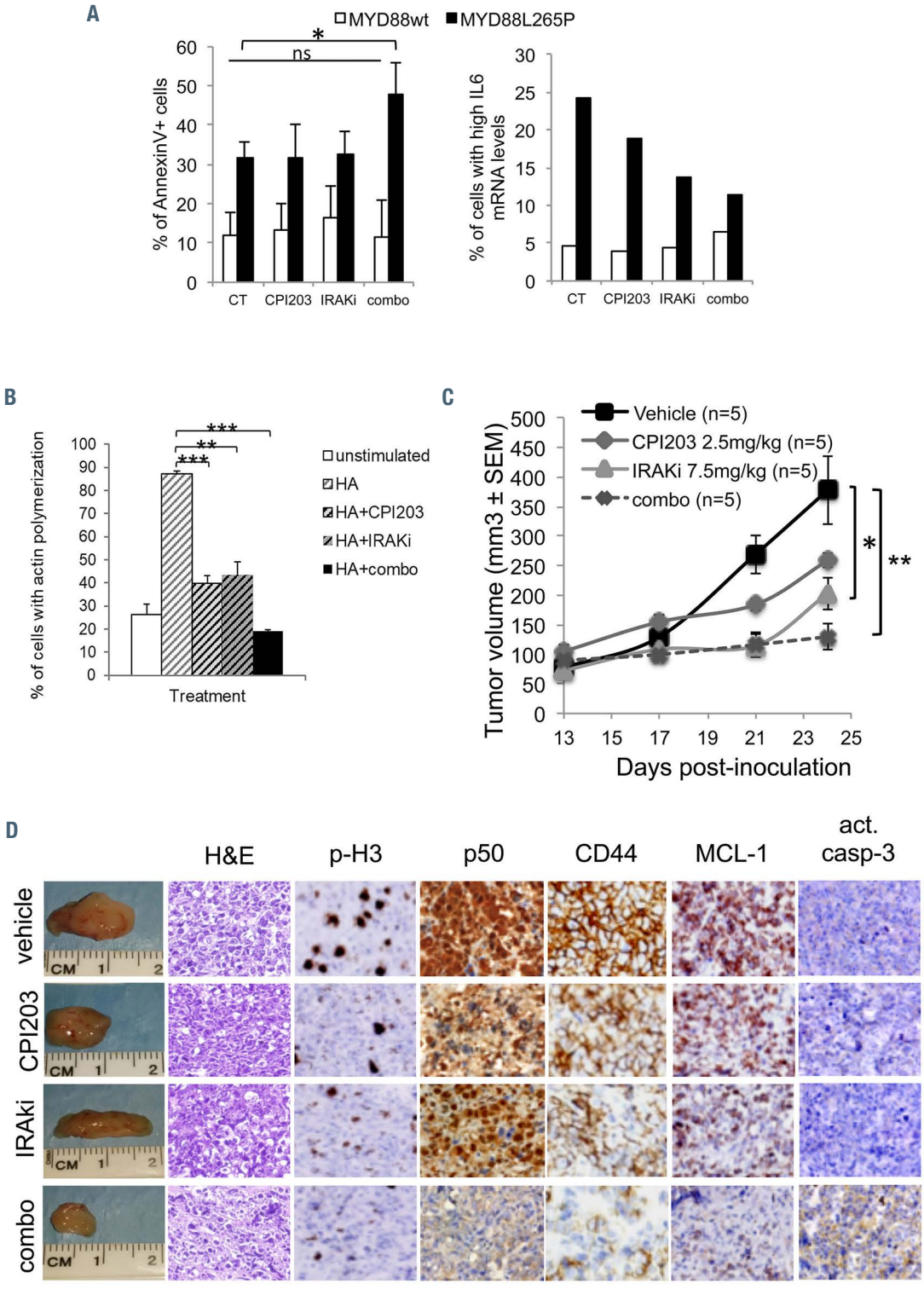

Figure 3. IRAKi and CPI203 combination is active in activated B-cell - diffuse B-cell lymphoma primary cultures and impairs tumor growth *in vivo*. (A) Left panel: antitumoral activity of CPI203 (0.5 μM) and/or IRAKi (50 μM) was evaluated after a 24-hour culture of primary lymph node biopsies from activated B-cell - diffuse B-cell lymphoma patients with either *MYD88*^{wt} or *MYD88* L265P by cytofluorimetric quantification of AnnexinV^{+} cells. Cell of origin (COO) and *MYD88* mutational status of the patients were determined by allele-specific polymerase chain reaction and gene expression analysis, as previously.[15] *Right panel*: DLBCL cultures treated as above were labeled with an IL-6 Hu-Cyanine 5 SmartFlare RNA detection probe (Merck Millipore), and percentage of viable cells with high contents in *IL6* mRNA was determined by flow cytometry, as previously.[16] (B) HBL-1 y OCI-LY3 cell lines were preincubated for 24 hours with 0.5 μM CPI203 and/or 50 μM IRAKi, followed by a 24-hour stimulation with 0.5 μM HA, labeling with 50 μM Phalloidin-TRITC (Sigma-Aldrich) and recounting of red fluorescent cells on a Nikon H5505 microscope by means of a 20X/1.30 NA oil objective (Nikon) with the use of Isis Imaging System v5.3 software (MetaSystems GmbH) (***P<0.001). (C) NOD/SCID IL2Rγ-null (NSG) mice were inoculated subcutaneously with 10^7 OCI-LY3 cells and after 13 days, tumor-bearing animals (n=5 mice per group) received intraperitoneal (i.p.) injection of 2.5 mg/kg CPI203 (BID) and/or i.p. administration of 7.5 mg/kg IRAKi (BID), or an equal volume of vehicle, for 11 days, in a five/two (on/off) schedule. Tumor volumes were measured each 2-3 days with external calipers. (D) Immunohistological analysis of consecutive tumor sections from representative animals reveals a notable decrease in mitotic index and in the NF-κB-regulated CD44, as well as a strong downregulation of MCL-1 and induction of apoptosis in IRAKi-CPI203 combo group.

CD44 by HA. In contrast, the anti-IL-6 antibody failed to sensitize ABC-DLBCL cells to IRAKi-based treatment (*Online Supplementary Figure S1B*). Thus, these results suggest a significant activity of the drug combination towards CD44 downstream signaling, while IL-6 expression may not be directly involved in the effect of these agents.

Finally, in order to assess the efficacy of the drug combination *in vivo*, NSG mice were subcutaneously injected with OCI-LY3 cells, and tumor-bearing animals received daily doses of either IRAKi (5 mg/kg, intraperitoneal [i.p.], BID), CPI203 (2.5 mg/kg, i.p., BID), the combination of both agents, or the equivalent volume of vehicle, for 11 days. Figure 3C shows that CPI203 and IRAKi single agents induced a 31.5% and 46.3% tumor growth inhibition (TGI), respectively, while the combination of both drugs significantly improved this effect with a 65.6% TGI, when compared to vehicle-receiving animals (*P=0.011; **P=0.007). No significant toxicity was observed in any of the treatment arms. Histological analysis of the corresponding tumors revealed an improved reduction of mitotic index together with an accumulation of apoptotic cells by the combination therapy, as assessed by phosphohistone H3 and activated-caspase-3 staining (Figure 3D). In agreement with the *in vitro* results, an enhanced reduction in the levels of CD44 and MCL-1, and an improved downregulation of nuclear p50 used as a read of NF-κB activity, was observed in the combination group when compared with the other arms (Figure 3D).

Collectively, our results suggest that IRAK1/4 inhibition is modestly effective in *in vitro* and *in vivo* models of ABC-DLBCL with *MYD88* L265P, achieving only a partial inhibition of NF-κB signaling. We confirm that BET inhibition is an efficient strategy to counteract NF-κB over-activation in these models, offering synergistic anti-tumoral and pro-apoptotic activities with IRAK inhibition, mediated by the downregulation of the NF-κB-regulated factors, CD44 and MCL-1, and the consequent blockade of cell motility and triggering of tumor cell death.

Ivan Dlouhy,[1,2] Marc Armengol,[3*] Clara Recasens-Zorzo,[2] Marcelo L. Ribeiro,[3,4] Patricia Pérez-Galán,[2] Francesc Bosch,[5] Armando López-Guillermo[1,2#] and Gaël Roué[3#]*

[1]Department of Hematology, Hospital Clínic, BarceIona, Spain; [2]Division of Hematology and Oncology, Institut d'Investigacions Biomèdiques August Pi i Sunyer (IDIBAPS), CIBERONC, Barcelona, Spain; [3]Lymphoma Translational Group, Josep Carreras Leukemia Research Institute (IJC), Badalona, Spain; [4]Post Graduate Program in Health Science, Universidade São Francisco (USF), Bragança Paulista, Brazil and [5]Laboratory of Experimental Hematology, Department of Hematology, Vall d'Hebron Institute of Oncology (VHIO), Vall d'Hebron University Hospital, Universitat Autònoma de Barcelona, Barcelona, Spain

**ID and MA contributed equally as co-first authors.*

#ALG and GR contributed equally as co-senior authors.

Correspondence:

GAËL ROUÉ - groue@carrerasresearch.org

doi:10.3324/haematol.2020.278258

Received: December 25, 2020.

Accepted: May 5, 2021.

Pre-published: May 13, 2021.

Disclosures: GR received research support from Celgene Corp and TG Therapeutics. CPI203 was kindly provided by Constellation Pharmaceuticals.

Contributions: ID and MA performed experiments, analyzed data and co-wrote the manuscript; CRZ provided support in animal studies; MLR interpreted the results and reviewed the manuscript; PP-G helped in analyzing the gene expression data; FB evaluated the data and reviewed the manuscript critically; AL-G and GR conceived and designed the study, analyzed data and wrote the manuscript.

References

1. Pasqualucci L. Molecular pathogenesis of germinal center-derived B cell lymphomas. Immunol Rev. 2019;288(1):240-261.
2. Miyazaki K. Treatment of diffuse large B-cell lymphoma. J Clin Exp Hematopathol. 2016;56(2):79-88.
3. Chapuy B, Stewart C, Dunford AJ, et al. Molecular subtypes of diffuse large B cell lymphoma are associated with distinct pathogenic mechanisms and outcomes. Nat Med. 2018;24(5):679-690.
4. Ngo VN, Young RM, Schmitz R, et al. Oncogenically active MYD88 mutations in human lymphoma. Nature. 2010;470(7332):115-119.
5. Kelly PN, Romero DL, Yang Y, et al. Selective interleukin-1 receptor–associated kinase 4 inhibitors for the treatment of autoimmune disorders and lymphoid malignancy. J Exp Med. 2015;212(13):2189-2201.
6. Knittel G, Liedgens P, Korovkina D, et al. B-cell–specific conditional expression of Myd88p.L252P leads to the development of diffuse large B-cell lymphoma in mice. Blood. 2016;127(22):2732-2741.
7. Wang Z, Sun D, Johnstone S, et al. Discovery of potent, selective, and orally bioavailable inhibitors of interleukin-1 receptor-associate kinase-4. Bioorg Med Chem Lett. 2015;25(23):5546-5550.
8. Li Z, Younger K, Gartenhaus R, et al. Inhibition of IRAK1/4 sensitizes T cell acute lymphoblastic leukemia to chemotherapies. J Clin Invest. 2015;125(3):1081-1097.
9. Lam LT, Davis RE, Pierce J, et al. Small molecule inhibitors of IκB kinase are selectively toxic for subgroups of diffuse large B-cell lymphoma defined by gene expression profiling. Clin Cancer Res. 2005;11(1):28-40.
10. Ceribelli M, Kelly PN, Shaffer AL, et al. Blockade of oncogenic IκB kinase activity in diffuse large B-cell lymphoma by bromodomain and extraterminal domain protein inhibitors. Proc Natl Acad Sci U S A. 2014;111(31):11365-11370.
11. Boi M, Gaudio E, Bonetti P, et al. The BET bromodomain inhibitor OTX015 affects pathogenetic pathways in preclinical B-cell tumor models and synergizes with targeted drugs. Clin Cancer Res. 2015;21(7):1628-1638.
12. Esteve-Arenys A, Valero JG, Chamorro-Jorganes A, et al. The BET bromodomain inhibitor CPI203 overcomes resistance to ABT-199 (venetoclax) by downregulation of BFL-1/A1 in in vitro and in vivo models of MYC+/BCL2+ double hit lymphoma. Oncogene. 2018;37(14):1830-1844.
13. Wei X, Xu M, Wei Y, et al. The addition of rituximab to CHOP therapy alters the prognostic significance of CD44 expression. J Hematol Oncol. 2014;7:34.
14. Dlouhy I, Filella X, Rovira J, et al. High serum levels of soluble interleukin-2 receptor (sIL2-R), interleukin-6 (IL-6) and tumor necrosis factor alpha (TNF) are associated with adverse clinical features and predict poor outcome in diffuse large B-cell lymphoma. Leuk Res. 2017;59:20-25.
15. Rovira J, Karube K, Valera A, et al. MYD88 L265P mutations, but no other variants, identify a subpopulation of DLBCL patients of activated B-cell origin, extranodal involvement, and poor outcome. Clin Cancer Res. 2016;22(11):2755-2764.
16. Vaidyanathan S, Friend S, Weldon D, Morrissey P. Measurement of IL-6 levels in live cells using RNA detection probe with Imaging Flow Cytometer. J Immunol. 2016;196(Suppl 1):S196.